PHYSICOCHEMICAL CHARACTERIZATION OF THE BACTERIAL Cu(I) SENSOR CsoR

A Dissertation

by

ZHEN MA

Submitted to the Office of Graduate Studies of
Texas A&M University
in partial fulfillment of the requirements for the degree of

DOCTOR OF PHILOSOPHY

December 2009

Major Subject: Biochemistry

PHYSICOCHEMICAL CHARACTERIZATION OF THE BACTERIAL Cu(I) SENSOR CsoR

A Dissertation

by

ZHEN MA

Submitted to the Office of Graduate Studies of
Texas A&M University
in partial fulfillment of the requirements for the degree of

DOCTOR OF PHILOSOPHY

Approved by:

Chair of Committee	David P. Giedroc
Committee Members	J. Martin Scholtz
	Gregory D. Reinhart
	Gary R. Kunkel
Head of Department	Gregory D. Reinhart

December 2009

Major Subject: Biochemistry

ABSTRACT

Physicochemical Characterization of the Bacterial Cu(I) Sensor CsoR. (December 2009)

Zhen Ma, B.S., Fudan University

Chair of Advisory Committee: Dr. David P. Giedroc

M. tuberculosis copper-sensitive operon repressor (*Mtb* CsoR) is the founding member of a new metalloregulatory protein family in prokaryotes that regulates the transcription of the *cso* operon in response to copper toxicity. *Mtb* CsoR tetramer binds 1 monomer mol equiv of Cu(I) with very high affinity (log K_{Cu}=18.0) via three conserved residues, Cys36, His61' and Cys65'. Binding of Cu(I) allosterically inhibits the CsoR binding to the DNA operator (CsoO) overlapping the *cso* promoter (ΔG_c=+3.6 kcal/mol, pH 7.0, 25 ^{o}C). These findings are consistent with a role of CsoR as a transcriptional repressor with Cu(I) binding inducing transcriptional derepression. To explore the mechanism of this regulation, His61 was substituted with 1-methylhistidine (MeH) or β-(2-thiazolyl)-alanine (Thz) using a native chemical ligation strategy. The CsoO binding affinities of the resultant H61MeH and H61Thz CsoRs are both refractory to inhibition by Cu(I) binding despite the fact that each forms a high affinity 3-coordinate complex with Cu(I). This suggests that while Cu(I) is coordinated by the $N^{\delta 1}$ atom of His61, the $N^{\varepsilon 2}$ atom plays an critical role in driving this allosteric switch. Evidence in support of a formation of a hydrogen bonding network involving the $N^{\delta 1}$ face of His61 and two conserved "second coordination shell" residues, Glu81' and Tyr35, is presented.

Remarkably, this mechanism is analogous to that proposed for the Zn(II) sensor CzrA from *S. aureus*. To test this, we employed the same native chemical ligation approach to substitute the key Zn(II) ligand His97 with 1-methylhistidine; with the preliminary findings fully consistent with an intersubunit allosteric switch involving the $N^{\varepsilon 2}$ face of this key His97 residue in CzrA.

Two predicted homologs of *Mtb* CsoR were also biochemically characterized to obtain additional support for the hypothesis that CsoR is a key Cu(I) regulatory protein in many bacterial species. *B. subtilis* CsoR, known to regulate the transcription of the *copZA* operon, was found to have biochemical properties similar to those of *Mtb* CsoR as to Cu(I) binding, DNA binding and Cu(I)-dependent allosteric regulation. Interestingly, *Bsu* CsoR also binds other divalent metal ions (Zn, Ni) with high affinity but with metal coordination geometries distinct from that of Cu(I). Binding of these divalent metal ions only weakly regulates *copZA* operator binding *in vitro*, suggesting that coordination number and geometry are most closely related to the allosteric regulation. Finally, a putative CsoR from the pathogenic *S. aureus* Newman strain was identified and characterized, and was found to exhibit biochemical properties similar to those of *Mtb* and *Bsu* CsoRs. Parallels between Cu(I)-sensing CsoRs and functional orthologs in the CsoR/RcnR family are further discussed in the context of the mechanism and evolutionary divergence of this new family of regulatory proteins.

DEDICATION

I would like to dedicate this work to my family and friends, especially my parents and my wife, for their continued support and help.

ACKNOWLEDGEMENTS

I would like to thank my advisor, Dr. David Giedroc for his support and guidance on this project. In addition, I would also like to thank all current and former members of the Giedroc laboratory, in particular Dr. Xiaohua Chen and Dr. Tong Liu for their help when I joined the lab and started on this project. I would also like to acknowledge those who helped me along the way including the professors on my committee: Dr. Martin Scholtz, Dr. Gregory Reinhart, Dr. Gary Kunkel and Dr. Paul Fitzpatrick.

Our collaborators have also made important contributions on different aspects of this project and I would like to thank them for their help. These include Dr. Adel Talaat (University of Wisconsin-Madison), Dr. James Sacchettini (Texas A&M University), Dr. Graham George (University of Saskatchewan), Dr. Robert Scott (University of Georgia), Dr. Richard DiMarchi (Indiana University) and Dr. Eric Skaar (Vanderbilt University).

ABBREVIATIONS

Mtb	*Mycobacterium tuberculosis*
Bsu	*Bacillus subtilis*
Sau	*Staphylococcus aureus*
BCS	bathocuproine disulfonate
BCA	bicinchoninic acid
MES	2-(*N*-morpholino)ethanesulfonic acid
HEPES	4-(2-hydroxyethyl)-1-piperazineethanesulfonic acid
Tris	tris(hydroxymethyl)aminomethane
DTNB	5,5'-dithiobis(2-nitrobenzoic acid)
XAS	X-ray absorption spectroscopy
cso	copper-sensitive operon
CsoR	copper-sensitive operon repressor
EMSA	electrophoretic mobility shift assay

TABLE OF CONTENTS

CHAPTER Page

LIST OF FIGURES

FIGURE Page

FIGURE Page

LIST OF TABLES

CHAPTER I

INTRODUCTION*

Transition metal ions have long been known as essential nutrients. These metal ions include manganese, iron, cobalt, nickel, copper, zinc and to a more specialized degree, molybdenum, tungsten and vanadium. These ions function either as structural components or enzyme cofactors, and are thus involved in many important biological processes (*1, 2*). Such roles cannot be carried out by any other entity in the cell, thus making metal ions essential for all life (*3*). On the other hand, each of these metal ions in excess is toxic to cells to various degrees, largely as a result of perturbation of homeostasis and/or by initiation of oxidative stress. Also, an individual metal ion can only fulfill limited roles (*1*). As a result, during the course of evolution, all cells have evolved mechanisms to ensure a delicate or optimized balance of each transition metal ion, thereby coordinating the control of inserting the "right" metal into a target protein at the "right" time and "right" place (*1, 2, 4, 5*).

METAL HOMEOSTASIS AND TRANSPORT

The homeostasis of essential metal ions is maintained by extensive regulatory and protein-coding machinery that controls the uptake, intracellular trafficking and

---

This dissertation follows the style of *Biochemistry*.

*This chapter is reproduced in part with permission from "Coordination chemistry of bacterial metal sensing and transport" Ma, Z., Jacobsen, F. E. and Giedroc, D. P., 2009, Chemical Review, in press. Copyright [2009] American Chemical Society.

efflux/storage of these metal ions. Metal homeostasis is defined as the process in which an optimal metal concentration or bioavailability is maintained in the cell, or in different intracellular compartments, in the case of eukaryotic cells (*1*). The scarcity of a particular metal ion may cause reprogramming of cellular events, possibly via increasing the uptake and/or lowering the requirement for this metal ion by down-regulating the proteins require that metal ion for function. On the other hand, under metal stress or an excess of metals, cells require the ability to efflux, store or otherwise detoxify metals to mitigate the effect of toxicity (Figure 1) (*6*). In prokaryotes, all of these processes are highly coordinated largely at the level of transcriptional regulation by a panel of metalloregulatory or metal sensor proteins (see below).

In bacteria, acquisition or uptake of essential transition metal ions requires special consideration. In gram-negative bacteria, metal ions have to pass through the outer membrane (OM), the periplasmic space and the inner or plasma membrane (PM) before they reach the cytosol where many metal ions are incorporated into the target proteins. Trimeric β-barrel proteins called porins in the outer membrane allow for non-selective diffusion of metal ions; in other cases, mostly for Fe, there are specific high affinity outer membrane receptors mediating the transport of low molecular weight Fe-chelates, *e.g.,* siderophores, across the outer membrane (*1*). To meet the demands of the cell, the cytosol effectively concentrates all metal ions by employing specific metal uptake transporters located in the plasma membrane (*7*). The uptake systems are driven either by the hydrolysis of ATP, *e.g.,* ATP-binding cassette (ABC) transporters and P-type ATPases, or via coupling to an energetically favorable process, such as co-transport

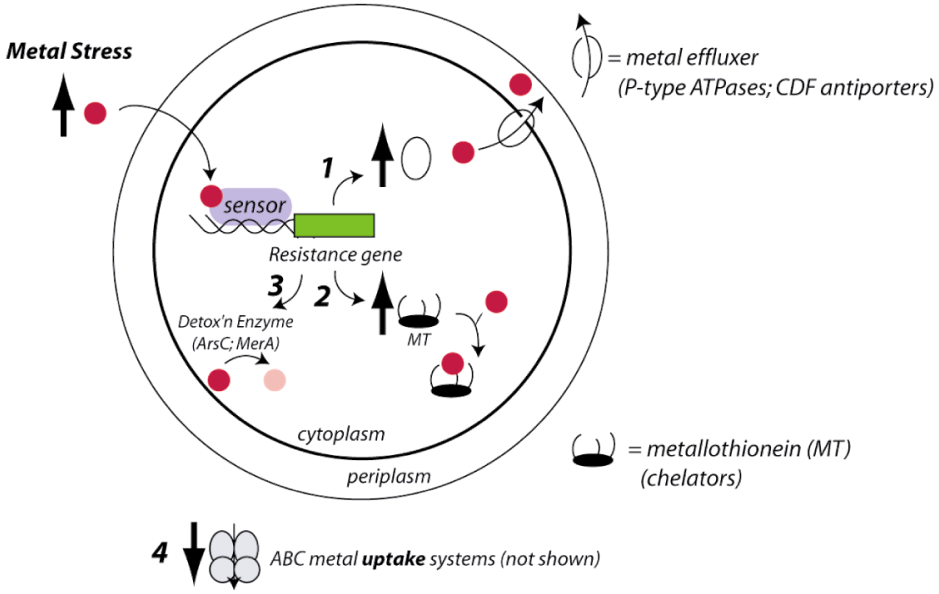

Figure 1. Cartoon representation of how a generic metal sensor protein affects resistance to toxic concentrations of a particular transition metal ion in the cytoplasm. Adapted from reference (*6*).

of protons or other small molecules across the lipid bilayer (symport or antiport). In gram-positive bacteria, an extra layer of lipopolysaccharide or complex carbohydrates is present and this may potentially affect the rate and mechanism of metal uptake.

In the cytosol and periplasmic space in gram-negative bacteria, certain metal ions, especially copper ions, seem to require specific trafficking mechanisms to target it to correct proteins (*5*). Such trafficking is usually mediated by proteins called metallochaperones, which have been reported for copper, nickel and iron-sulfur protein biogenesis. Recent work also suggests that in *E. coli*, a periplasmic Zn(II) binding prtotein, YodA, has characteristics consistent with a role as a Zn chaperone (*8-11*). The metal transfer from these metallochaperones to an acceptor protein occurs by formation of a transient protein-protein interaction mediated by intermolecular metal complexes, as described for Cu trafficking via a ligand exchange reaction (*12*).

To mitigate the possible toxicity generated by excess metals, different metal efflux transporters have evolved, such as P-type ATPases, CDF antiporters and RND type transporters (*13-16*). In some cases, Cys-rich metallothioneins such as those described for Zn and Cu detoxification, or ferritin-like bacterioferritins and Dps-type proteins for iron storage, can function to sequester excess metal ions in the cytosol (*17-19*). This storage mechanism is likely to be crucial for iron homeostasis, since iron availability is usually very limited. Bacteria have also evolved highly specific small molecule chelators, such as siderophores, for iron sequestration in the extracellular milieu and uptake. Such processes are energetically expensive; therefore, these cytosolic

stores allow the cell to mobilize Fe when the extracellular iron source in the immediate milieu becomes limiting (*19*).

The expression of these proteins relevant to metal homeostasis is controlled mainly by various transcriptional regulators in bacteria (see below). Since the requirement for each metal is different, a hypothesis that emerges is that the homeostasis machinery and the regulation must be selective in order to effectively control the intracellular availability of a particular metal ion. Therefore, each individual component is thought to be "tuned" so that the affinity or sensitivity matches the prevailing conditions in the cell (*1*). In fact, the concentrations of different metal ions in different organisms may vary widely and so far, there is only limited experimental data on this fundamental aspect of metal homeostasis. Further investigation of this may provide considerable insights into intracellular mechanisms of metal homeostasis.

COPPER IN BIOLOGY

The total copper concentration in an *E. coli* cell grown aerobically in minimal media is low (10^{-6} M), but still much higher than the concentration of copper outside of the cell in the same media (10^{-8} M) (*7*). Copper has two accessible redox states, Cu(I) (cuprous) and Cu(II) (cupric), which can be reversibly interconverted. The standard reduction potential for Cu(II)/Cu(I) is 150 mV, while a range of 200-800 mV can be achieved when Cu is coordinated by proteins; therefore, Cu is an excellent cofactor for well-known oxidoreductases, such as cytochrome c oxidase and superoxide dismutase (SOD) (*20, 21*), and indeed in any reaction that requires electron transfer. In fact, it has

been estimated that 93% of Cu-containing enzymes are used as conduits for electron transfer via reversible redox cycling of Cu(I)/Cu(II) (*2*).

Uncomplexed copper ions are extremely toxic to the cell. Free Cu(I) ion can react with hydrogen peroxide through a Fenton like reaction to produce reactive hydroxyl radicals, which can readily react with proteins, lipids and nucleic acids (*20*). In support of this, recent microarray and proteomics studies shown that copper stress can induce the genes related to oxidative stress defense, suggesting a connection between Cu homeostasis and oxidative stress, although the underlying mechanism remains unclear (*22, 23*). A more recent report suggests that in *E. coli*, Cu(I) may directly damage the solvent exposed iron-sulfur clusters in proteins and significantly interrupt their functions in the absence of molecular oxygen; iron release caused by such damage may induce mis-regulation of Fe homeostasis and, in aerobic conditions, Fe mediated oxidative stress (*24*). On the other hand, free Cu(II) ion is capable of directly oxidizing amino acid side chains as well as inducing amyloid formation, and thus is associated with many amyloid-related diseases in mammals (*25-28*). Therefore, the bioavailable copper levels must be strictly controlled inside the cell and is proposed to be buffered at a concentration in the 10^{-18} M range. As such, it is widely accepted that in bacterial and yeast cells, there is no free or bioavailable copper in the cell (*29*). Control of Cu homeostasis in bacteria is particularly important since most prokaryotes lack a cytosolic Cu requirement. Thus, virtually any Cu(I) in the cytoplasm in a non-photosynthetic bacterium is toxic. In fact, Cu has long been used as a bactericidal agent in water purification, plants, and recent efforts have attempted to exploit the sensitivity of the

major hospital pathogen, MRSA (methicillin-resistant *Staphylococcus aureus*), to Cu(I) (*30*).

Another important motivation for understanding bacterial copper homeostasis is that proteins involved in Cu-transport, trafficking and sensing can be tied in some way to the viability or the virulence of human pathogenic bacteria (*31, 32*). Although the molecular details of this are unknown, the immediate milieu that must be colonized by these microbes in the host may be characterized by metal concentrations that are either too high or greatly limiting, with metal homeostasis required for successful adaptation to these changing conditions (*33*).

METALLOREGULATORY PROTEINS IN PROKARYOTES

Prokaryotes typically contain a panel of metalloregulatory proteins that collectively manage metal ion homeostasis in the cell. These specialized "metal receptor proteins" function as transcriptional regulators of genes that encode membrane-bound transporters that mediate metal ion uptake and efflux from the cytosol, and to a lesser degree, genes that encode intracellular chelators, *e.g.*, metallothioneins, and, in the case of Hg and As, metal detoxification enzymes (Figure 1) (*34-36*). These systems collectively and globally coordinate homeostasis of individual metal ions in the cytosol. Seven major transcriptional regulator families have thus far been structurally and/or functionally characterized in some detail, with new ones (at least three more) emerging from other transcriptional regulator families in which the majority members play no role in metal homeostasis (Figure 2) (*6*).

Figure 2. Structural families of metalloregulatory proteins. For each family, boxes for metals that are known to be sensed are shaded *red* on the abbreviated periodic table, while *green* boxes on the left denote known family members that are known to sense cytosolic oxidative stress. Boxes identifying putative metal sensors and non-metal sensing oxidative stress regulators are shaded *pink* or *yellow*, respectively. The four-letter designations for individual proteins that perform the function listed in the nearby box are given (see text for details). The mechanism of regulation of gene expression is indicated as is the DNA-binding domain that mediates operator-promoter DNA binding. Ribbon representations of selected representative members are shown on the right with individual protomers shaded *red* and *blue* in each case. Structures are from top to bottom: 1) apo *S. aureus* pI258 CadC with structural α5-Zn(II) ions shaded *yellow* (1U2W pdb code) (*37*); 2) *E. coli* Cu(I)-sensor CueR with regulatory Cu(I) ions in *red* (1Q05) (*38*); 3) *M. tuberculosis* Cu(I)-sensor CsoR with regulatory Cu(I) ions shaded *red* (2HH7) (*39*); 4) *S. aureus* BlaI as a model for *Enterococcus* CopY (1SD4) (*40*); 5) TetR-Tc-Mg DNA complex structure as model for *S. pneumonia* SczA (3CDL) (*41*); 6) apo *B. subtilis* PerR with structural Zn(II) ions in *yellow* (2FE3) (*42*); 7) *B. subtilis* MntR with Mn_A/Mn_C binuclear cluster ions in *green* (2F5F) (*43*); 8) Ni(II)-bound *E. coli* NikR-*nik* operator DNA complex with high affinity Ni(II) ions shown in *green* and regulatory K^+ ions in *purple* (2HZV) (*44*); 9) *B. subtilis* OhrR-DNA complex (1Z9C) (*45*); 10) Molybdate sensor ModE with molybdate shaded *green* (1O71) (*46*).

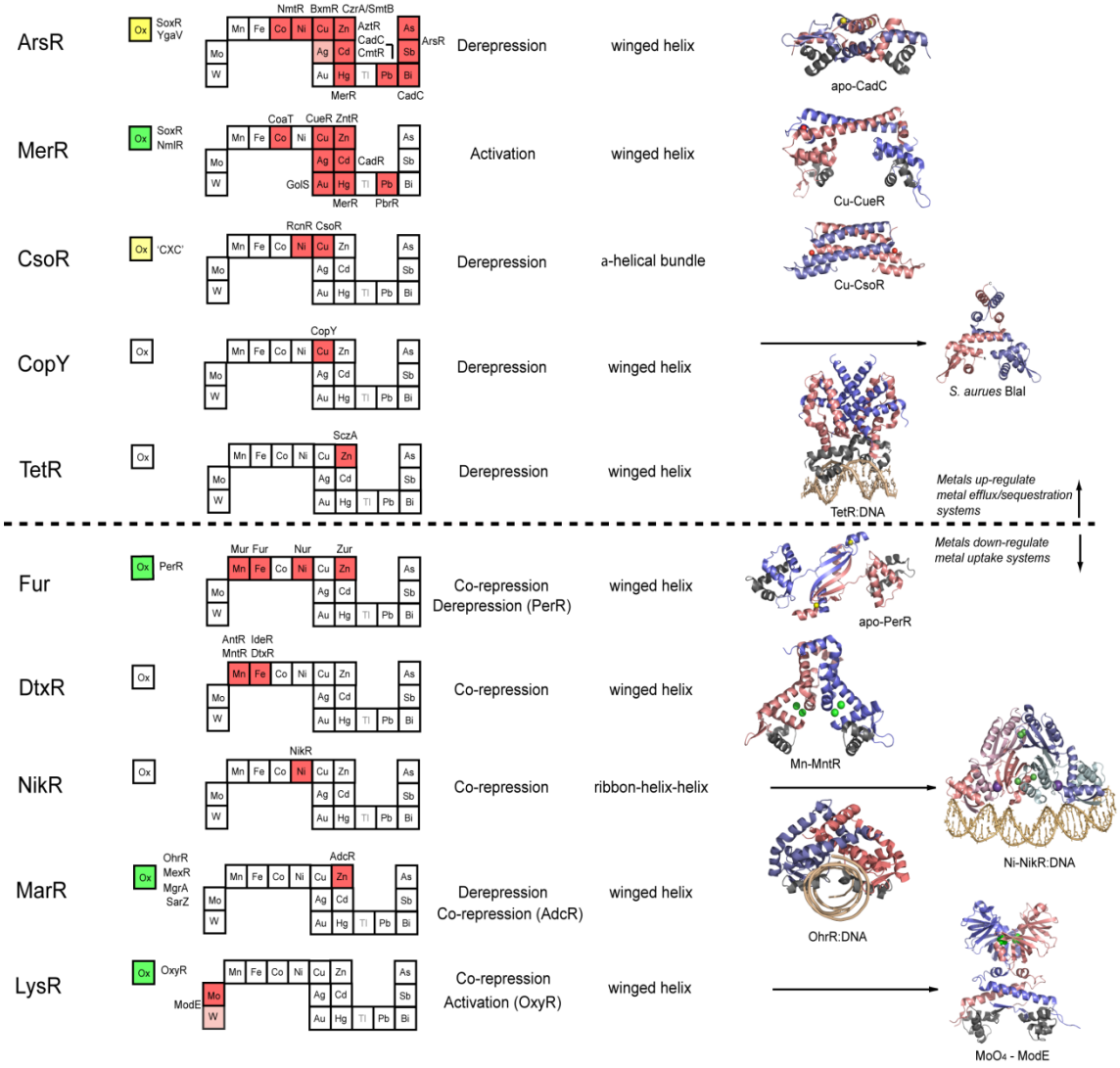
ArsR
NmtR BxmR CzrA/SmtB
SoxR YgaV
Ox
AztR
CadC
CmtR
ArsR
MerR
CadC
Derepression
winged helix
apo-CadC
MerR
SoxR NmlR
CoaT CueR ZntR
CadR
GolS
MerR
PbrR
Activation
winged helix
Cu-CueR
CsoR
RcnR CsoR
'CXC'
Derepression
a-helical bundle
Cu-CsoR
CopY
CopY
Derepression
winged helix
S. aurues BlaI
TetR
SczA
Derepression
winged helix
TetR:DNA
Metals up-regulate metal efflux/sequestration systems
Metals down-regulate metal uptake systems
Fur
Mur Fur Nur Zur
PerR
Co-repression
Derepression (PerR)
winged helix
apo-PerR
DtxR
AntR IdeR MntR DtxR
Co-repression
winged helix
Mn-MntR
NikR
NikR
Co-repression
ribbon-helix-helix
Ni-NikR:DNA
MarR
OhrR MexR MgrA SarZ
AdcR
Derepression
Co-repression (AdcR)
winged helix
OhrR:DNA
LysR
OxyR
ModE
Co-repression
Activation (OxyR)
winged helix
MoO4 - ModE

Transcriptional regulators from different sensor families sometimes regulate the expression of genes with identical functions in different organisms, consistent with a "mix-and-match" approach for the evolution of metal sensing operons or regulons in a particular organism, perhaps aided by horizontal gene transfer and subsequent convergent evolution (*47*). For example, individual members of a set of Cu(I)-specific effluxing P-type ATPases that share high pairwise sequence similarity are regulated by CsoR in *M. tuberculosis,* CueR (a MerR family member) in *E. coli* and CopY in *E. hirae,* each of which are characterized by distinct mechanisms of metalloregulation of transcription (Figure 2) *(39, 48, 49)*. Even in the same organism, *E. coli*, the transcription of functionally orthologous metal uptake transporters, *e.g.,* ABC transporters specific for Ni(II) and Zn(II), are regulated by metal sensor proteins from distinct structural families, which are NikR and Zur (a Fur family member), respectively (*50, 51*). The functional equivalent of Zur from gram-negative proteobacteria is hypothesized to be a MarR family member AdcR in at least some gram-positive organisms (Figure 2).

ArsR/SmtB and MerR proteins, as two most extensively studied families of metalloregulatory proteins, will be discussed in detail here in order to summarize common features and outstanding questions regarding the mechanism of metal sensing in the cell. CopY, as the only other known family of Cu-sensors in prokaryotes, will also be briefly described. From this discussion, an understanding of metal specificity and mechanisms of metal-dependent allosteric regulation of DNA binding allows us to place our studies of the new CsoR family proteins in context. It should be pointed out that the

molecular details by which an individual metalloregulatory protein selectively responds to one or a small overlapping subset of metal ions remain elusive, due in part to limited number of high resolution structures of each functionally relevant "allosteric" state within any regulating systems (*6*).

ArsR/SmtB FAMILY OF TRANSCRIPTIONAL REPRESSORS

The ArsR/SmtB (ArsR) family is the most extensively studied and likely the largest and most functionally diverse metalloregulatory protein family known to date (*52, 53*). This family of proteins is named for its founding members, the *E. coli* plasmid R773 As(III)/Sb(III) sensor ArsR and the *Synechococcus* PCC 7942 Zn(II) sensor SmtB (*54, 55*). Many bacterial genomes across virtually every bacterial taxonomy encode at least one ArsR-family regulator as annotated by the NCBI Cluster of Orthologous Groups (COG0640) and the number of unique ArsR/SmtB-encoding genes is conservatively in excess of 500 (*53*). Notably, the Actinobacteria *Mycobacterium tuberculosis* and *Streptomyces coelicolor* appear to encode ten and thirteen ArsR/SmtB proteins, respectively, the majority of which have not yet been functionally or structurally characterized. Detailed comparative studies of ArsR/SmtB sensors therefore provides an excellent opportunity to investigate how nature employs the same protein fold to create proteins with distinct or orthologous functions (*56, 57*).

The ArsR/SmtB family includes proteins responsible for sensing a wide variety of metal ions, ranging from essential metal ions Zn(II), Cu(I) and Ni(II), to toxic metal pollutants such as As(III), Cd(II) and Pb(II) (Figure 2). Genes regulated by ArsR/SmtB

family proteins are usually responsible for effluxing, scavenging, or detoxifying excess metal ions found in the cytosol. As transcriptional repressors, apo ArsR/SmtB proteins bind to a DNA operator which physically overlaps the promoter where they repress transcription of downstream genes. Metal binding induces a low affinity conformation that mediates dissociation from the DNA and thus drives transcriptional derepression. One striking aspect of ArsR/SmtB family proteins is that diverse metal ion binding sites have evolved at structurally distinct places on what is likely the same protein fold. These have been designated α3N/α3 (or metal site 1 in *S. aureus* pI258 CadC), α4C (as in *M. tuberculosis* CmtR) and α5 (or site 2 in *S. aureus* pI258 CadC), α5C and α5-3 (Figure 3). This nomenclature derives from the secondary structural element, *e.g.*, the α3 helix, or the N- or C-terminal "tail" region, that are known, or projected on the basis of mutagenesis experiments, to provide ligand donor atoms to the metal ion in each case. These metal coordinating residues are also highlighted on a multiple sequence alignment of representative ArsR-family sensors discussed here (Figure 4) (*47, 52, 53, 56*). The α3/α3N and α4C metal binding sites nearly exclusively utilize cysteine residues to coordinate metal ions, and as a result, thiophilic or "soft", highly polarizable, metals such as Cd(II), Pb(II) and As(III) bind here (Figure 3-4). In three cases where Zn(II) is known to bind to the α3N sites to carry out regulation in the cell, *e.g.*, in the cyanobacterial Zn(II) sensors *Anabaena* AztR, *O. brevis* BxmR, and *Synechocystis* ZiaR, a His residue replaces one of the Cys to create a S_3N donor set, distinct from the S_3 [Pb(II)] and S_4 [Cd(II)] donor sites of the related Cd(II)/Pb(II) sensor, *S. aureus* CadC (*58-63*).

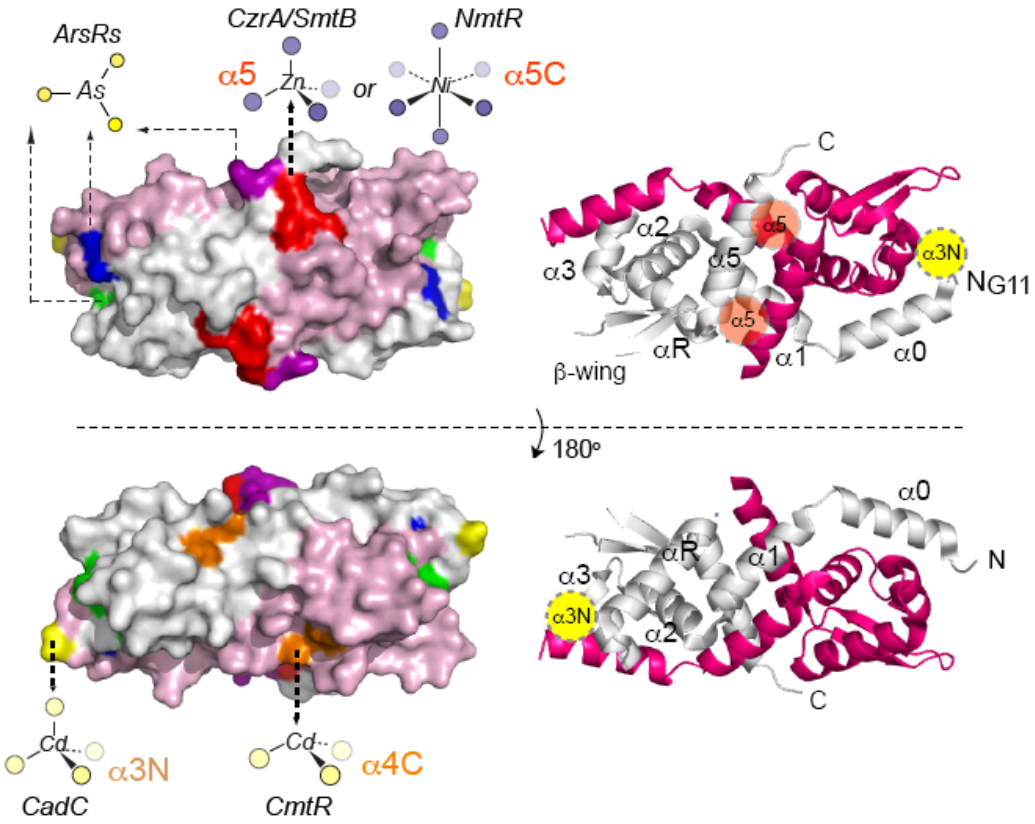

Figure 3. Summary of the known metal binding sites of ArsR/SmtB family repressors on the structure of *S. aureus* pI258 CadC homodimer.(*37*) *Left*, spacefilling models of two views of CadC adapted from ref. (*64*) with ribbon representations of the same view shown on the *right*. One protomer is shaded *pink* and the other *grey*, with the α-helices labeled consecutively from the N-terminus α0-α5 of the ribbon diagrams (which correspond to α1-α6 in the Ye *et al*. structure), along with schematic locations of the α3N (*yellow*) and α5 (shaded *red*) sensing sites on each view of the dimer (*37*). The approximate locations and schematic renderings of representative coordination complexes of distinct sensing sites are shown on the *left* and correspond to *S. aureus* pI258 CadC (*yellow*, α3N), *E. coli* plasmid R773 ArsR (*green*, α3), *S. aureus* CzrA/*Synechococcus* SmtB and *M. tuberculosis* NmtR (*red*, α5 and α5C, respectively), *M. tuberculosis* CmtR (*orange*, α4C), *C. glutamicum* ArsR1 (*blue*) and *A. ferrooxidans* ArsR (*purple*). The α5-3 metal site characterized in the Ni/Co sensor *M. tuberculosis* KmtR (*53*) is not explicitly shown, but partially overlaps the α5 site. See text for details and Figure 4 for a multiple sequence alignment that highlights these metal sensor sites in the ArsR/SmtB family.

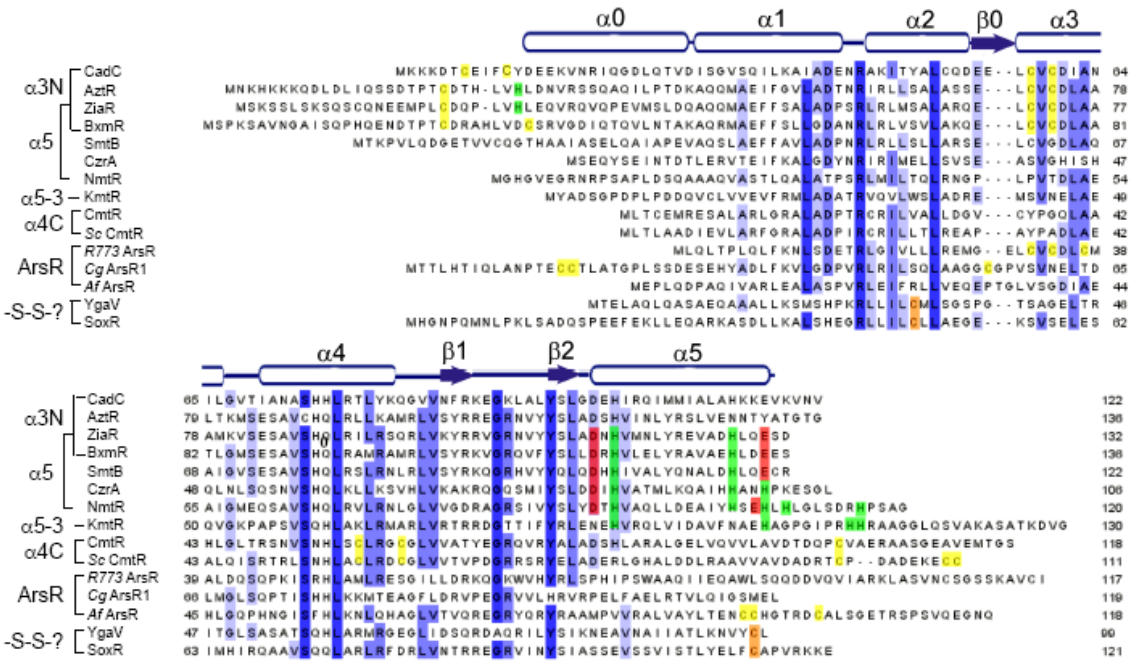

Figure 4. Multiple sequence alignment of ArsR/SmtB family repressors with the secondary structural units of apo-CadC shown (*37*). These secondary structural units align well with those known for *S. aureus* CzrA (*65*) and *Synechococcus* SmtB (*66*). The residues known to coordinate *regulatory* metal ions in each sequence are shaded *yellow* (Cys), *green* (His) or *red* (Asp/Glu) in each sequence, with degree of residue-specific conservation at each position in the alignment indicated by the *blue* shading.

Recent work reveals that As(III)-sensing ArsRs have evolved a range of regulatory binding sites that are structurally distinct from the canonical *E. coli* R773ArsR. This provide significant support for the hypothesis that the ArsR/SmtB family protein matrix is particularly adaptable or evolutionarily "plastic" relative to the nature and number of regulatory metal binding sites (Figure 3-4). This is projected to occur as a result of convergent evolution in response to environmental pressures (*64*). For example, in *Corynebacterium glutamicum* ArsR1, As(III) is coordinated by three cysteine residues in a trigonal S_3 coordination complex at a site distinct from the canonical α3 or α4C sensing sites, in linking two consecutive Cys from the N-terminal α0 helix and single Cys in the opposite protomer just N-terminal to the CVC sequence of *E. coli* R773 ArsRs and *S. aureus* CadC (*64*). Thus, while reminiscent of the S_4 Cd(II) sensing site of CadC, it is clearly structurally distinct, consistent with independent evolution of this metal site (Figure 4).

A recently characterized ArsR/SmtB family repressor, BxmR from the cyanobacterium *O. brevis*, provides an illustration of the evolution of *functional* diversity and redundancy of metal binding sites within a single family member (*60*). BxmR regulates the expression of metallothionein and P-type ATPase in response to both Cu(I)/Ag(I) and Zn(II)/Cd(II), as well as the thiol-specific oxidant diamide, all novel properties (*60, 67, 68*). BxmR, like its closest ortholog, *Synechocystis* ZiaR, retains all the metal binding residues in both the α3N and α5 sites (Figure 4). The α3N site is capable of binding Cd(II), Ag(I) and Cu(I), the latter through formation of a binuclear Cu_2S_4 cluster analogous to that of *E. hirae* CopY, while the α5 site is capable

of binding only Zn(II) with high affinity. Unlike CadC, which binds a structural Zn(II) ion at α5 site with no regulatory function, metal binding to either the α3N or α5 site in BxmR is capable of negatively regulating operator DNA binding in vitro (*37, 61*). Strikingly, however, the functional metal specificity profile of each site differs. The cysteine-rich α3N site adopts a range of coordination structures that mediate metalloregulation of DNA binding by all metals that induce gene expression in the cell, Cd(II), Zn(II), Ag(I) and Cu(I); in contrast, the α5 site is capable of driving only Zn(II) regulation (*60*). Thus, BxmR exhibits the novel property of possessing a relaxed metal response, and has retained a functional redundancy in the ability to sense Zn(II). The biological significance of these findings is not yet known.

The C-terminal α5 helical region of ArsR/SmtB family repressors has also been subjected to evolutionary modification in a way that changes the metal specificity of a particular sensor. For example, the canonical α5 sensing site, first structurally characterized in the zinc sensors *Synechococcus* SmtB and *S. aureus* CzrA adopts an evolutionarily conserved tetrahedral N_2O_2 or N_3O coordination geometry, respectively (*66, 69, 70*). In contrast, the Ni(II)/Co(II) sensing site of *M. tuberculosis* NmtR forms an octahedral N/O-rich coordination complex that incorporates the same four Zn(II)-site α5 ligands, but adds two additional ligands, thought to be provided by the C-terminal tail found in NmtR but missing in SmtB/CzrA, to create an *n*=6 complex optimized for Ni(II)/Co(II) sensing (Figure 4) (*70, 71*). Interestingly, KmtR, a second Ni(II)/Co(II) sensor in *M. tuberculosis* that functions independently of NmtR, may also form an octahedral histidine-rich coordination site for Ni(II) and Co(II), but with a different set

of ligating residues relative to NmtR, in a metal site designated α5-3 (*53*). Finally, *Af* ArsR forms a trigonal S_3 As(III) coordination site derived from consecutive Cys that align with the C-terminus of the α5 helix, and a third more C-terminal Cys (Figure 3-4) (*72*).

Several metal-free (apo) and metal-bound ArsR/SmtB repressor structures have been solved for individual members of this large protein family by x-ray crystallography or NMR spectroscopy. These include crystallographic structures of the apo- and Zn(II)-bound α5 Zn(II)/Co(II) sensor *Synechococcus* SmtB, the apo- and Zn(II)-bound α5 Zn(II)/Co(II) sensor *S. aureus* CzrA, the apo-structure of α3N Cd(II)/Pb(II) sensor *S. aureus* CadC, as well as a solution structure for Cd(II)-bound α4C Cd(II)/Pb(II) sensor *M. tuberculosis* CmtR (*37, 66, 73*). As shown on the structure of a representative ArsR/SmtB repressor, *S. aureus* pI258 CadC, all ArsR/SmtB proteins are dimeric and possess a similar fold with a winged helix-turn-helix motif (α3-turn-αR) used for DNA binding (*37*). Remarkably, the structures of CadC and *Synechococcus* SmtB can be described as "flat" or "open" molecules, with the winged helical domain an integral part of the dimer, the primary interface of which is formed by the N-terminal α1 and C-terminal α5 helices; in CadC, the N-terminal α0 helix also packs against the winged helix domain. In other metal sensor families, the winged helix domain constitutes a folded subdomain within the molecule.

Our understanding of the molecular basis of allosteric negative regulation of operator DNA binding in ArsR/SmtB family repressors remains confined to Zn(II)-sensing α5 family sensors. Crystallographic structures of the apo- and Zn(II)-bound

forms of SmtB and CzrA along with solution NMR studies suggest a quaternary structural switching model for allosteric regulation (*66*). This model involves a hydrogen bonding network formed upon metal binding, which connects the metal binding α5 helix and the DNA binding domain. The hydrogen bonding network is proposed to drive a quaternary structural change upon metal binding, resulting in a "closed" conformation with poor DNA binding affinity (*66*). Although it has been proposed that this hydrogen bonding pathway substantially contributes to the large observed coupling free energy ΔG_c of ≈ +6 kcal/mol, the origin of the driving force for this allosteric switch remains unclear (*70, 74*). Recent dynamics and thermodynamics studies provide additional details into this aspect (*65, 74*). Our recent NMR determination of the solution structure of CzrA in the DNA-bound state reveals a model by which Zn(II) binding results in a large conformational change that drives CzrA off the DNA operator (*65*).

Although most ArsR/SmtB family proteins are proposed to be metalloregulatory repressors, some family members have been reported to regulate genes involved in other cellular processes. For example, *Vibrio cholerae* HlyU regulates the expression of the hemolysin gene *HlyA,* and its homolog has been proposed to function as a master transcriptional regulator for virulence in *Vibrio vulnificus* (*75*). *Pseudaminobacter salicylatoxidans* KCT001 SoxR is the regulator of a cluster of genes required for sulfur oxidation, which is induced by reduced sulfur compounds, *e.g.*, thiosulfate, in the chemolithotrophic α-proteobacteria (*76*). *Xylella fastidiosa* BigR regulates the transcription of genes related to biofilm formation, while *E. coli* YgaV represses the expression of the *ygaVP* operon encoding a membrane-associated protein YgaP that

displays a sulfur transferase (rhodanese) activity (*77*). Each of these proteins are predicted to be ArsR/SmtB family repressors with a similar fold but lack all of the known metal binding sites thus far characterized; each contains two conserved Cys, however, that are predicted to be close to another in the tertiary structure to perform cysteine disulfide or persulfide chemistry (Figure 4).

MerR FAMILY OF TRANSCRIPTIONAL ACTIVATORS

The mercuric ion resistance regulator, MerR, first studied in transposons Tn501 from *P. aeruginosa* and Tn21 from *Shigella flexneri* R100 plasmid, is the prototype metalloregulatory protein, upon which the word "metalloregulatory" was originally coined (*35, 78, 79*). The Hg(II) sensor MerR is now known to be the founding member of a large class MerR family regulators (COG0789) that function as transcriptional activators of the expression of genes required for metal efflux or detoxification, or in some cases, defense against oxidative stress and drug resistance (*80-82*). MerR proteins collectively possess very similar N-terminal winged helical domains comprised of a helix-turn-helix-β-hairpin structure, followed by a long dimerization helix, but quite divergent C-terminal effector binding domains. The structural diversity in the C-terminal region makes it possible for individual MerR family proteins to sense not only various metal ions, including Zn(II) by ZntR, Cu(I) by CueR, Hg(II) by MerR, Au(I) by GolS, Cd(II) by CadR and Pb(II) by PbrR, but also oxidative stress by SoxR via an [2Fe-2S] cluster, and small molecule drugs in the case of BmrR and MtaN (*38, 83-89*).

Insights into the coordination chemistry of MerR regulators was first determined in MerR itself by ^{199}Hg NMR spectroscopy and site-directed mutagenesis experiments to adopt a subunit-bridging trigonal planar Hg(II) coordination site formed by three cysteine residues (Figure 5) (*90, 91*). In striking contrast to ArsR/SmtB family repressors which have evolved an impressive panel of regulatory metal binding sites at distinct locations on the protein scaffold (see Figure 3) as a means to evolve metal selectivity, the metal binding sites in individual MerR family proteins are all composed of residues derived from two symmetry-related metal binding loops at the periphery of the dimer, positioned just C-terminal to the long dimerization helix, which itself is followed by a short C-terminal helix. This single metal binding site region in MerR proteins has evolved to sense a wide range of divalent as well as monovalent metal ions, each of which is characterized by a signature disposition of metal ligands (Cys/His), in the metal binding loop and elsewhere (*38, 82*). A comparison between Cu(I)-bound *E. coli* CueR and Zn(II)-bound *E. coli* ZntR structures reveals several key determinants for metal specificity of monovalent metal ions (CueR) over divalent metal ions (ZntR). Change in the coordination number, charge neutralization and hydrogen bonding interactions all play important roles in specific metal binding (Figure 5) (*38, 90*). On the other hand, the amino acids in the metal binding loop have shown to be crucial to distinguish between similar monovalent metal ions, such as Cu(I) vs. Au(I), in the case of *Salmonella* GolS and *R. metallidurans* CupR (*85, 92*).

MerR family proteins are unique in the mechanism of transcription activation among all the metalloregulatory proteins (*81*). The DNA sequences MerR proteins

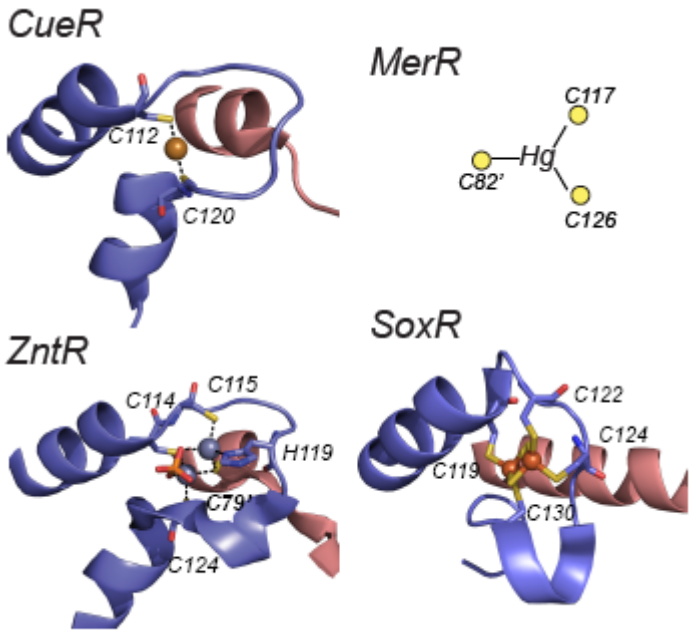

Figure 5. Ribbon representations of the metal binding loops of various MerR family metalloregulators. In all cases, only one of the two symmetry-related metal sites are shown with one protomer is shaded *blue* and the other *red*; annotated metal donor ligands shown in *stick*. The structures shown are the Cu(I) bound form of *E. coli* CueR(*38*), the $Zn(II)_2$ sulfate anion (shown in *red/orange*)-bridged binuclear structure of *E. coli* ZntR (*38*), and the $[2Fe\text{-}2S]^{2+}$ center of *E. coli* SoxR (*93*). A schematic of the single subunit-bridging Hg(II) site of Tn501 MerR consistent with spectroscopic and functional data but of unknown structure is also shown for comparison (*90, 91*).

apo recognize have one common feature, that is a long 19- or 20-bp spacer between the -35 and -10 promoter elements, which results in poor RNA polymerase binding affinity and transcription initiation efficiency (*94*). As originally determined for MerR itself, both theand effector-bound forms are capable of binding to their cognate operator DNA sequences with similar affinities (*95*). However, only the effector-bound form can significantly unwind and distort the DNA helix, bringing the -35 and -10 elements into the same side of the DNA helix in a position optimized for RNA polymerase binding and ultimately transcriptional activation (*94*). Thus, both RNA polymerase and the effector-bound MerR family member are predicted to bind to the promoter simultaneously. This mechanism of allosteric modulation of the DNA structure was first documented at high resolution by the crystallographic structure of a multidrug efflux regulator *B. subtilis* BmrR bound to a small lipophilic drug, tetraphenylphosphonium (TPP), in complex with its cognate 22-base pair DNA operator; this was followed by several other multidrug transporter regulator-DNA complex structures (*88*). Unfortunately, there is as yet no high resolution structure for any MerR family *metal sensor* in complex with DNA. However, the recently published structure of the oxidative stress sensor *E. coli* SoxR-DNA complex sheds considerable light on this. SoxR contains an oxidized $[2Fe\text{-}2S]^{2+}$ cluster coordinated by four cysteines from the metal binding loop (Cys119, Cys122, C124 and Cys130) that is analogous to that found in metal sensing MerR proteins (Figure 5) .

The activated, oxidized $[2Fe\text{-}2S]^{2+}$ form of SoxR bound to DNA uncovers at high resolution what may be a general structural mechanism of activation from a 20-bp spacer

promoter. A 20-bp spacer is most commonly found in the cognate operator-promoter sequences for many metal ion sensors in the MerR family, including MerR, ZntR and CueR (*93*). This structure is distinct from the previously reported BmrR-DNA and MtaN-DNA complexes, each of which is characterized by a 19-bp spacer in the promoter (*88*). In the SoxR-DNA structure, the long dimerization helix (α5) exhibits the largest differences relative to the drug-BmrR-DNA structures, in that it is twisted into a unique position relative to BmrR and is stabilized by hydrophobic interactions. The DNA in the complex is also more significantly bent (≈65^{o}) than that in BmrR- and MtaN-DNA complexes (≈47~50^{o}) (Figure 6A), resulting in further shortening of ≈3.4 Å, which compensates for the additional 1-bp spacer in the DNA relative to the 19-bp spacer DNA for the BmrR and MtaN complexes. Furthermore, signal transduction between the sensing domain and the DNA-binding domain is proposed to be mediated by direct interactions between the two domains (Figure 6B and C) (*93*). An analogous set of interactions are also found in the recent drug bound BmrR-DNA complex to be crucial for transcription activation, and may well be common to all MerR family regulators (*96*).

CopY FAMILY OF Cu-SENSORS

CopY represents a small family of copper-specific metalloregulatory proteins restricted largely to the Firmicutes, and was first characterized in *Enterococcus hirae* (*39, 49*). It is proposed to be a member of MecI/BlaI family of repressors associated with antibiotic resistance due to the high sequence similarity in the N-terminal DNA binding

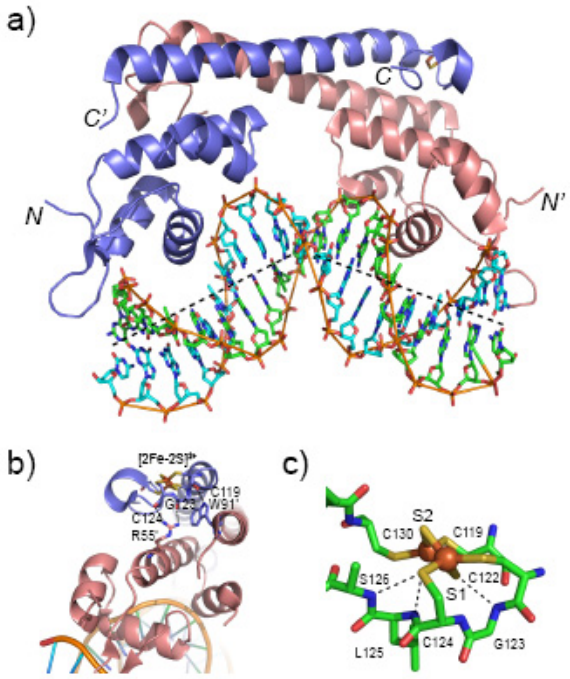

Figure 6. Crystallographic structure of the oxidized (activated) *E. coli* SoxR-DNA complex (*93*). (A) Overall view of the structure of SoxR-DNA complex showing a significant bend (~65^{o}) in the *sox* operator DNA. The DNA strands are colored *green* and *cyan* and shown in *stick* representation; the two protomers of the SoxR homodimer are shown as ribbon structures, and shaded as in Figure 5. (B) Intersubunit hydrogen bonding interactions that link main chain carbonyl oxygen atoms from G123 and C124 in the metal binding loop that coordinates the $[2Fe\text{-}2S]^{2+}$ cluster with the side chain of R55' from the DNA binding domain of the opposite protomer. A main chain-side chain hydrogen bond between C119 and W91' from the dimerization helix of the opposite protomer is also shown. (C) A close-up view of the $[2Fe\text{-}2S]^{2+}$ cluster revealing how electrostatic interactions around the bridging S^{2-} anion S1 may facilitate the conformational change upon reversible reduction/oxidation of the cluster (*93*).

domain and the fact that CopY and MecI/BlaI recognize identical cognate DNA sequences (*97*). *E. hirae* CopY regulates the transcription of the *copYZBA* operon which encodes two copper-specific P-type ATPases (CopA and CopB) thought to be involvedin copper uptake and efflux, respectively, and the copper chaperone CopZ. It has been shown that Zn(II)-bound CopY binds to the operator-promoter region of the *copYZBA* operon and represses the transcription; Cu(I)-bound CopZ then transfers Cu(I) to Zn(II)-bound CopY, forming Cu(I)-CopY which dissociates from the DNA and leads to transcriptional derepression of the operon (*98*). Nearly all CopYs possess a conserved **C**X**C**XXXX**C**X**C** motif close to the C-terminus. Spectroscopic studies suggested that each CopY protomer within the dimer is capable of binding 2 equivalents of Cu(I) per monomer to form a highly luminescent binuclear S_4Cu_2 cluster exactly analogous to Cu(I) formed by the ArsR/SmtB family regulator BxmR (*60, 98*). The degree to which this mechanistic scenario characterizes other CopYs has not yet been tested.

Recent functional and structural studies of the CopY family Cu-sensor *Lactococcus lactis IL1403* CopR provides new insights into the CopR regulon as well as high resolution structure of the N-terminal winged helix DNA binding domain (*23, 99*). Expression profiling experiments reveal that the CopR regulon consists, as expected, of Cu-homeostasis related genes including *copB* and the *copRZA* operon, but also genes related to oxidative stress resistance, *e.g.,* lactate oxidase (*lctO*), nitroreductase (*ytjD*) and glyoxalase I (*yaiA*) (*23*). Similar findings characterize *M. tuberculosis* and are all consistent with the physiological scenario in which excess Cu(I) may be capable of engaging in redox cycling and generation of reactive oxygen species either directly by

Fenton chemistry or indirectly by damaging iron-sulfur cluster which may further lead to Fe-mediated oxidative stress (*22, 24, 100*). The solution structure of the CopR N-terminal DNA binding domain monomer reveals, as anticipated, a winged helix-turn-helix domain similar to the N-terminal domain of *S. aureus* MecI and BlaI, the regulators of the genes encoding the penicillin binding protein and β-lactamase, whose crystal structures with and without DNA bound have been previously reported (*40, 99*). Further biophysical and structural characterization of the C-terminal Cu(I) binding domain in the context of the intact homodimeric repressor, however, will be required to fully understand how Cu(I) is capable of mediating an allosteric or regulatory response upon DNA binding, while Zn(II) is not.

CsoR/RcnR FAMILY

Unlike other Cu(I) sensors such as *E. coli* CueR and *E. hirae* CopY which are largely confined to the Proteobacteria and Firmicutes, respectively, genes encoding CsoRs are widely distributed through most other major bacterial species (*39*). As the founding member, *M. tuberculosis* CsoR (*Mtb* CsoR) has been characterized using biological, biophysical and structural methods. CsoR is the transcriptional repressor for the *cso* (Cu-sensitive operon) which encodes CsoR itself, a gene of unknown function but limited to mycobacteria (*rv0968* in *Mtb*), and a Cu(I)-effluxing P-type ATPase CtpV (Figure 7). Apo-CsoR binds to the operator-promoter region upstream of the *csoR* gene, with the addition of Cu(I), but not other divalent metals, resulting in derepression of transcription. Physiological Cu(I) stress induces the expression of a relatively small

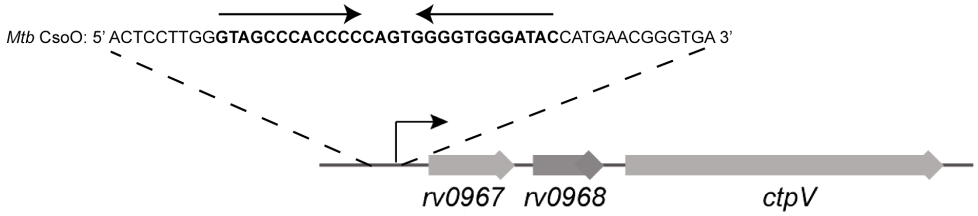

Figure 7. Genetic organization of the *Mtb* copper-sensitive operon (*cso*) with the CsoO sequence in bold.

number of genes in *M. tuberculosis*, and it is not known as yet how many of these are regulated by CsoR (*22*). It is also not known as yet if the expression of a recently characterized Cu(I)-binding metallothionein MymT is regulated by CsoR (*17*).

The 2.6 Å crystallographic structure of Cu(I)-bound CsoR reveals a homodimeric structure with a core antiparallel four-helix bundle (α1, α1', α2, α2') and the short C-terminal α3 helix stacked against the base of the molecule, proximate to α2' helix of the opposite protomer (Figure 8). The Cu(I) ion is coordinated to an intersubunit metal binding site formed by two conserved cysteines (Cys36 and Cys65') and one conserved histidine (His61') (Figure 9) (*39*). Due to the lack of a classical DNA binding motif such as winged helix-turn-helix domain commonly found in other metalloregulatory proteins, how apo-CsoR binds to the cognate DNA operator remains unclear, as well as the mechanism by which Cu(I) binding induces allosteric negative regulation of operator DNA binding.

E. coli RcnR is a Co(II)/Ni(II) sensor that regulates the expression of a nickel and cobalt efflux protein RcnA (*101*). RcnA is proposed to be a member of the major facilitator superfamily (MFS) family of membrane permeases that are unrelated to NiCoT permeases (*102*). Although RcnR shares low sequence similarity with CsoR, it is predicted to be an all α-helical protein with a fold similar to that of CsoR; thus, RcnR and CsoR are considered to be distantly related orthologs that represent two major subfamilies in this new metalloregulatory protein family (*103*). Unlike Cu(I)-sensing CsoRs, RcnRs possess a His-Cys-His-His W-X-Y-Z metal binding fingerprint (Figure 10); recent Ni(II) and Co(II) binding experiments coupled with characterization by

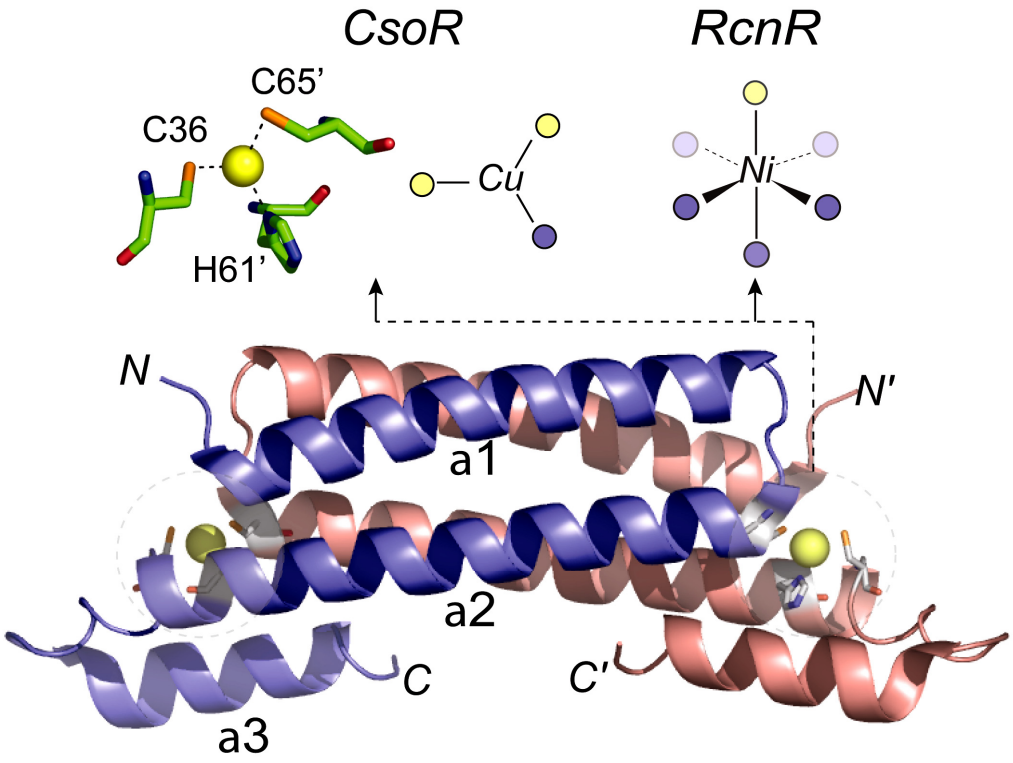

Figure 8. Ribbon representation of the 2.6 Å crystallographic structure of the Cu(I)-bound *M. tuberculosis* CsoR homodimer (*39*). The crystallographically defined structure of the Cu(I) coordination complex is shown in stick representation, while schematic representations of Cu(I) and Ni(II) complexed of CsoR and *E. coli* RcnR (*103*), respectively, are also shown. Cys sulfur ligands are shaded *yellow* while N/O ligands are given by the *blue* spheres. The α-helices of the blue protomer in CsoR are labeled α1-α3.

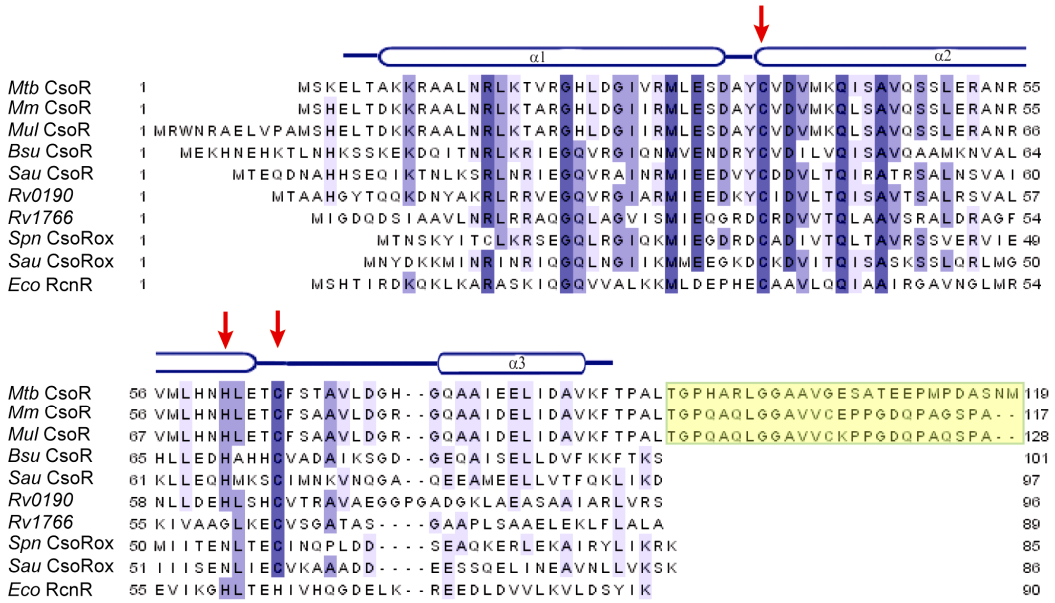

Figure 9. Multiple sequence alignment of CsoR/RcnR family proteins. Organisms and (locus tags) for the other entries are as follows: *M. tuberculosis* (Rv0967, Rv0190 and Rv1766), *M. marinum* (MM4874), *M. ulceran* (MUL0425), *B. subtilis* (BSU33520), *S. aureus* (NWMN1991and an unannotated ORF encoded by the complementary strand of 37974-38234), *S. pneumoniae* (SPD0073) and *E. coli* RcnR (b2015). The three conserved Cu(I) ligands in Cu-sensing CsoRs are indicated by the red arrows. The C-terminal tails in several pathogenic mycobacterial species are highlighted in yellow. Secondary structure is annotated based on the crystal structure of Cu(I) bound *Mtb* CsoR (*39*).

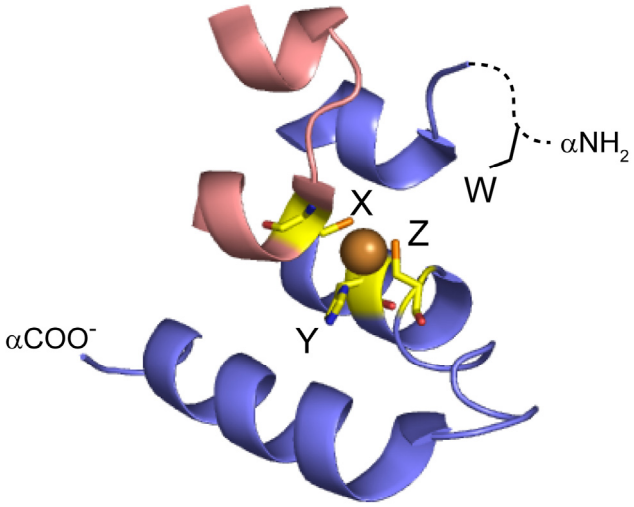

Fingerprint:	W-X-Y-Z
Cu(I) CsoR:	x-**C**-**H**-**C**
Ni(II) RcnR:	**H**-**C**-**H**-**H**
Redox (?):	x-**C**-x-**C**
FrmR (redox):	x-**C**-**H**-x

Figure 10. A schematic representation of the W-X-Y-Z "fingerprint" of individual CsoR/RcnR family repressors. The X-Y-Z region of the fingerprint is defined by the ligands to the Cu(I) ion in Cu(I)-sensing CsoRs, corresponding to C36, H61' and C65' in opposite protomers of *M. tuberculosis* CsoR (shaded *red* and *blue*, respectively) (*39*). W corresponds to H3 in *E. coli* RcnR which must occupy the third position relative to the Met1 αNH_2 group (*103*). The invariant Cys in the X position is shaded *red*.

electronic and x-ray absorption spectroscopies reveal that RcnR binds both Ni(II) and Co(II) with a 6-coordinate octahedral geometry, clearly distinct from that of the Cu(I)-CsoR complex (Figure 8). Although the Ni(II) and Co(II) coordination spheres may differ slightly, they both include all four of the signature residues conserved in CsoR/RcnR-like proteins, with a fifth ligand thought to be donated from the α-amino group at the N-terminus which would be in close proximity. The identity of the sixth ligand remains unknown, with the possible recruitment of a backbone amide or a solvent molecule into the first coordination shell (*103*). The obvious differences between coordination geometries of Cu(I)-bound CsoR and Ni(II)-bound RcnR reinforce the notion that coordination geometry controls metal selectivity, with a higher coordination number far more favorable for Ni(II) and Co(II), relative to Cu(I).

In a striking parallel with ArsR/SmtB α5-site sensors as well as MerR family sensors, a comparison of CsoR and RcnR illustrates the degree to which metal sites with distinct selectivities can be evolved from a common "core" of primary coordinating residues, which in this case likely corresponds to the Cys pair across the protomer interface, Cys36 and Cys65' in *M. tuberculosis* CsoR. Metal binding here, or even reversible disulfide bond formation or derivatization of one or both Cys in other CsoR orthologs, might be anticipated to alter the structure of the dimer (or oligomer), which in turn might be necessary, albeit not sufficient in the case of CsoR and RcnR, to drive allosteric negative regulation of DNA binding. The characterization of non-metal ion sensing CsoRs is thus of interest.

An extensive multiple sequence alignment of CsoR/RcnR family proteins (formerly annotated as DUF156; now COG1937) reveals other members with "fingerprint" residues distinct from the x-Cys-His-Cys and His-Cys-His-His W-X-Y-Z residues of CsoR and RcnR, respectively (Figure 9-10) (*39, 103*). These putative CsoR homologs are proposed to be involved in some way in oxidative stress sensing or antibiotic resistance, based solely on the immediate genomic neighborhood (Figure 10); there is no evidence as yet that these CsoRs actually bind DNA, although this seems likely (*103*). Inspection of the structure of *M. tuberculosis* CsoR reveals that these two conserved cysteine residues in an x-Cys-x-Cys CsoR are predicted to be in close proximity, which makes it possible for these residues to undergo reversible disulfide bond formation as a result of oxidative stress. Such a mechanism has been shown to be operative in other antibiotic and redox sensing repressors, as exemplified by the MarR family member *Pseudomonas aeruginosa* MexR (*104*). However, to qualify as a cytosolic redox sensor, the reduction potential of this cysteine pair must be tuned in a way that tracks with changes in that potential that occur under conditions of oxidative stress. Therefore, both functional biological and biochemical studies will be required to understand this non-metal-sensing subgroup of this newly discovered metalloregulatory protein family (see Chapter VI) (*39*).

SCOPE OF THE RESEARCH

Extensive studies on the ArsR/SmtB and MerR families of metalloregulatory proteins summarized above reveal common features and unresolved issues regarding

how these metal sensor proteins specifically respond to a particular metal ion. In order to gain further insights into the CsoR/RcnR family of metalloregulatory proteins, this dissertation focuses on understanding common features of the Cu(I)-sensing subgroup of this new protein family. Three CsoR family members, including the founding member *M. tuberculosis* CsoR (*Mtb* CsoR) (*39*), *B. subtilis* CsoR (*Bsu* CsoR) (*105*) and a predicted CsoR from *S. aureus* (*Sau* CsoR), are characterized in Chapters II, IV and V, respectively. General biochemical and biophysical properties including metal binding and DNA binding of these CsoRs are presented as are insights into the structural mechanism of Cu(I)-mediated negative allosteric regulation of DNA binding (Chapter III). Conventional mutagenesis approaches have been combined with a native chemical ligation strategy to specifically incorporate an unnatural amino acid analog into *Mtb* CsoR in order to explore the underlying molecular details of the regulation. A parallel strategy has also been applied to CzrA, a SmtB/ArsR family Zn(II)-sensing transcriptional repressor with the findings consistent with a common mechanism of metal-dependent allosteric regulation involving the $N^{\varepsilon 2}$ face of metal coordinated histidine.

CHAPTER II

BIOCHEMICAL PROPERTIES OF *M. tuberculosis* CsoR

INTRODUCTION

As the founding member of the new family of Cu-sensing transcriptional repressors, *M. tuberculosis* CsoR (*Mtb* CsoR) was first shown to regulate the transcription of an operon encoding CsoR itself, a small protein of unknown function and a P-type ATPase for Cu effluxing (Figure 7) (*39*). Apo-CsoR represses the transcription by binding to an operator (denoted *Mtb* CsoO) in the operator-promoter region upstream of the *csoR* gene. Cu(I) binding to CsoR causes dissociation of the protein-DNA complex and leads to derepression of transcription(*39*).

The crystal structure of Cu(I)-bound *Mtb* CsoR solved at 2.6 Å reveals a homodimeric α-helical protein. Each protomer consists of two long helices (α1, α2) and one short helix (α3) in which α1, α1', α2 and α2' form a four-helix bundle stabilized by several conserved salt bridges between α1and α1' (Figure 8) (*39*). The Cu(I) ion is bound at two symmetry-related intersubunit sites via Cys36, His61' and Cys65'. However, there are no classical DNA binding motifs found in the structure and it is therefore not yet known how *Mtb* CsoR binds DNA. *Mtb* CsoR is also different from many other predicted or known Cu-sensing CsoR homologs in that it has a long C-terminal tail (~30 amino acids) which is not present in the crystal structure, possibly due to its flexible nature. This C-terminal tail is only found in several CsoR homologs in pathogenic mycobacterial species and its function remains unknown.

In this chapter, a characterization of the biochemical and biophysical properties of *Mtb* CsoR in solution are presented. Direct Cu(I) titrations in the absence or presence of bathocuproine disulfonate (BCS) reveal that *Mtb* CsoR binds 1 mol equiv Cu(I) ion per monomer with very high affinity (log K_{Cu}= 18.0). X-ray absorption spectroscopy (XAS) followed by site-directed mutagenesis shows Cu(I) is coordinated by Cys36, His61 and Cys65, forming a trigonal planar S_2N complex. Apo-CsoR binds a 50 bp DNA derived from the operator-promoter region (*Mtb* CsoO) with high affinity as determined by fluorescence anisotropy, while the affinity of Cu(I)-bound CsoR decreases significantly. Interestingly, either full deletion (Δ89-119) or partial deletion (Δ99-119) of the C-terminal tail causes a significant decrease in the DNA binding affinity, while deletion of the C-terminal 13 residues (Δ107-119) retains wild-type DNA binding affinity. Finally, substitution of two residues in a positively charged surface patch, Arg15 and Arg55 with Ala, results in undetectable DNA binding by fluorescence anisotropy assay. Based on these observations, further mutagenesis experiments as well as a unnatural amino acid substitution strategy were carried out in order to understand the mechanism of how Cu(I) binding regulates the DNA binding. These experiments are described in Chapter III.

MATERIALS AND METHODS

Plasmid construction, protein overexpression and purification. The *Mtb csoR* gene was amplified from *M. tuberculosis* H37Rv genomic DNA and cloned into the pET3a vector (Novagen, WI) between the NdeI and BamHI restriction sites (*39*). Amino acid

substitutions were introduced by site-directed quick-change mutagenesis. The integrity of resultant plasmids was confirmed by DNA sequencing.

For both wild-type and mutant CsoRs, the expression plasmids were transformed into *E. coli* BL21(DE3). A single colony from the LB plate containing 100 mg/L ampicillin was inoculated into 200 mL LB medium containing 100 mg/L ampicillin and grown overnight in a 37 ^{o}C shaker. 20 mL of the overnight culture was then inoculated into 1 L of the same LB medium and grown at 37 ^{o}C until the OD600 reached 0.6-0.8. 0.4 mM IPTG was then added and cells were grown for additional 2 h before harvesting by low speed centrifugation. Cell pellets were resuspended in 200 mL Buffer A (25 mM MES, 2 mM DTT, 1 mM EDTA, pH 5.8) and lysed by sonication. The lysate was centrifuged and 0.15% (v/v) polyethyleneimine (PEI) was added to the supernatant to precipitate the nucleic acids. *Mtb* CsoR remained in the pellet and was resuspended by washing the pellet with Buffer A containing 0.5 M NaCl overnight. After centrifugation, the supernatant was subjected to $(NH_4)_2SO_4$ precipitation and the pellet was resuspended in Buffer A and dialyzed against Buffer A containing 0.05 M NaCl. The sample was then subjected to purification by cation-exchange chromatography using a sulfoprophyl (SP)-sephadex Fast Flow column with Buffer A using a salt gradient of 0.05 – 0.75 M NaCl. Fractions containing *Mtb* CsoR were combined and concentrated to a final volume of ~3 mL. 1 mL of the resultant protein was then loaded onto a Superdex 200 30/100GL size exclusion column (GE Healthcare, NJ) pre-equilibrated with Buffer A containing 0.4 M NaCl. Fractions containing *Mtb* CsoR were combined and dialyzed against Buffer B (25 mM Tris, 2 mM DTT, 1 mM EDTA, pH 8.0) containing 0.05 M NaCl. The protein

was further purified on a quadramine (Q)-sephadex Fast Flow column with Buffer B using a salt gradient of 0.05 – 0.5 M NaCl. The resultant protein fractions were pooled, concentrated and dialyzed against Buffer S (10 mM HEPES, 0.2 M NaCl, pH 7.0) in an anaerobic Vacuum Atmospheres glovebox (Vacuum Atmospheres, CA). The purity of the final products was estimated by visualization of Coomassie-stained 18% Tris-glycine SDS-PAGE gels to be ≥90%. The protein concentration was determined by amino acid analysis carried out by the Texas A&M University Protein Chemistry Laboratory (PCL) or using a ε_{280}=1615 $M^{-1}cm^{-1}$. The free thiol content was determined by the DTNB (5, 5'-dithiobis-(2-nitrobenzoic acid)) assay to be more than 95% of expected value (*39, 105*). Less than 0.1% copper was detected by atomic absorption spectroscopy in all purified protein samples.

Cu(I) binding and BCS competition monitored by UV-vis absorption spectroscopy. 250 µL aliquots of 20 µM *Mtb* CsoR monomer with or without 50 µM bathocuproine disulfonate (BCS) (Sigma, MO) in buffer S were prepared in an anaerobic glovebox. Different amounts of CuCl (Sigma, MO) were added to each aliquot and the UV-vis absorption spectrum was taken. The copper concentration was determined by atomic absorption spectroscopy. Samples with BCS were equilibrated in the glovebox at ambient temperature (≈22 ^{o}C) for 3 h before recording the spectrum to ensure that equilibrium was reached. Absorption at 240 nm and 483 nm was plotted against total Cu concentration. The Cu(I) binding affinity was determined by fitting the data to a simple competition model using Dynafit (*106*) with the overall affinity constant β_2 for $Cu(I)(BCS)_2$ fixed at $10^{19.8}$ M^{-2} (Figure 11) (Appendix A) (*107*).

Alternatively, 10 to 15 μM CsoRs were mixed with 50, 250 and 500 μM BCS (or BCA) in buffer S anaerobically. 20 μM Cu(I) was then added to the mix in a total volume of 250 μL. The mixtures were incubated at ambient temperature (≈22 ^{o}C) for 3 h before the absorption spectrum of each sample was taken. The $Cu(I)(BCS)_2$ concentration in these samples was determined by comparing the absorbance at 483 nm with 20 μM $Cu(I)(BCS)_2$ complex in the same buffer. The CsoR-Cu(I) affinity constant which assumes identical and independent sites on the CsoR oligomer (K_{Cu}) was then calculated using the following equation (*107, 108*):

$$K_{Cu} = \frac{\beta_2[Cu^{I}CsoR][BCS]^2}{[Cu^{I}(BCS)_2][apoCsoR]}$$

Here $\beta_2=10^{19.8}$ M^{-2} is the overall formation constant of $Cu(I)(BCS)_2$ complex (*107*). The average and standard deviation of the binding constants at three different BCS concentrations is reported. For the similar competition assay with bicinchoninic acid (BCA) (Sigma, MO), $\beta_2=10^{17.2}$ M^{-2} for $Cu(I)(BCA)_2$ complex was used and the formation of this complex was monitored by absorbance at 562 nm (Figure 11) (*109*).

Cu(I) X-ray absorption spectroscopy. Both wild-type and mutant *Mtb* CsoRs were mixed with 0.8 mol equiv of Cu(I) in 10 mM HEPES, 0.2 M NaCl, 30% (v/v) glycerol, pH 7.0 in an anaerobic environment and concentrated to ≈0.5~1.0 mM final protein concentration. Samples were loaded into standard XAS cuvettes or 5-well polycarbonate XAS cuvettes and immediately frozen in liquid N_2. XAS data were collected at Stanford Synchrotron Radiation Lightsource (SSRL) on beamline 9-3 or at the Canadian Light Source (CLS) on the HXMA beamline. EXAFS data analysis was performed using

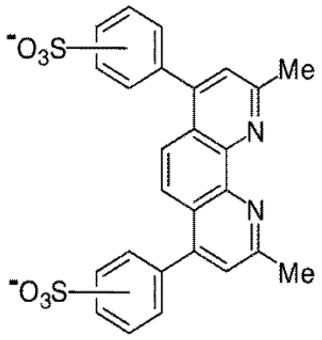

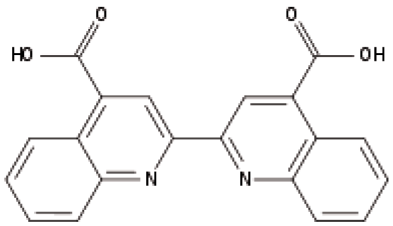

bathocuproine disulfonate (BCS)

β_2=19.8

bicinchoninic acid (BCA)

β_2=17.2

Figure 11. Structures of BCS and BCA used in the competition assay with overall Cu(I) binding constant β_2 for formation of the BCS_2:Cu or BCA_2:Cu complexes at pH 7.0 indicated (*107, 109*).

EXAFSPAK software, using *ab initio* phase and amplitude functions computed with FEFF v7.2, according to standard procedures as described before (*110, 111*).

Fluorescence anisotropy. A 50 bp 5'-fluorescein (FL) labeled DNA (5'-FL-CGACT CCTTGG**GTAGCCCACCCCCAGTGGGGTGGGATAC**CATGAACGGGTG-3') (Operon, AL) containing the 28 bp inverted repeat in bold letters was used (Appendix B) (*39*). The double stranded DNA was made by mixing the labeled strand with 1.1 mol equiv of the unlabeled complementary strand. The mixture was heated at 95 ^{o}C for 10 min and then slowly cooled to room temperature. Formation of double stranded DNA was confirmed by native TBE polyacrylamide gel electrophoresis. A typical anisotropy experiment was carried out with 10 nM DNA in 10 mM HEPES, 0.2 M NaCl, 2 mM DTT, pH 7.0 at 25 ^{o}C unless noted otherwise. To verify the stoichiometry of DNA binding, 10 μM DNA was mixed with different concentrations of *Mtb* CsoR monomer up to 100 μM in the same buffer in room temperature. 100 μL of each mixture was loaded onto a Tricon Superdex 200 column (GE Healthcare, NJ) on an Äkta-10 purifier. Elution profiles were obtained by monitoring the absorption at 220 nm, 260 nm and 280 nm simultaneously.

The anisotropy of the fluorescein fluorescence was monitored by exciting fluorescein at 490 nm (1.0/1.0 slits). With apo- or Cu(I)-bound *Mtb* CsoRs added, the average anisotropy of 5 measurements was reported for each addition. The resulting data were fitted to a stepwise model involving the binding of two non-dissociable tetramers to one DNA using Dynafit assuming a linear change in anisotropy with fractional saturation of the DNA (see Appendix C) (*106, 110*). Since Cu(I)-bound *Mtb* CsoR does

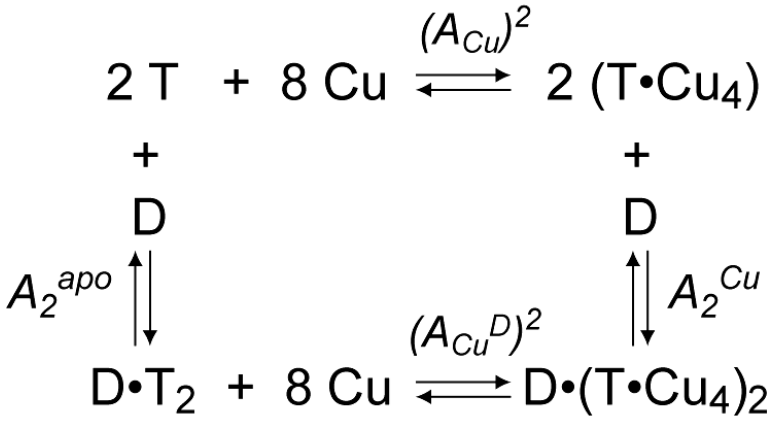

Figure 12. Coupled equilibria of *Mtb* CsoR tetramer (T)-DNA (D) complexes as a function of Cu. $A_{Cu}=K_{Cu}{}^4$, where K_{Cu} is the microscopic binding constant to each protomer. A_{Cu} represents the macroscopic binding constant of four Cu(I) ions bound to a CsoR tetramer. $A_2{}^{apo}$ and $A_2{}^{Cu}$ represent the macroscopic binding constants of two CsoR tetramers binding to one DNA in absence or presence of Cu(I), respectively.

not reach saturation of the DNA under conditions of the experiment, the maximum anisotropy value was fixed to the same value as that measured for apo-*Mtb* CsoR. The coupling free energy, ΔG_c, is operationally defined here by $\Delta G_c = -RT\ln(A_2^{Cu}/A_2^{apo})$, where A_2^{apo} and A_2^{Cu} are the macroscopic DNA binding constants for apo- and Cu(I)-bound CsoRs, respectively (Figure 12).

Circular Dichroism Spectroscopy. For circular dichroism, protein samples were dialyzed against 10 mM sodium phosphate pH 7.0, 0.2 M NaF anaerobically. ~8 μM CsoR monomer was then loaded into a 1 mm pathlength rectangular quartz cuvette. The circular dichroism spectrum for each sample was collected using an Aviv DS62 circular dichroism spectrometer with 3 individual scans from 180–260 nm. The data was converted to mean residue ellipticity [θ_{MRW}] using the equation $[\theta_{MRW}] = \theta/10C_r l$, where θ is the millidegrees as collected by the spectrometer, C_r is the mean residue concentration and l is the pathlength.

RESULTS

Mtb CsoR binds 1 mol equiv Cu(I) per monomer with very high affinity. Direct titration of Cu(I) into wild-type *Mtb* CsoR causes a ligand to metal charge transfer (LMCT) at 240 nm with an $\varepsilon_{240} \approx 12{,}500\ M^{-1}cm^{-1}$. This absorption is saturable upon addition of ~1 mol equiv Cu(I) per monomer and reports on Cys thiolate-Cu(I) coordination (Figure 13A and inset) (*39*). The small increase of absorbance after saturation may be due to slight precipitation of the protein (Figure 13A, inset). In order to further verify the stoichiometry, Cu(I) binding was monitored by tyrosine fluorescence. Interestingly,

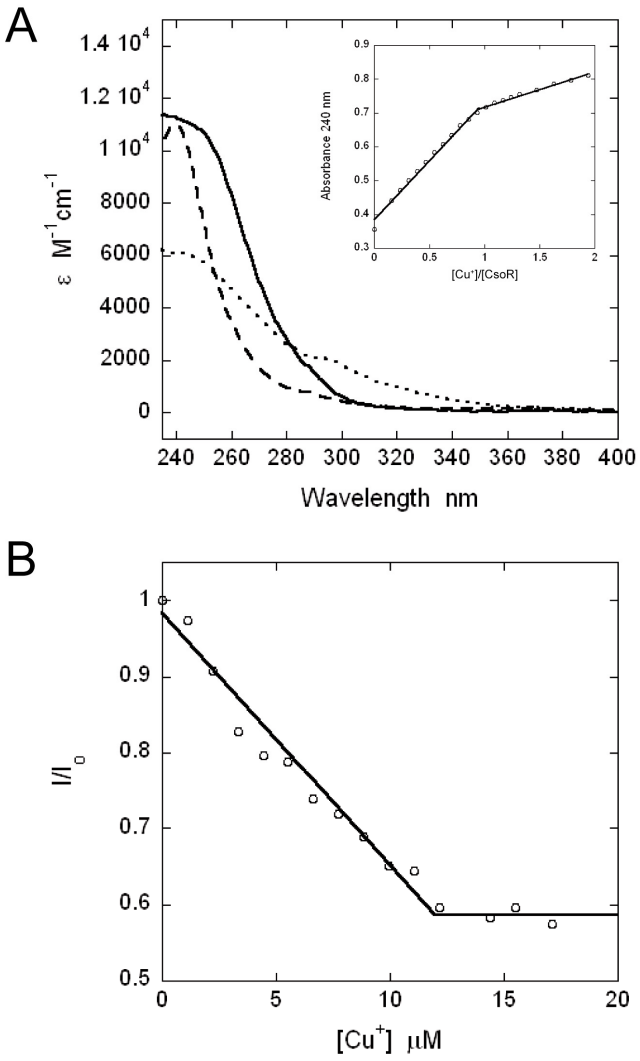

Figure 13. Cu(I) binding to *Mtb* CsoR. (A) Apoprotein-subtracted molar absorptivity spectrum of 20 μM Cu(I):*Mtb* CsoR wild-type (solid line), H61A (dashed line) and C36A (dotted line) CsoRs mixture at a 1:1 molar ratio. Inset: Cu(I) binding isotherm of wild-type CsoR. (B) Anaerobic titration of 10 μM apo-*Mtb* CsoR with Cu(I) as monitored by change in tyrosine fluorescence. Conditions: 10 mM HEPES, 0.2 M NaCl, pH 7.0, at ambient temperature (panel A) and 25.0±0.1 ^{o}C (panel B).

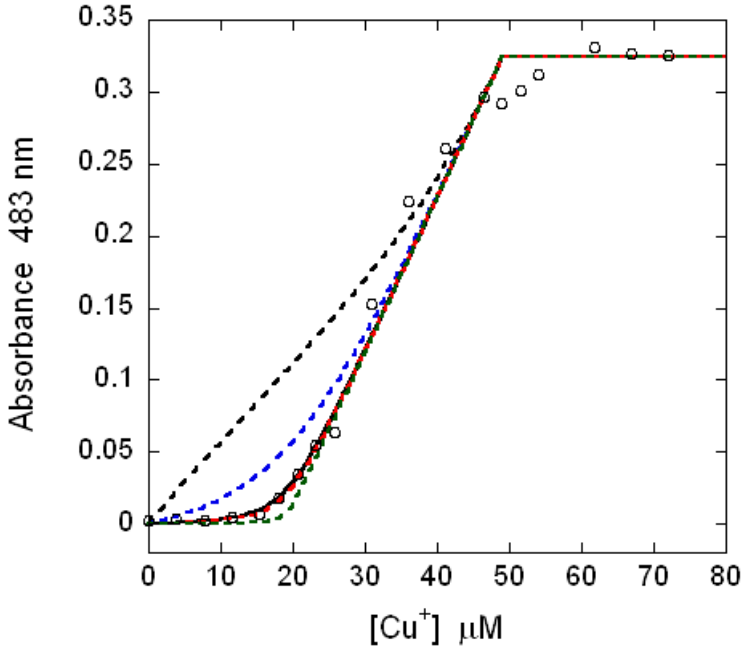

Figure 14. A representative wild-type CsoR-BCS competition titration. 19 μM CsoR (monomer) and 60 μM BCS were mixed with different concentrations of CuCl in an anaerobic chamber (10 mM HEPES, 0.2 M NaCl, 25 ^{o}C). Log K_{Cu} is fitted by a simple competition model by Dynafit to be 17.9 ± 0.4 as shown by the black solid line, consistent with the affinity determined using a different experimental strategy as described in Methods. The dashed lines represent simulations with log K_{Cu}=16 (black), 17 (blue), 18 (red) and 19 (green) under the same conditions.

Cu(I) binding causes dramatic quenching (~40%) of tyrosine fluorescence from the single tyrosine residue (Y35) in CsoR and this change is saturable at about 1 monomer mol equiv Cu(I) (Figure 13B). These data taken collectively establish the Cu(I) binding stoichiometry as one Cu(I) per monomer.

The Cu(I) binding affinity was further determined by a competition assay using bathocuproine disulfonate (BCS) as a competitor ligand (Figure 11A). As shown in Figure 14, when increasing concentrations of Cu(I) are added to a mixture of 19 μM CsoR monomer and 60 μM BCS, no change in absorbance at 483 nm is observed until about 19 μM Cu(I). This suggests that no $Cu(I)(BCS)_2$ complex is formed until virtually all of the CsoR is saturated with Cu(I). Data fitting using simple competition model by Dynafit reveals the Cu(I)-CsoR binding affinity to be $\log K_{Cu}$=17.9±0.4 (Figure 14) (Appendix A) (*106, 111*).

Using an alternative approach as described in Methods, different concentrations of BCS were mixed with CsoR and Cu(I) present at the same concentration. The formation of $Cu(I)(BCS)_2$ complex was quantified by absorbance at 483 nm and therefore K_{Cu} of CsoR can be calculated (see Methods). Using this assay, log K_{Cu} for wild-type CsoR is determined to be 18.1±0.1, in excellent agreement with the direct titration result (Figure 14). Therefore, this assay was used to determine the binding affinities of CsoR mutants in the studies that follow. An average of log K_{Cu}=18.0 (±0.2) obtained by both methods is thus reported in Table 1.

Mtb CsoR coordinates Cu(I) with Cys36, His61 and Cys65. The Cu(I) coordination geometry in solution was determined by x-ray absorption spectroscopy (XAS). For wild-

Table 1. Cu(I) and DNA binding affinities of *Mtb* CsoR[a]

Mtb CsoR		log K_{Cu}[b]	DNA binding affinity[d] A_2 (x10^{14} M^{-2})	ΔG_c (kcal/mol)
wild-type	apo	18.0 (±0.2)	3.7 (±1.0)	
	Cu(I)		0.0079 (±0.0023)	3.6 (±0.2)
wild-type 1-106	apo	17.3 (±0.4)	17 (±7.8)	
	Cu(I)		0.10 (±0.03)	3.0 (±0.3)
H61A	apo	14.5 (±0.3)	n.d.[e]	
		14.9 (±0.4)[c]		
C36A	apo		3.7 (±0.9)	
	Cu(I)		10.5 (±8.4)	-0.6 (±0.5)
R15A/C36A/R55A	apo		n.d.	
C36A CsoR 1-98	apo		0.055 (±0.011)	
C36A CsoR 1-88	apo		n.d.	

[a] Conditions: 10 mM HEPES, 0.2 M NaCl, pH 7.0, 25 ºC, with 2 mM DTT present only in the DNA binding experiments.

[b] Determined by competition with the chromophoric complex $Cu^I(BCS)_2$ (log β_2=19.8) as described in Methods.

[c] BCA is used as a competitor with a log β_2=17.2 for $Cu^I(BCA)_2$ complex used in calculation.

[d] Determined using fluorescence anisotropy-based titrations.

[e] n.d., not detected, $K_i \leq 10^5$ M^{-1} under these conditions.

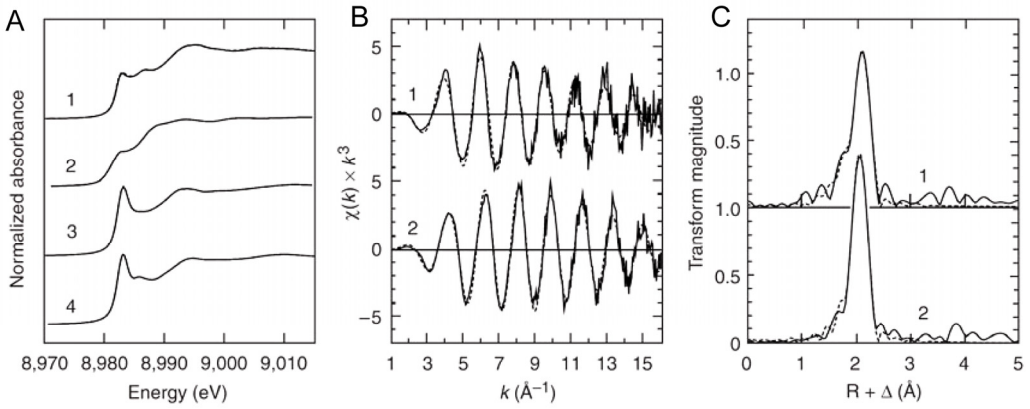

Figure 15. X-ray absorption spectroscopy (XAS) of Cu-CsoR. (A) Copper K-edge X-ray absorption near-edge spectra of CsoR with 1.0 (solid line) and 0.5 (broken line) metal stoichiometries (solid and broken lines overlap) (curve 1), compared with the spectrum of the trigonally coordinated cuprous model ($[Cu_4(SPh)_6]^{2-}$) (curve 2). Also shown is the near-edge spectrum of H61A CsoR (curve 3), compared with the spectrum of the two-coordinate species ($[Cu(SR)_2]^-$) (curve 4). (B) Cu-S phase-corrected EXAFS Fourier transforms (solid lines) plus best fits (broken lines) of CsoR (1) and H61A CsoR (curve 2). (C) EXAFS data (solid lines) plus best fit (broken lines) of CsoR (1.0 stoichiometry) (curve 1) and H61A CsoR (curve 2). Parameters that derive from the fitted curves are compiled in Table 2.

Table 2. XAS fitting parameters for *Mtb* CsoR[a]

Sample		*N*	*R* (Å)	σ^2 (Å2)	ΔE_0 (eV)	*F* [b]
WT CsoR	Cu-S	2	2.204(3)	0.0038(1)	-19.5(10)	0.335
	Cu-N	1	1.955(21)	0.0093(2)		
H61A CsoR	Cu-S	2	2.143(1)	0.0031(6)	-17.9(4)	0.233

[a]Coordination numbers *N*, interatomic distances *R* are given in Å, Debye-Waller factors σ^2 (the mean-square deviations in interatomic distance) in $Å^2$, and the threshold energy shifts ΔE_0 are given in eV. The values in parentheses are the estimated standard deviations obtained from the diagonal elements of the covariance matrix.

[b]The fit-error function *F* is defined by $F = \sqrt{\sum k^6(\chi(k)_{calcd} - \chi(k)_{expt})^2 / \sum \chi(k)^2_{expt}}$

where $\chi(k)$ are the EXAFS oscillations and *k* is the photo-electron wave number.

type CsoR, the pre-edge peak at 8940 eV in the edge spectrum shown in Figure 15A is consistent with a 1s→4p excitation typical for 3-coordinate Cu(I) (*111*). Data analysis of the Cu K-edge extended X-ray absorption fine structure (EXAFS) spectrum (Figure 15C) as well as the Fourier transforms as shown in (Figure 15B) reveals a trigonal Cu(I) complex with two S-Cu interactions at 2.20 Å and a N/O interaction at 1.97 Å (Table 2).

To confirm the identity of the Cu(I) ligands in CsoR, two substitution mutants, C36A and H61A, were purified and characterized. Interestingly, the LMCT molar intensity for C36A CsoR is only about half of what is observed for wild-type CsoR, consistent with only one S-Cu coordination bond (Figure 13A). In addition, preliminary EXAFS data for C36A CsoR shows only one S-Cu interaction at 2.23 Å and two Cu-(N/O) interactions at 1.98 Å (data not shown). Therefore, Cu(I) is likely to be coordinated by Cys65, His61 and possibly a third ligand from the solvent. Although the UV spectrum of Cu(I)-substituted H61A CsoR is different from wild-type CsoR, the molar intensity is consistent with 2 Cu(I)-thiolate coordination bonds. The Cu(I) binding affinity as determined by BCS and BCA competition assays is decreased by ~5000 fold relative to wild-type CsoR (Table 1). Remarkably, x-ray absorption spectroscopy of H61A CsoR suggests a 2-coordinate Cu(I)-complex with two S-Cu interactions at 2.14 Å (Figure 15, Table 2). All of these data are consistent with the crystal structure where Cu(I) is coordinated by Cys36, His61 and Cys65 in CsoR. Both the XAS and Cu(I) binding affinity studies also reveal that decrease of coordination number from 3 to 2 in the H61A mutant causes a significant decrease in the Cu(I) binding affinity by $>10^3$ fold;

however, the two Cu(I)-thiolate coordination bonds provide the largest contribution to the Cu(I) binding free energy.

DNA binding of wild-type Mtb CsoR is regulated by Cu(I). To determine the DNA binding affinity of CsoR to the operator DNA (*Mtb* CsoO), a fluorescence anisotropy based assay was employed (see Methods). To fit the anisotropy data, a model invoking the binding of two non-dissociable tetramers to one DNA was used on the basis of the size exclusion chromatography profile shown in Figure 16A, in which 80 μM CsoR monomer is required to saturate 10 μM input DNA, consistent with our findings with *Bsu* CsoR (see Chapter IV) . The normalized binding isotherms shown in Figure 16B reveal that apo-CsoR binds to the DNA with much higher affinity than Cu(I)-bound CsoR, with an overall binding affinity, A_2^{apo}=3.7 x 10^{14} M^{-2} vs. A_2^{Cu}=7.9 x 10^{11} M^{-2} in the absence and presence of Cu(I), respectively. Therefore, Cu(I) binding strongly negatively regulates the *cso* operator binding affinity of *Mtb* CsoR, corresponding to a ΔG_c of +3.6 (±0.2) kcal/mol (Table 1).

The positively charged patch and the C-terminal tail are important for DNA binding. The crystal structure of Cu(I)-bound *Mtb* CsoR reveals an all α-helical structure with no classic DNA binding motifs (Figure 8) (*39*). A positively charged patch was observed in the structure which was proposed to be important for DNA binding (*39*). To test this, two arginine residues in this patch were substituted with alanine in the context of C36A CsoR, which although poorly regulated by Cu(I) binding, retains high affinity for the CsoO DNA (Figure 17A, Table 1). This mutant was also easier to purify with high yield. Surprisingly, the resultant protein, R15A/R55A/C36A CsoR binds the DNA with an

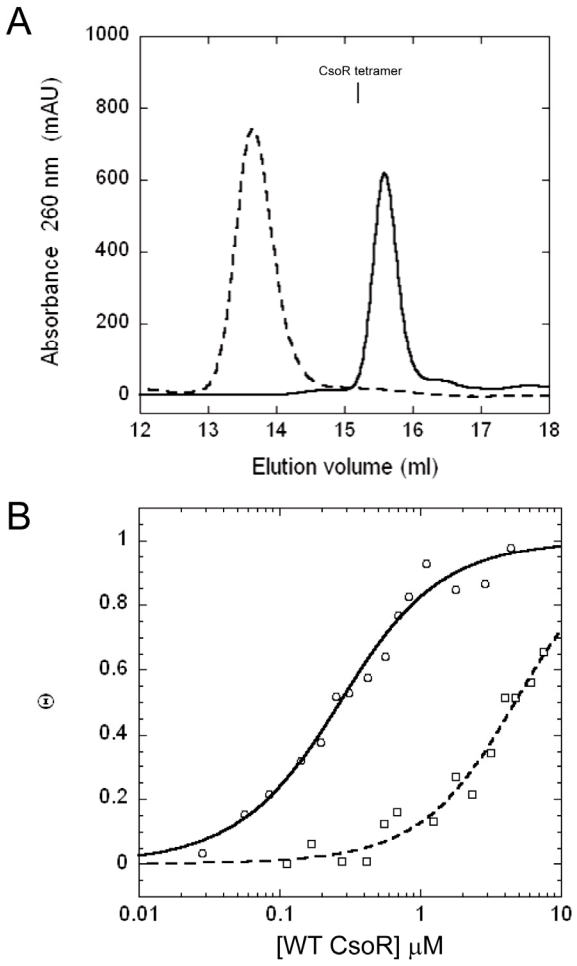

Figure 16. DNA binding of wild-type *Mtb* CsoR. (A) Two CsoR tetramers (8 monomers) bind to one 50 bp DNA. Elution profile obtained with 10 μM DNA only (solid line) and 10 μM DNA mixed with 80 μM CsoR monomer from a Superdex 200 column as monitored by absorption at 260 nm. (B) Normalized fluorescence anisotropy-based DNA binding isotherms acquired in the absence (○) and presence (□) of Cu(I). Curves represent the best fit using a stepwise two tetramer DNA binding model (Appendix C). Conditions: 10 mM HEPES, 0.2 M NaCl, 2 mM DTT, pH 7.0, 25 ^{o}C.

undetectably low affinity under the standard experimental conditions used ($K \leq 10^5\ M^{-1}$) (Figure 17A). To verify that this mutant is folded normally, the far UV-CD spectrum was acquired and compared to that of C36A CsoR (Figure 17B). No significant differences are observed, suggesting the mutant protein is folded with no significant perturbation in secondary structure. Therefore, this positively charged patch may be important for DNA binding, possibly via electrostatic interactions with the DNA phosphate backbone.

In the crystal structure of Cu(I)-bound *Mtb* CsoR, essentially all of the C-terminal tail (residues 89-119) is not observed in the final model (*39*). Since this tail is only present in CsoR homologs from pathogenic mycobacterial species (Figure 9), it is of interest to determine how the deletion of the tail influences the functional properties of CsoR. Surprisingly, deletion of the entire C-terminal tail in the context of C36A CsoR (C36A CsoR 1-88), *i.e.*, that which directly corresponds to the crystal structure, results in an undetectable DNA binding affinity ($K \leq 10^5\ M^{-1}$) in the anisotropy assay under standard solution conditions (0.2 M NaCl, pH 7.0, 25 ^{o}C). Adding back 10 residues to create C36A CsoR 1-98 CsoR partially restores DNA-binding affinity, but not to a level comparable to that of full-length C36A CsoR (Figure 18, Table 1). These data suggest that this C-terminal tail is also important for DNA binding, although the detailed mechanism by which this occurs remains unknown (see Chapter VI).

A more detailed comparison of the amino acid sequence of the C-terminal tail of CsoRs from other pathogenic mycobacterial species reveals that the tail sequence is highly conserved until residue 106 (Figure 9). Therefore, CsoR 1-106 in the context of

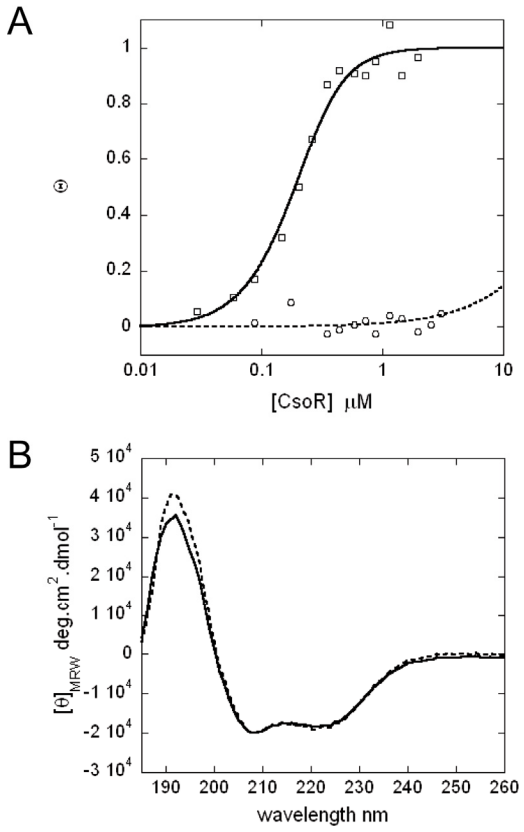

Figure 17. Arg15 and Arg55 are important for DNA binding. (A) Normalized fluorescence anisotropy-based DNA binding isotherms of C36A (○) and R15A/C36A/R55A (□) *Mtb* CsoRs. Curves represent the best fit using a stepwise two tetramer DNA binding model. DNA binding R15A/C36A/R55A CsoR is not detected in this assay. Conditions: 10 mM HEPES, 0.2 M NaCl, 2 mM DTT, pH 7.0, 25 ^{o}C. (B) Circular dichroism spectra comparison of CsoR C36A (solid) and R15A/C36A/R55A (dash) CsoRs. Conditions: 10 mM sodium phosphate pH 7.0, 0.2 M NaF.

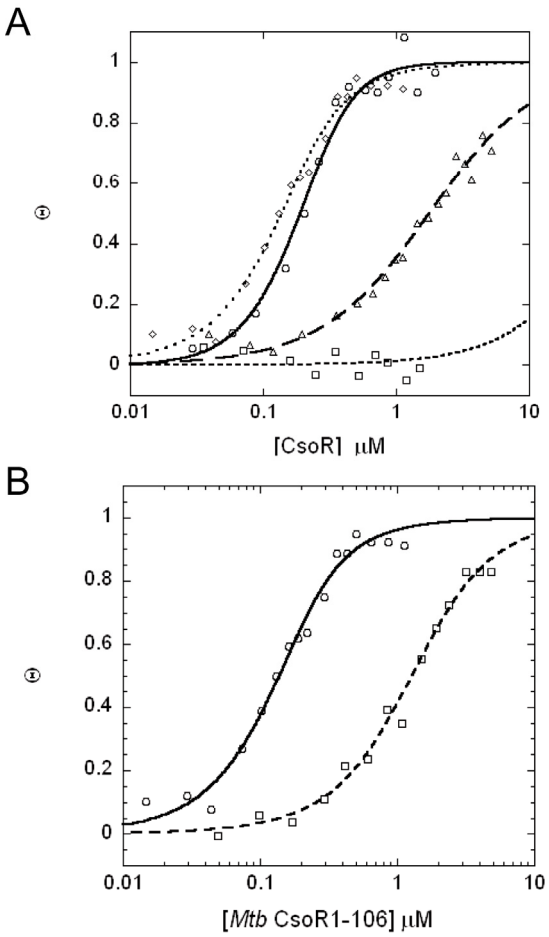

Figure 18. DNA binding of C-terminal deletion mutants. (A) Normalized fluorescence anisotropy-based DNA binding isotherms of C36A 1-119 (○), C36A 1-98 (Δ), C36A 1-88 (□) and wild-type 1-106 (◊) *Mtb* CsoRs. (B) Normalized fluorescence anisotropy-based DNA binding isotherms of wild-type 1-106 acquired in the absence (○) and presence (□) of Cu(I). All curves represent the best fit using a stepwise two tetramer DNA binding model. Conditions: 10 mM HEPES, 0.2 M NaCl, 2 mM DTT, pH 7.0, 25 ^{o}C.

wild-type CsoR was constructed and purified. The overall DNA binding was determined to be A_2=1.7x10^{15} M^{-2} in the apo form which is comparable to that of wild-type CsoR (Table 1). The DNA binding affinity is also significantly decreased by Cu(I) binding, resulting a coupling free energy of ΔG_c=3.0 kcal/mol for CsoR 1-106 (Figure 18, Table 1). The Cu(I) binding affinity is determined by BCS competition assay to be log K_{Cu}=17.3 (Table 1). These data provide support for the assertion that 1-106 are necessary and sufficient to maintain the functional properties of wild-type CsoR, a finding that we further exploit in the following Chapter III.

DISCUSSION

The Cu(I) binding affinity reported here (log K_{Cu} =18.0) reveals that CsoR binds Cu(I) very tightly. Such high affinity is not unprecedented for Cu(I) binding proteins however. In fact, another Cu(I) regulatory protein CueR from *E. coli* is proposed to be induced by zeptomolar (10^{-21} M) Cu concentrations (*38*). Some of the metal binding domains of the Cu(I) P-type ATPase as well as the Cu chaperones are also reported to bind Cu(I) with very high affinity (*107, 111, 112*). These observations are consistent with the hypothesis that there is no free or bioavailable Cu(I) ion in the cytosol of bacterial or yeast cells, likely due to it its toxicity (*38*). This is probably one of the reasons why a high affinity trigonal planar 3-coordinate Cu(I) complex appears to have been evolved in all the putative Cu(I)-sensors in this family (Figure 10). A 2-coordinate Cu(I) complex as found in H61A CsoR, may not bind Cu(I) with sufficient affinity to function as a Cu(I)-sensor in the cell. A similar scenario likely also characterizes the

CsoRs that harbor only x-Cys-x-Cys signature (see Figure 10); thus these CsoRs may not bind Cu(I) with sufficient affinity to carry out Cu-sensing under physiological conditions in the cell.

The Cu-efflux P-type ATPase (Rv0969; Figure 7) regulated by CsoR in *Mtb* represents one mechanism by which excess amounts of Cu can be effluxed from the cytosol. The recent report of a Cu-metallothionein, MymT, provides another possible copper detoxification mechanism, although it remains unclear if and how the expression of MymT is regulated (*17*). However, one important component required to carry out Cu trafficking in the cytosol, the Cu chaperone, still remains to be identified in *Mtb*. No putative Cu chaperone can be identified in *Mtb* by sequence alignment using the bacterial Cu chaperone *B. subtilis* CopZ sequence as query. However, there are two other CsoR homologs encoded in the *Mtb* genome, annotated as *rv0190* and *rv1766*. The protein encoded by *rv0190* retains all three conserved Cu(I) binding ligands, in a fashion similar to the *bona fide* Cu-sensing CsoRs (Figure 9). Interestingly, microarray data obtained with *Mtb* grown in liquid culture reveal that *rv0190* is highly induced by elevated Cu concentration added to the growth media (0.5 mM), suggesting a possible function in Cu homeostasis. Since *rv0190* does not contain the C-terminal tail which is important for DNA binding at least for *Mtb* CsoR, it is unlikely to regulate the *cso* operon via binding to the operator DNA. It cannot be ruled out though that *rv0190* encodes a transcriptional repressor that regulates different gene(s) distinct from that of CsoR. Alternatively, it may function as a Cu chaperone or a Cu-storage protein, a hypothesis that requires further biological and biochemical support. Interestingly, *rv0190*

is positioned next to a putative major facilitator superfamily (MFS) transporter (*rv0191*) of unknown substrate specificity. Rv1766, on the other hand, contains an x-Cys-x-Cys sequence and its biological function remains totally unknown.

Although it is not known yet how *Mtb* CsoR binds the cognate DNA operator, the unique C-terminal tail seems to be important for this interaction. The tail is highly conserved as shown in Figure 9, but consists mainly of neutral and hydrophobic rather than basic amino acids. Other CsoR homologs do not contain such tails, and yet can bind DNA with high affinity at least as shown for *Bsu* CsoR (*111*). Therefore, it seems unlikely that this tail forms crucial directly interactions with DNA, although direct experimental support for or against this proposal are lacking. Alternatively, this tail may be indirectly involved in DNA binding, possibly via stabilizing the tetrameric oligomerization state or stabilizing a certain conformation of CsoR for high affinity DNA binding (see Chapter VI).

The minimal DNA sequence that *Mtb* CsoR recognizes is a 28 bp GC-rich inverted repeat as previously described (*39*). A 50 bp DNA containing this 28 bp was used in the DNA binding studies here to avoid incomplete double strand formation especially under low DNA concentration in fluorescence anisotropy experiments (Appendix B). To identify the DNA sequences crucial for the interactions with CsoR, several deletion and mutant CsoO DNA operators were prepared and the DNA binding activity of each qualitatively determined by gel filtration chromatography at 10 μM DNA concentration (Appendix B). Deletion of 7 bp at either side of the 28 mer results in only very weak DNA binding as reported by a broad peak of 220 nm absorption in these

elution profiles (data not shown). These preliminary data suggest that both the GC-rich regions and the inverted repeat are important for specific high affinity interactions with *Mtb* CsoR.

The data presented in this chapter document the biochemical properties of the founding member of this new metalloregulatory protein family, *Mtb* CsoR (*39*). In the following chapter, the mechanism by which Cu(I) allosterically inhibits DNA operator binding is further investigated by conventional mutagenesis as well as native chemical ligation, the latter approach used to incorporate a single unnatural amino acid in a key position in the protein.

CHAPTER III

EXPLORING THE MECHANISM OF ALLOSTERIC NEGATIVE REGULATION OF CsoO BINDING BY *M. tuberculosis* CsoR

INTRODUCTION

Metalloregulatory or metal sensor proteins control the intracellular availability of essential transition metal ions and collectively mediate metal homeostasis (*1, 6*). These specialized metal receptor proteins regulate gene expression by binding a specific metal ion, which, in turn, allosterically activates or inhibits operator DNA binding, thus leading to derepression, co-repression or activation of transcription of metal homeostasis genes (*1, 6*). Metal ion-dependent regulation of operator DNA binding likely requires a change in the structure and/or dynamics of the regulator. However, the structural and molecular details in many cases are poorly understood due mainly to a lack of high resolution structural and dynamical information for functionally important allosteric states in any one system (*1, 6*).

Amino acid substitution is a commonly used tool to investigate the roles of individual amino acid residues in driving functional regulation. However, this approach has limited application in specific cases when the residue of interest is thought to perform multiple functions. For example, as discussed in Chapter I, in the Zn(II)-sensor *S. aureus* CzrA, His97 is hypothesized to play two roles in the regulation of the operator-promoter binding (*66, 113*). In one, the $N^{\delta 1}$ donates a coordination bond to the Zn(II), while in the other, the $N^{\varepsilon 2}$ face is proposed to initiate the formation of a hydrogen

bonding network that physically links the zinc binding and DNA binding sites of the repressor (*66, 113*). As might be anticipated, conventional site-directed mutagenesis of His97 induces a non-native octahedral Zn(II) coordination geometry with K_{Zn} decreased by more than 10^5-fold; the same substitutions abrogate Zn(II)-dependent allosteric negative regulation of *czr* operator binding and thus are mechanistically uninformative (*113*). It is therefore impossible to probe these two roles separately by conventional mutagenesis. A more powerful approach is to site-specifically incorporate a unnatural amino acid, *e.g.,* a specific His analog, to create mutant proteins with defined *atom* substitutions rather than *residue* substitutions in a way that retains many of the physicochemical characteristics of the wild-type amino acid (*114, 115*).

As shown in Chapter II, Cu(I) binding to *Mtb* CsoR negatively regulates the DNA binding affinity, resulting in an allosteric coupling free energy ΔG_c of 3.6 ± 0.2 kcal/mol at 25 ^{o}C. Interestingly, substitution of the key Cu(I) ligand His61 with alanine results in a 2-coordinate Cu(I) geometry with a significantly lower Cu(I) affinity (log K_{Cu}=14.5) and undetectable DNA binding affinity ($K<10^5$ M^{-1}); as a result, the coupling free energy cannot be determined. Thus, H61 in CsoR may play multiple key roles, and conventional mutagenesis will not be capable of probing these roles separately. To better understand the mechanism, we incorporated 1-methyl-His (MeH) or β-(2-thiazolyl)-Ala (Thz) into *Mtb* CsoR by native chemical ligation in replacement of His61 to specifically perturb the possible function of the $N^{\varepsilon 2}$ face of His61. We postulate that this face of His61 initiates hydrogen bonding interactions to other "second coordination shell" residues which may include Tyr35 and Glu81 (Scheme 1). Consistent with this model,

we show that the DNA binding activity of H61MeH and H61Thz CsoRs is not strongly regulated by Cu(I) binding, despite the maintenance of a 3-coodinate Cu(I) geometry and high Cu(I) binding affinity. Amino acids substitutions of the proposed "second shell" residues Tyr35 and Glu81 also result in a significant decrease in allosteric coupling free energy with no significant perturbation of either the Cu(I) binding affinity or Cu(I) coordination geometry. Formation of such a hydrogen bonding network may drive the conformational change that decreases the DNA binding affinity thus contributing to the observed coupling free energy. To our knowledge, this is the first example where the native chemical ligation approach is applied to specifically interrupt a possible hydrogen bond interaction crucial for allosteric regulation. This approach was further applied to the Zn(II) sensor CzrA and the preliminary findings from these experiments are also discussed.

MATERIALS AND METHODS

Unnatural amino acid incorporation by native chemical ligation. The C-terminal peptide of *Mtb* CsoR (residue 58-106, L58 substituted with Cys) was synthesized with incorporation of MeH (1-methylhistidine) or Thz (β-(2-thiazolyl)-alanine) analog (obtained as a Boc-derivative from Bachem, CA) at residue 61 by standard Boc-based solid phase peptide synthesis in collaboration with Dr. Richard DiMarchi at Indiana University. The DNA sequence encoding the N-terminal CsoR peptide (residue 1-57) was cloned into the pTXB1 vector (New England Biolabs, MA) between NdeI and SpeI restriction sites in frame to a C-terminal intein domain to express as an intein fusion

protein. The fusion protein was expressed in *E. coli* BL21(DE3) as described in Chapter II and the cells were lysed in Buffer C (25 mM Tris, 0.5 M NaCl, 2 mM TCEP, pH 8.0). Sodium 2-mercaptoethanesulfonate (MESNA) (Sigma, MO) was added to the lysis supernatant which contained CsoR 1-57-intein to a concentration of 100 mM and stirred at 4 ^{o}C for 24 h to cleave the intein. The resultant CsoR 1-57 containing a C-terminal thioester was then purified using an SP column and concentrated to a final volume of 2 mL to about 2 mM (monomer) in Buffer C with 5 mM MESNA. 1 mL of CsoR1-57 thioester was used to dissolve 12 mg (about 1.8 mM in 1 mL) of the C-terminal peptide 58-106. 7 M urea, 10 mM TCEP and 100 mM MESNA were added to the ligation reaction and pH adjusted to 7.5 using 1 M NaOH (Figure 19A). The reaction was carried at room temperature in air overnight. The ligated CsoR was then purified by a μRP (GE Healthcare, NJ) reverse phase column using a 0.1% TFA solution with 0-75% acetonitrile gradient. Fractions containing CsoR were combined and refolded into Buffer S (10 mM HEPES, 0.2 M NaCl, pH 7.0) containing 2 mM DTT by stepwise increasing the pH. The final preparation was dialyzed in the glovebox against Buffer S as described in Chapter II. The purity of the protein was estimated to be >90% by SDS-PAGE gel and the number of reduced Cys residues (3 expected) was confirmed by the DTNB assay. The integrity of the resultant proteins was analyzed by MALDI-TOF as well as trypsin digestion followed by tandem MS/MS sequencing (Figure 20).

Construction and purification of H97MeH CzrA using native chemical ligation. The C-terminal peptide of CzrA (residues 96-106, H96 substituted with Cys) was synthesized with incorporation of MeH (1-methylhistidine) at residue 97 by standard Boc-based solid

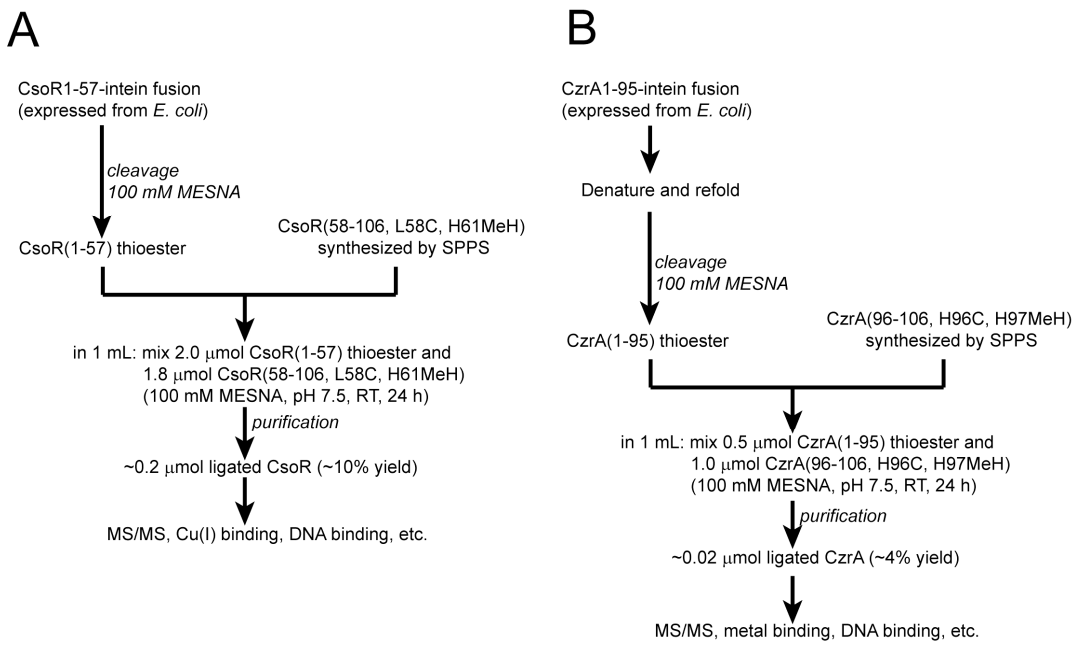

Figure 19. Semi-synthesis of H61MeH CsoR (A) and H97MeH CzrA (B) (see Methods for details). The H61Thz CsoR was made using the same scheme as shown in panel (A).

phase peptide synthesis in collaboration with Dr. Richard DiMarchi at Indiana University. The DNA sequence encoding the N-terminal peptide (residue 1-95) was cloned into the pTXB1 vector (New England Biolabs) between NdeI and SpeI restriction sites in frame to a C-terminal intein fusion. The CzrA 1-95-intein fusion was then expressed in *E. coli* BL21(DE3) as described above. After sonication using Buffer C, the CzrA 1-95-intein fusion was found to be insoluble and remained in the low speed lysis pellet. This pellet was then resuspended in Buffer C containing 7 M urea and refolded by stepwise decreasing the urea concentration in Buffer C. The resultant soluble fraction of CzrA 1-95-intein was cleaved with the addition of 100 mM MESNA as described above with CzrA 1-95-thioester further purified on a C18 reverse phase column by running a 0-75% acetonitrile gradient in 0.1% TFA. Fractions containing CzrA 1-95 thioester were pooled and concentrated to ~1 mL and ligated to the C-terminal peptide using conditions analogous to those as described above for CsoR (Figure 19B). The resultant H97MeH CzrA was further purified on a μRP (GE Healthcare, NJ) reverse phase column under denaturing conditions and finally refolded into Buffer P by stepwise increasing pH (10 mM HEPES, 0.4 M NaCl, pH 7.0) with 2 mM DTT.

Purification of H96C CzrA. An overexpression plasmid containing *S. aureus* H96C CzrA was constructed by site-directed quick-change mutagenesis using pET3a-CzrA as template (*113*). The protein was expressed in *E. coli* BL21(DE3) in M9 minimum medium containing 100 mg/ml ampicillin supplemented with $^{15}NH_4Cl$ as the sole nitrogen source and purified using the published procedure (*70, 113*) except that 2 mM DTT was added to all the buffers used during the purification. Purified H96C CzrA was

extensively dialyzed in the glovebox against Buffer P. The protein concentration was determined using ε_{280nm}=4470 $M^{-1}cm^{-1}$ and the mol equiv of free reduced thiol was determined by the DTNB assay to be 0.9 (1.0 expected).

Purfication of CsoR mutants. See Methods in Chapter II.

Cu(I) binding affinity determination of CsoR mutants. The Cu(I) binding affinities for various CsoR mutants were determined by varying the BCS concentration in a competition assay as described in Chapter II.

X-ray absorption spectroscopy. See Methods in Chapter II.

Fluorescence anisotropy. DNA binding experiments of CsoR were carried out as described in Chapter II. The DNA binding activity of H96C and H96C/H97MeH (hereafter referred to as simply H97MeH CzrA) CzrAs was measured in 10 mM HEPES, 0.4 M NaCl, 2 mM DTT, pH 7.0 with 10 μM Zn(II) or 1 mM EDTA present in the solution. 4 nM fluorescein labeled 28 bp with the 12-2-12 inverted repeat underlined was used (5'-FL-T<u>AATATATGAACA</u>AA<u>TATTCAGATGAA</u>A-3'). The data were fitted using Dynafit with a 1:1 dimer:DNA binding model with the dimerization constant fixed at K_{dim}=1.7x10^5 M^{-1} (*70, 116*).

Co(II) and Zn(II) binding to CzrA. $CoCl_2$ titrations with 100 μM CzrA monomer (50 μM dimer) were carried out in Buffer P anaerobically as previously described (*70, 117*). For the Zn(II) titrations, $ZnSO_4$ was titrated into a mixture of 2.4 μM magfura-2 and 1.7 μM CzrA monomer in Buffer P. The excitation spectrum from 265-455 nm with λ_{em}=497 nm was measured after each addition. Fluorescence intensities at 325 and 379

nm were plotted against total Zn(II) concentration and the data were simultaneously fitted to a simple competition model using Dynafit as described (Appendix D) (*118*).

NMR spectroscopy NMR spectra were acquired on a Varian Unity Inova 600 MHz spectrometer equipped with a cryo-probe in the MetaCyt Biomolecular NMR Laboratory at Indiana University. NMR samples contained ≈0.25 mM ^{15}N-labeled H96C CzrA or 0.07 mM ^{15}N-labeled H97MeH CzrA in 10 mM MES, 50 mM NaCl and 2 mM DTT with or without 1.1 monomer mol equiv of Zn(II) added (pH 6.0). ^{1}H–^{15}N HSQC spectra were acquired at 40 °C as described previously(*113*). All spectra were processed and analyzed using NMRPipe and SPARKY (*119, 120*).

RESULTS

L58C CsoR 1-106 was chosen to incorporate His-analogs. *Mtb* CsoR is 119 residues in length with two key Cu(I) coordinating Cys residues. We chose a semisynthetic route using an intein fusion strategy (see Methods) (*115*). As shown in Chapter II, the C-terminal tail (residues 89-119) is essential for high affinity DNA binding by CsoR. However, partial truncation at residue 106 results in a protein with near wild-type Cu(I) binding and DNA binding properties. Therefore, the C-terminal peptide that would have to be made by solid-phase peptide synthesis was truncated at residue 106 to maximize the synthesis efficiency without significantly affecting the properties of the ligated protein. The most efficient semisynthesis of a chemically ligated protein also requires a non-native Cys residue to be incorporated at the ligation junction (*121*). We settled on a non-conserved and solvent exposed residue, Leu58, at the C-terminus of the α2 helix.

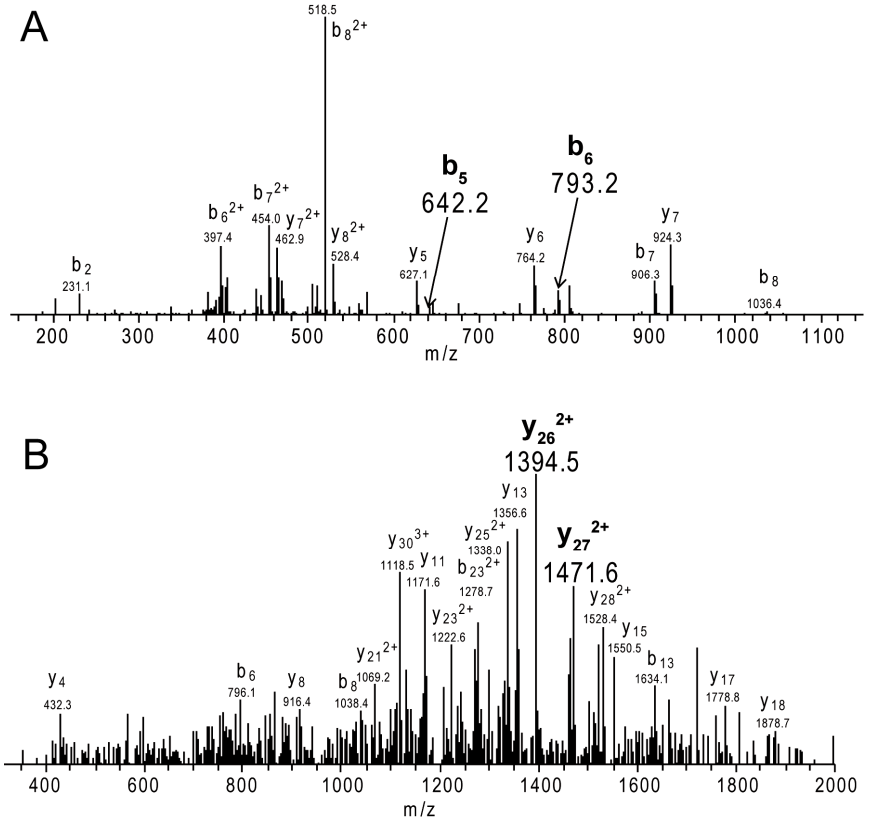

Figure 20. MS/MS results of the ligated CsoRs. (A) Tandem mass spectrum of doubly-charged peptide ^{56}VMCHN(MeH)LET^{64} from precursor ion m/z 578.1 with several identified fragment ions labeled. Fragment ions b_5 and b_6 confirm the location of the methyl group on His61. The underlined C corresponds to the L58C substitution which also defines the ligation junction. (B) Tandem mass spectrum of triply-charged peptide ^{56}VMCHN(Thz)LETCFSTAVLDGHGQAAIEELIDAVK^{87} from precursor ion m/z 1195.4 with several identified fragment ions labeled. Fragment ions y_{26} and y_{27} confirm the location of the thiazole substitution in place of His61.

To insure that these modifications did not significantly affect the properties of *Mtb* CsoR, the parent molecule L58C CsoR 1-106 was purified and extensively characterized. This mutant maintains a high Cu(I) binding affinity with log K_{Cu}=17.3 (±0.3) as determined by the BCS competition assay (Table 3). XAS reveals a 3-coordinate Cu(I) complex similar to that of wild-type CsoR (Figure 21, Table 4). More importantly, apo-L58C CsoR 1-106 binds the DNA with an affinity similar to wild-type CsoR 1-106, with Cu(I) binding significantly decreasing the DNA binding affinity; this results in a coupling free energy ΔG_c of +3.0 kcal/mol, a value close to that of wild-type CsoR (Figure 22A, Table 3). These data clearly reveal that L58C CsoR1-106 is characterized by properties very similar to that of wild-type CsoR and CsoR 1-106. We therefore chose this context with which to incorporate both H61MeH and H61Thz substitutions by native chemical ligation.

Cu(I) does not regulate the DNA binding of either H61MeH or H61Thz CsoRs. The His-analogs were incorporated into CsoR as described in Methods. The integrity of the resultant proteins were verified by tandem MS/MS spectroscopy as described in Figure 20. As shown in Figure 22B, C and Table 3, both H61MeH and H61Thz CsoRs in their apo forms bind to the DNA with affinities close to the parent L58C CsoR 1-106, suggesting both proteins are folded correctly and retain high CsoO binding affinity. Strikingly, Cu(I) binding to either of the two proteins only weakly regulates the DNA binding, resulting in a coupling free energy close to zero (Figure 22B and C, Table 3).

To confirm that the Cu(I) binding properties were not perturbed in H61MeH and H61Thz substituted L58C CsoR 1-106, both XAS and BCS competition assays were

Table 3. Cu(I) affinities, DNA binding affinities, and allosteric coupling free energies for various *Mtb* CsoRs[a]

Mtb CsoR		log K_{Cu}[b]	DNA binding affinity[d] A_2 (x10^{14} M^{-2})	r_0	r_∞	ΔG_c (kcal/mol)
Wild-type	apo	18.0 (±0.2)	3.7 (±1.0)	0.0975	0.1100	
	Cu(I)		0.0079 (±0.0023)	0.1040	0.1170	3.6 (±0.2)
WT 1-106	apo	17.3 (±0.4)	17 (±7.8)	0.1100	0.1250	
	Cu(I)		0.10 (±0.03)	0.1135	0.1285	3.0 (±0.3)
L58C 1-106	apo	17.3 (±0.3)	2.6 (±1.4)	0.1197	0.1290	
	Cu(I)		0.015 (±0.01)	0.1160	0.1270	3.0 (±0.4)
H61MeH	apo	18.4 (±0.2)	0.67 (±0.23)	0.1170	0.1310	
	Cu(I)		0.7 (±0.3)	0.1175	0.1300	0 (±0.4)
H61Thz	apo	16.7 (±0.1)	3.1 (±1.0)	0.1056	0.1210	
	Cu(I)		1.4 (±0.4)	0.1092	0.1240	0.5 (±0.2)
H61A	apo	14.5 (±0.3) 14.9 (±0.4)[c]	n.d.[e]			
	Cu(I)		n.d.			n.d.
E81A	apo	17.7 (±0.4)	14.7 (±5.7)	0.1000	0.1150	
	Cu(I)		5.3 (±2.4)	0.0980	0.1143	0.6 (±0.3)
E81Q	apo	17.6 (±0.5)	26.6 (±10.0)	0.1085	0.1205	
	Cu(I)		1.0 (±0.2)	0.1030	0.1145	1.9 (±0.3)
E81D	apo	17.8 (±0.4)	4.3 (±1.8)	0.1060	0.1190	
	Cu(I)		0.36 (±0.2)	0.1050	0.1200	1.5 (±0.3)
E81N	apo	17.3 (±0.4)	2.8 (±1.1)	0.1075	0.1205	
	Cu(I)		0.19 (±0.1)	0.1040	0.1170	1.6 (±0.4)
Y35F	apo	16.7 (±0.4)	14.3 (±3.6)	0.1000	0.1160	
	Cu(I)		0.24 (±0.07)	0.1075	0.1230	2.4 (±0.2)
Y35F/E81Q	apo	17.6 (±0.3)	10 (±2.9)	0.1080	0.1240	
	Cu(I)		1.7 (±0.8)	0.1117	0.1240	0.8 (±0.3)[f]

[a]Conditions: 10mM HEPES, 0.2 M NaCl, pH 7.0, 25 ºC, with 2 mM DTT present only in the DNA binding experiments. [b]Determined by competition with the chrmophoric complex $Cu^I(BCS)_2$ (log β_2=19.8) (or [c]$Cu^I(BCA)_2$) as described in Chapter II. [d]Determined using fluorescence anisotropy-based titrations like those shown in Figure 22. [e]n.d., not detected, $K_i \leq 10^5$ M^{-1} under these conditions. [f]$\delta = \Delta\Delta G_c^{Y35F/E81Q} - (\Delta\Delta G_c^{Y35F} + \Delta\Delta G_c^{E81Q}) = +0.1$ kcal/mol indicates the pairwise interaction between Y35F and E81Q, where $\Delta\Delta G_c^{mut} = \Delta G_c^{mut} - \Delta G_c^{WT}$.

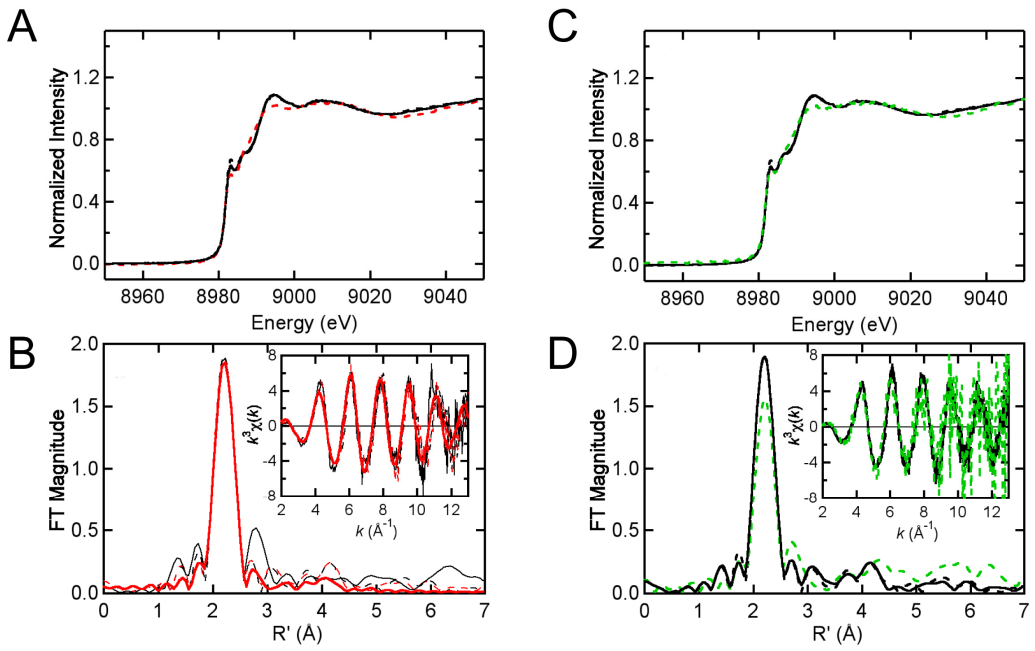

Figure 21. X-ray absorption spectroscopy (XAS) of Cu(I)-bound WT 1-106 (dashed black), L58C (solid black), H61MeH (dashed red) and H61Thz (dashed green) CsoRs. (A) and (C) Cu K-edge X-ray absorption edge spectra with (B) and (D) EXAFS spectra and the Fourier transforms (k^3 weighted, k=2-12 Å^{-1}) in the inset are shown. The bold red curve represents the best fit for H61MeH CsoR with the fitting parameters compiled in Table 4. The spectra for CsoR 1-106 and L58C CsoR 1-106 shown in (C) and (D) are the same as those in (A) and (B).

Table 4. XAS fitting parameters for various *Mtb* CsoR mutants [a]

Sample (*k* range) $\Delta k^3\chi$	Fit	Shell	R_{as} (Å)	σ_{as}^2 (Å^2)	ΔE_0 (eV)	f[b]
WT CsoR 1-106	1	Cu-S_2	2.21	0.0017	-9.191	0.070
		Cu-N_1	1.96	0.0016	[-9.191][c]	
		Cu-C_1	[2.95]	[0.0032]	[-9.191]	
		Cu-C_1	[3.00]	[0.0033]	[-9.191]	
		Cu-N_1	[4.13]	[0.0020]	[-9.191]	
		Cu-C_1	[4.17]	[0.0020]	[-9.191]	
L58C 1-106	1	Cu-S_2	2.22	0.0022	-8.654	0.067
		Cu-N_1	2.03	0.0016	[-8.654]	
		Cu-C_1	[3.01]	[0.0032]	[-8.654]	
		Cu-C_1	[3.06]	[0.0033]	[-8.654]	
		Cu-N_1	[4.19]	[0.0020]	[-8.654]	
		Cu-C_1	[4.23]	[0.0020]	[-8.654]	
H61MeH	1	Cu-S_2	2.25	0.0014	-2.850	0.89
		Cu-N_1	2.04	0.0016	[-2.850]	
		Cu-C_1	[3.02]	[0.0032]	[-2.850]	
		Cu-C_1	[3.07]	[0.0033]	[-2.850]	
		Cu-N_1	[4.20]	[0.0020]	[-2.850]	
		Cu-C_1	[4.24]	[0.0020]	[-2.850]	

[a] Shell is the chemical unit defined for the multiple scattering calculation. Subscripts denote the number of scatterers per metal. R_{as} is the metal-scatterer distance. σ_{as}^2 is a mean square deviation in R_{as}. ΔE_0 is the shift in E_0 for the theoretical scattering functions.

[b] f' is a normalized error (chi-squared):

$$f' = \frac{\left\{\sum_i \left[k^3\left(\chi_i^{obs} - \chi_i^{calc}\right)\right]^2 / N\right\}^{1/2}}{\left[\left(k^3\chi^{obs}\right)_{max} - \left(k^3\chi^{obs}\right)_{min}\right]}$$

[c] Numbers in square brackets were constrained to be either a multiple of the above value (σ_{as}^2) or to maintain a constant difference from the above value (R_{as}, ΔE_0).

carried out. As shown in Figure 21 and Table 4, the near edge spectra show similar pre-edge features at about 8940 eV, consistent with a 3-coordinate Cu(I) complex in both proteins (*122*). Quantitative analysis of the EXAFS spectrum of H61MeH CsoR further confirms that this CsoR forms a Cu(I) complex that is structurally very similar to the parent L58C and wild-type CsoR 1-106. Consistent with this, the Cu(I) binding affinity is not significantly decreased in these mutants and is at least $\geq$100 fold greater than that of H61A CsoR (Table 3). Therefore, the Cu(I) binding affinity and structure of the chelate in each ligated protein is not significantly changed relative to CsoRs containing a native His in this position. These findings clearly establish that the $N^{\varepsilon 2}$ face of His61 in CsoR is specifically required to thermodynamically and functionally link Cu(I) binding to DNA binding, likely via hydrogen bond interactions with nearby "second coordination shell" residues (Scheme 1).

Conserved residues Tyr35 and Glu81 are also essential for the allosteric negative regulation by Cu(I). A multiple sequence alignment of proposed Cu(I)-sensing CsoRs reveals that Tyr35 and Glu81 are highly conserved and are in close proximity to His61 in the Cu(I)-bound *Mtb* CsoR structure (Figure 8-9). Therefore these residues are excellent candidates that might interact directly with $N^{\varepsilon 2}$ face of His61 and mediate allosteric regulation in this system (Scheme 1) (*39, 111*). Inspection of the CsoR structure suggests a hydrogen bonding network involving Tyr35, Glu81 and His61 in the Cu(I) bound state, formation of which would allosterically inhibit DNA binding. Consistent with this, Y35F CsoR reveals a 33% decrease in coupling free energy, while the inhibition of DNA binding of E81A CsoR by Cu(I) is greatly diminished, with a coupling free energy of

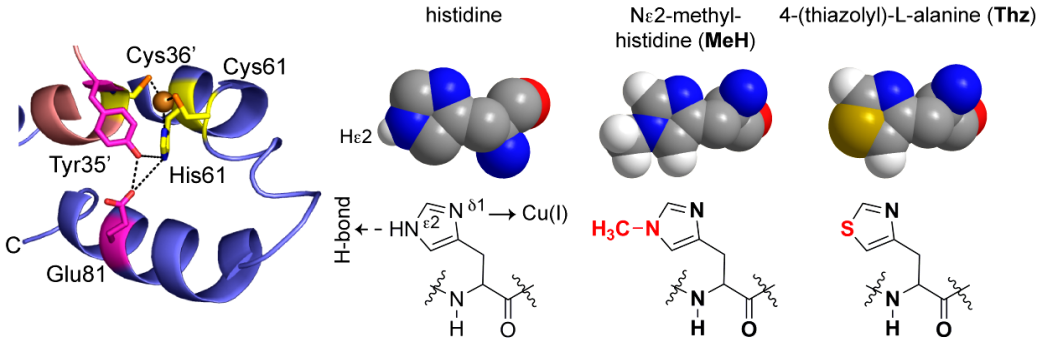
Cys36'
Cys61
Tyr35'
His61
C
Glu81
histidine
Nε2-methyl-
histidine (MeH)
4-(thiazolyl)-L-alanine (Thz)
Hε2
H-bond
Cu(I)
H3C–N
S

Scheme 1.

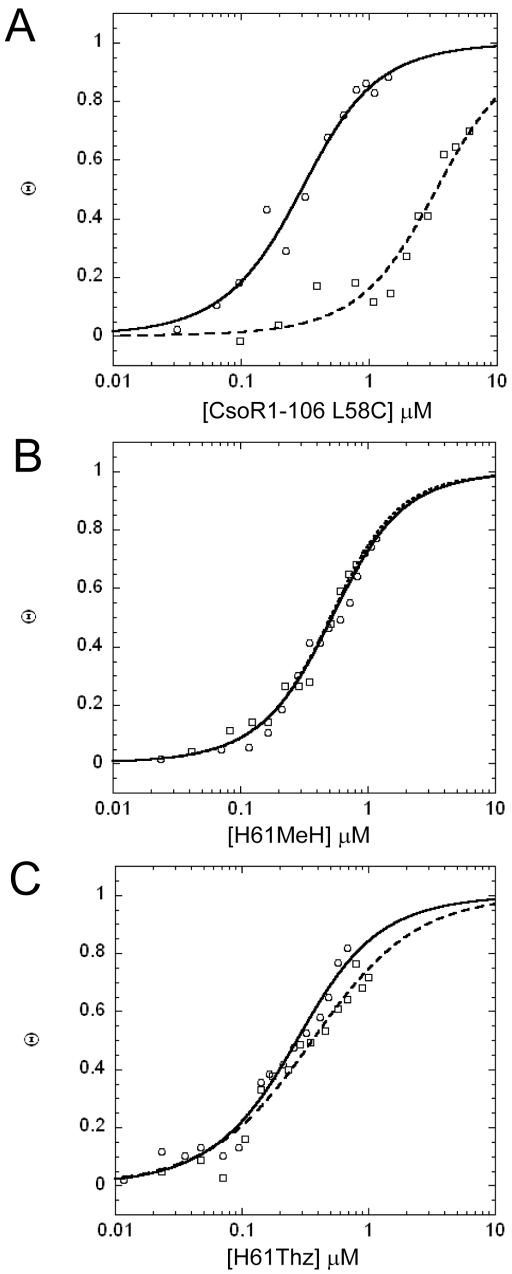

Figure 22. Normalized fluorescence anisotropy-based DNA binding isotherms of L58C CsoR 1-106 (A), H61MeH (B) and H61Thz (C) CsoRs acquired in the absence (○) and presence (□) of stoichiometric Cu(I). The solid curves represent the best fit using a stepwise, two-tetramer DNA binding model (Appendix C) with A_2 (Table 3) defined by $K_1 \cdot K_2$ (Figure 12). Conditions: 10 mM HEPES, 0.2 M NaCl, 2 mM DTT, pH 7.0, 25 ^{o}C.

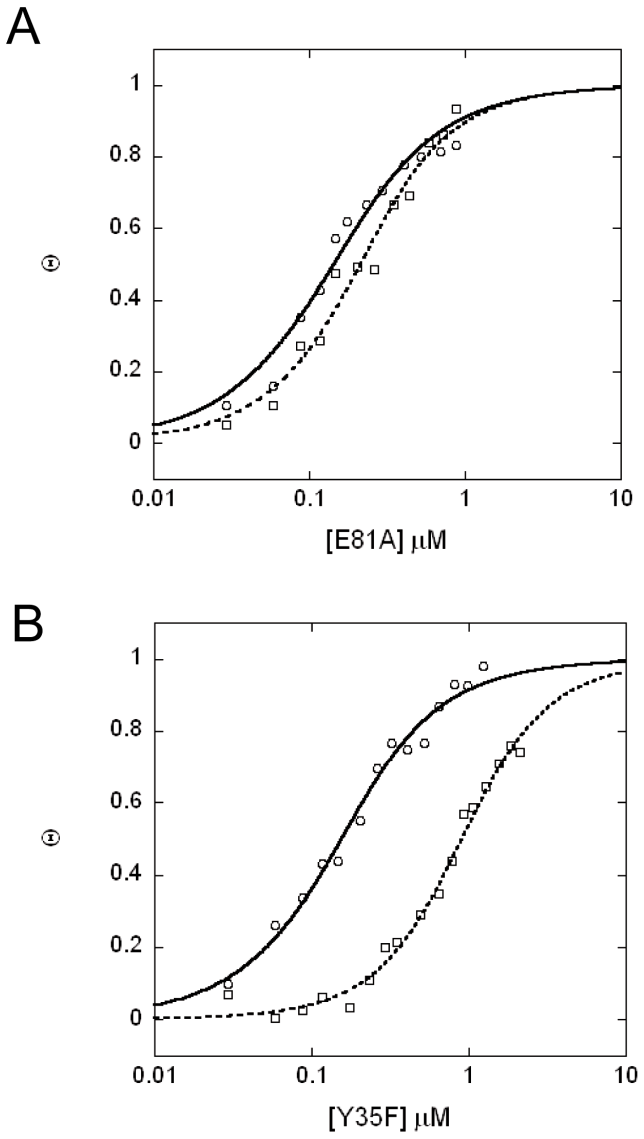

Figure 23. Normalized fluorescence anisotropy-based DNA binding isotherms of E81A (A) andY35F (B) CsoRs acquired in the absence (○) and presence (□) of stoichiometric Cu(I). Curves represent the best fit using a stepwise two tetramer DNA binding model with the fitting parameters given in Table 3. Conditions: 10 mM HEPES, 0.2 M NaCl, 2 mM DTT, pH 7.0, 25 ^{o}C.

just 0.6 kcal/mol (Figure 23, Table 3). The Cu(I) binding affinity and coordination geometry as measured using the BCS competition assay and x-ray absorption spectroscopy, respectively, reveal that the decrease in the coupling free energy is not caused by change in Cu(I) binding affinity or coordination structure, but specifically from "second coordination shell" interactions (Table 3).

More conservative substitutions of Glu81, *i.e.,* with Gln, Asp or Asn, also give rise to significant decreases in ΔG_c, to about 50% of that of wild-type CsoR, while Cu(I) binding affinities remain unaffected (Table 3). Inspection of the magnitude of ΔG_c for a double mutant, Y35F/E81Q CsoR, reveals a near additivity of $\Delta\Delta G_c$ value measured for the component single mutants ($\delta = \Delta\Delta G_c^{Y35F/E81Q} - (\Delta\Delta G_c^{Y35F} + \Delta\Delta G_c^{E81Q}) = +0.1$ kcal/mol) (see Table 3). In this case as well, the Cu(I) binding affinity is not significant decreased, consistent with a 3-coordinate Cu(I) complex. This finding reveals that these residues, while playing important functional roles, only weakly interact energetically to drive allosteric negative regulation of CsoR by Cu(I). This suggests that hydrogen bonds from Tyr35 and Glu81 *to* His61, but not to each other (Scheme 1), are most critical for Cu(I)-dependent metalloregulation in this system (Figure 24A).

Interestingly, this proposed allosteric coupling mechanism in CsoR is analogous to the proposed mechanism of zinc dependent regulation of the DNA binding affinity of the ArsR/SmtB Zn(II) sensor *S. aureus* CzrA (*66*). In CzrA, the Zn(II) ligand His97 is proposed to initiate a hydrogen bond network through its $N^{\varepsilon 2}$ face that physically links the Zn(II)-binding site via $N^{\delta 1}$ and the DNA binding site, thus stabilizing a low affinity DNA binding conformation (Figure 24B) (*66*). The native chemical ligation method

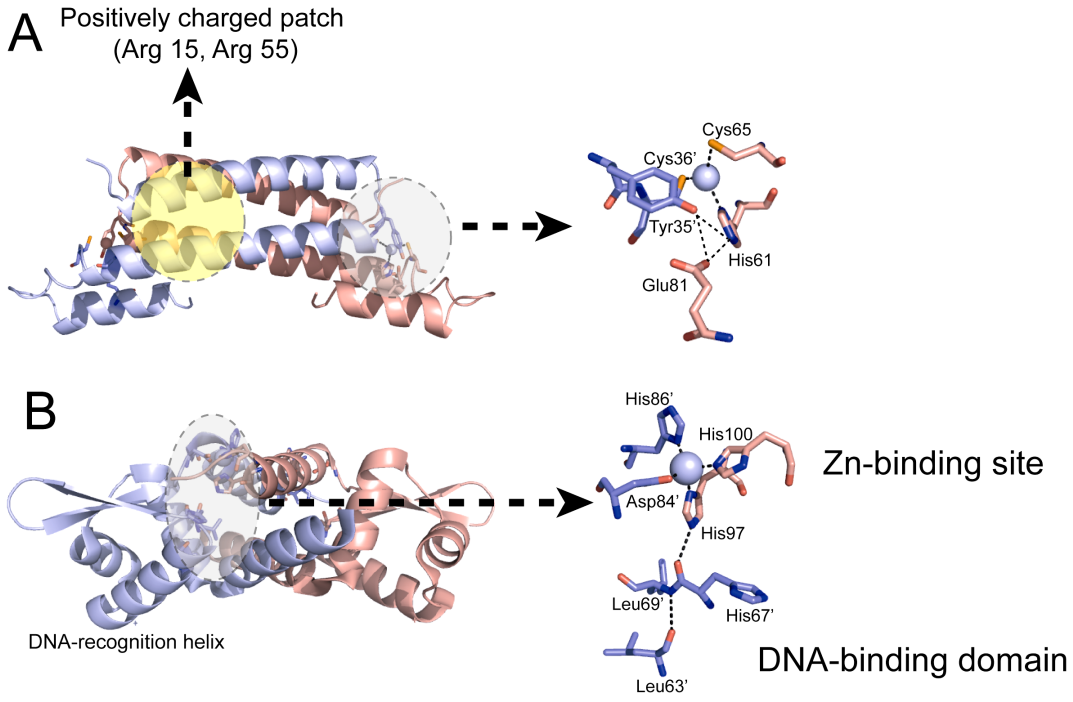

Figure 24. Proposed models for metal-dependent allosteric regulation by Cu(I) in *M. tuberculosis* CsoR (A) and by Zn(II) in *S. aureus* CzrA (B).

used here provides an excellent opportunity to specifically probe the role of this hydrogen bonding network, both energetically and possibly structurally provided sufficient ligated protein can be obtained. Below, we describe the purification scheme and present preliminary findings obtained for ligated CzrA.

A H96C substitution was first chosen to define the ligation junction with which to prepare H97MeH CzrA. As mentioned above, this strategy requires incorporation of a single non-native Cys residue at the ligation junction. Based on the structure of CzrA (*66*), His96 is solvent exposed in the C-terminal α5 helix and a previous mutagenesis study revealed that substitution of this residue (H96A CzrA) resulted in a protein with wild-type properties (Lee S. and Giedroc D.P., unpublished observations).

To verify this, ^{15}N-labeled H96C CzrA was purified. As expected, H96C CzrA retained high affinity binding to Zn(II) with $K_{Zn} \geq 10^9$ M^{-1} as measured by a competition assay with magfura-2 (Figure 25A, Table 5) (*70, 113*). More importantly, H96C CzrA binds 1 mol equiv Co(II) per monomer and binding of Co(II) gives rise to a d-d transition envelope at ~570 nm of $\varepsilon \approx 400$ $M^{-1}cm^{-1}$, consistent with a tetrahedral or distorted tetrahedral Co(II) coordination complex (Figure 25B and inset) (*70*). This spectrum is quite similar to that observed for the N_3O-Co(II) formed by wild-type CzrA (*70*). In particular, ligand to metal charge transfer (LMCT) absorption is *not* observed in the far UV region, revealing that the non-native Cys96 (the only Cys residue in H96C CzrA) is not recruited into the Co(II) coordination complex.

The DNA binding properties of H96C CzrA were next determined by fluorescence anisotropy assay. Apo-H96C CzrA binds to a 28 bp DNA derived from the

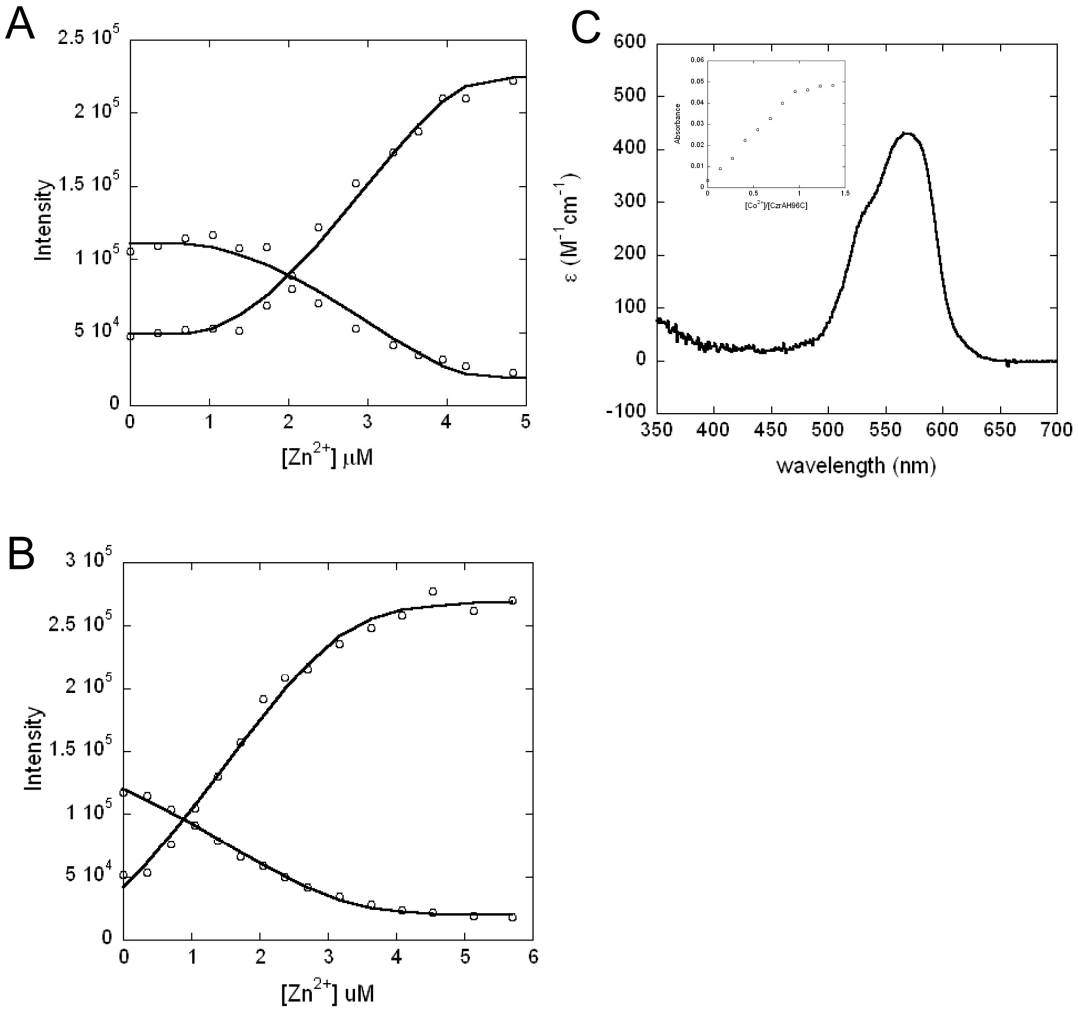

Figure 25. Zn(II) and Co(II) binding to various *S. aureus* CzrAs. Zn(II) titration into a mixture of 1.7 μM H96C CzrA (A) or H97MeH CzrA (B) in presence of 2.4 μM magfura-2. The solid curve shows a best fit using a simple competition model by Dynafit (Appendix D) with the binding parameters compiled in Table 5. (C) Apoprotein-subtracted molar absorptivity spectra of Co(II):H96C CzrA mixture at 1:1 molar ratio. The binding isotherm is shown in the inset. Conditions: 10 mM HEPES, 0.4 M NaCl, pH 7.0.

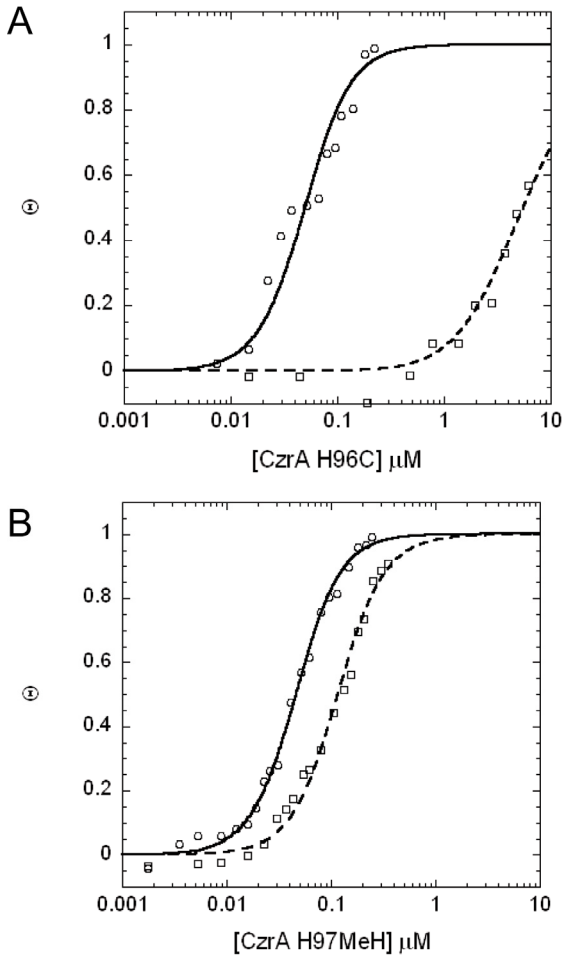

Figure 26. Normalized fluorescence anisotropy-based DNA binding isotherms of H96C (A) and H97MeH (B) CzrAs acquired in the absence (○) and presence (□) of 10 μM Zn(II). Curves represent the best fit using a 1:1 dimer:DNA binding model with the dimerization constant K_{dim} fixed at 1.7×10^5 M^{-1} with the binding parameters compiled in Table 5 (*70*). Conditions: 10 mM HEPES, 0.4 M NaCl, 2 mM DTT, pH 7.0, 25 ^{o}C, with 1 mM EDTA (○) or 10 μM Zn(II) (□).

Table 5. Summary of fitting parameters for H96C and H97MeH CzrAs in comparison with wild-type and H97D CzrAs measured previously

CzrA	K_{Zn1} (M^{-1})	K_{Zn2} (M^{-1})	K^{apo} (M^{-1})	K^{Zn} (M^{-1})	ΔG_c (kcal/mol)
Wild-type[a]	2.5 (±0.3) x 10^{12}	3.4 (±0.6) x 10^{10}	2.7 (±0.5) x 10^{10}	5.7 (±1.2) x 10^{5}	6.3 (±0.2)
Wild-type[b]	1.2 (±0.2) x 10^{12}	6.0 (±1.0) x 10^{10}	1.3 (±0.9) x 10^{11}	n.d.[d]	6.0 (±1.0)
H97D[a]	1.5 (±0.1) x 10^{7}	$\leq 10^{5}$	$\geq$ 5 x 10^{9}	$\geq$ 5 x 10^{9}	0
H96C	$\geq 10^{9}$	$\geq 10^{9}$	2.9 (±0.5) x 10^{9}	7.4 (±0.1) x 10^{5}	4.9 (±0.1)
H97MeH[c]	3.9 (±0.9) x 10^{8}	3.5 (±1.6) x 10^{6}	3.4(±0.3) x 10^{9}	5.0(±0.7) x 10^{8}	1.1 (±0.1)

[a] Numbers determined by UV-vis and fluorescence spectroscopies adapted from reference (*113, 116*). A 57 bp DNA involving the 28 bp inverted repeat was used in the DNA binding experiments and the stepwise binding constant K_1 was shown here.

[b] Numbers determined by isothermal titration calorimetry (ITC) adapted from reference (*74*).

[c] Average values of two determinations with different concentrations of H97MeH CzrA and magfura-2.

[d] Not determined.

operator-promotor region of the *czr* operon (CzrO) with an affinity of K^{apo}=2.9(±0.5) x 10^9 M^{-1}, while Zn(II)-bound H96C binds the same DNA with much lower affinity of K^{Zn}=7.4(±0.1) x 10^5 M^{-1}, resulting in a coupling free energy of +4.9 kcal/mol (Figure 26A, Table 5). These affinities as well as the coupling free energy are very similar to those reported for wild-type CzrA (*70, 113, 116*). As expected, the ^{1}H-^{15}N HSQC spectra of apo and Zn(II)-bound H96C CzrA are virtually identical to that of wild-type CzrA outside of the site of the substitution consistent with the finding that H96C CzrA exhibits near wild-type Zn(II) binding and DNA binding properties (*113, 123*).

Zn(II) only weakly regulates the DNA binding of H97MeH CzrA. Due to the fact that the CzrA1-95-intein fusion was not soluble, the yield for the CzrA1-95 peptide was very low; as a result, only limited amounts of H97MeH CzrA were obtained. The preliminary data suggest both the apo and Zn(II)-bound CzrA bind to the DNA operator with an affinity that is more similar than different (K^{apo}=3.4(±0.3) x 10^9 M^{-1}; K^{Zn}=5.0(±0.7) x 10^8 M^{-1}), resulting in an allosteric coupling free energy of +1.1 kcal/mol, significantly lower than that of the parent H96C CzrA (Figure 26B, Table 5). The Zn(II) binding affinity of H97MeH CzrA determined by a magfura-2 competition assay was found to be K_{Zn1}=3.9(±0.9) x 10^8 M^{-1} and K_{Zn2}=3.5(±1.6) x 10^6 M^{-1}(Figure 25C, Table 5). Although >1000 fold lower than wild-type CzrA, H97MeH CzrA still binds stoichiometric Zn(II) with an affinity ≥30-fold higher than other site-directed mutants of H97, *e.g.*, H97D CzrA, which binds one Zn(II) per dimer with a measurable affinity but with a non-native coordination octahedral geometry (*113*). The measurable decrease of the Zn(II) binding affinity suggests that the proposed hydrogen bond involving $N^{\varepsilon 2}$ of His97 in wild-type

CzrA may be energetically connected to Zn(II) binding, perhaps by restricting the relative conformation of the imidazole side chain and optimizing the orientation of the $N^{\delta 1}$ for Zn(II) binding. Alternatively, the methyl group might potentially perturb the local structure and therefore decrease the Zn(II) binding affinity. To test this latter idea, we have acquired ^{1}H-^{15}N HSQC spectra of H97MeH CzrA (^{15}N-labeled from residues 1-95) at 70 μM monomer in the presence and absence of saturating Zn(II) and compared these spectra with those of the parent H96C CzrA. Although the quality of these spectra of H97MeH CzrA is poor due to the low sample concentration, several key conclusions can be reached by inspection of the chemical shift perturbation maps shown (Figure 27). Incorporation of the methyl group in H97MeH CzrA causes only a local perturbation in the structure of the CzrA dimer, since the chemical shift differences between H97MeH and parent H96C CzrAs are small and localized in both the absence and presence of saturating Zn(II) (Figure 27A and B). Remarkably, Zn(II) binding to H97MeH CzrA causes a conformational change in the dimer that is essentially indistinguishable from that of H96C CzrA, as shown by the similar chemical shift perturbation maps (Figure 27C and D). These observations suggest that the hydrogen bonding network initiated by the $N^{\varepsilon 2}$ atom of H97 is not required to drive the conformational change in CzrA upon Zn(II) binding, the importance of which will be further discussed below.

DISCUSSION

In this chapter, unnatural amino acid incorporation was used to probe what we hypothesize is the “second coordination shell” that links metal binding to DNA binding

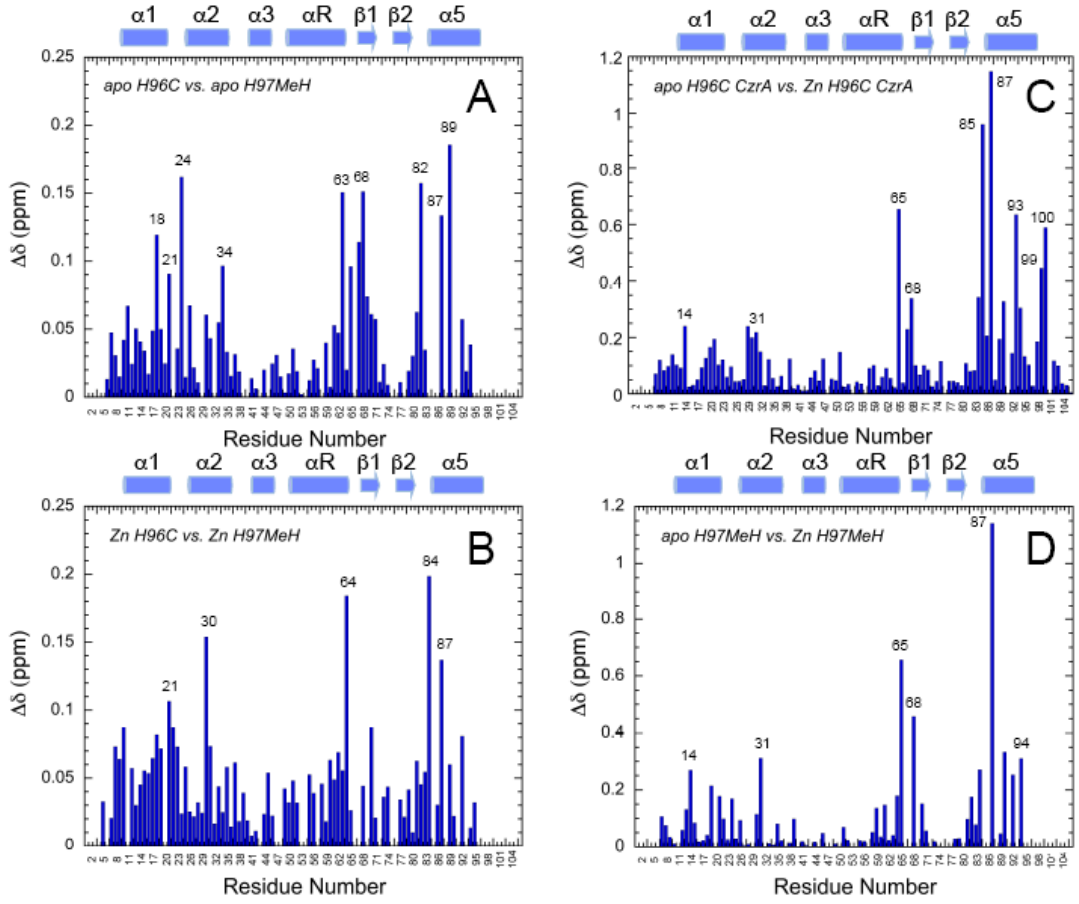

Figure 27. Chemical shift perturbation maps of H96C and H97MeH CzrAs. Each shows chemical shift perturbation of apo H96C vs. apo H97MeH CzrA (A), Zn(II)-bound H96C vs. Zn(II)-bound H97MeH (B), apo H96C vs. Zn(II) bound H96C CzrA and apo H97MeH vs. Zn(II)-bound H97MeH CzrA (D). In H97MeH CzrA, residues 96-106 are not ^{15}N-labeled and thus cannot be observed. Other residues for which crosspeaks could not be unambiguously assigned are given a $\Delta\delta$=0. These data were acquired, processed and analyzed by Alfredo J. Guerra (Guerra A.J., Ma Z. and Giedroc D.P., unpublished results). Conditions: 10 mM MES, 50 mM NaCl, pH 6.0, 40 ^{o}C.

in both *Mtb* CsoR and *S. aureus* CzrA. This strategy allows us to surgically perturb the hydrogen bonding interactions involving the $N^{\varepsilon 2}$ face of a key liganding histidine without affecting the other roles that this His could play, *e.g.*, in metal coordination by $N^{\delta 1}$. Such a semisynthetic approach is capable of introducing amino acid analogs anywhere into a protein; however, this approach is clearly limited by the length of the peptide to be synthesized by solid phase peptide synthesis and the potentially poor solubility of the intein fusion and cleaved proteins. An alternative strategy is to fully synthesize the entire protein in pieces, methods of which have been optimized and developed (*124*). Such a strategy involves dividing the protein into several peptides and stepwise ligating them together. However, as determined by the nature of the ligation reaction, a Cys residue is required at each ligation junction; as a result it is important to verify that the incorporation of non-native Cys residues does not affect the functional properties of the resultant protein. The application of such a strategy to metal binding proteins requires extra caution since Cys residues are very good metal binding ligands. Introducing multiple Cys residues into these proteins may cause an unanticipated change in metal coordination structure, enhance non-specific metal binding or lead to unanticipated disulfide bond formation, each of which might significantly interfere with the structure and function of the protein.

Another complementary methodology to site-specifically incorporate an unnatural amino acid is via utilization of an orthologous tRNA-aminoacyl-tRNA synthetase pair which can specifically incorporate amino acid analogs or other biochemical and biophysical probes into a protein co-translationally in vivo, typically

via terminator codon supression (*114*). However, such a strategy requires a bacterial strain carrying a specific orthologous tRNA synthetase that can charge the tRNA corresponding to an amber codon with an amino acid analog. Therefore, to incorporate different His analogs into either CsoR or CzrA would require screening procedures to obtain such strain (*114*). Since such a strain to incorporate His analogs is not yet available to our knowledge, due to the relatively small size of each protein studied here, a semisynthetic approach was chosen in this study.

The proposed allosteric regulation mechanism for *Mtb* CsoR is analogous to that previously proposed for CzrA and is further investigated here. This is remarkable since these two proteins belong to different families of metalloregulatory proteins with completely different structures (Figure 24). And yet, nature has evolved in these two proteins analogous mechanisms for metal regulation. The approach outlined here provides a tool to probe such a mechanism when high resolution structures of different allosteric states of the protein are not available. Such mechanism may not be operative in CsoR orthologs, including the Ni(II)/Co(II) sensor RcnR or the putative CsoR-like oxidative stress sensors simply because that Tyr35 and Glu81 are not conserved in these proteins (see alignment in Figure 9).

Both H61MeH and H61Thz *Mtb* CsoRs are capable of forming 3-coordinate Cu(I) complexes with an equilibrium affinity close to wild-type CsoR. In contrast, our preliminary studies on H97MeH CzrA reveal a ≈1000 fold decrease Zn(II) affinity of each of the two sites in the homodimer (Table 5). Previous crystallographic and NMR studies of apo and Zn(II)-bound CzrA suggest that formation of the hydrogen bond

network initiated by the $N^{\varepsilon 2}$ face of His97 physically links the Zn(II) binding and DNA binding sites, and is used to drive a conformational change that greatly reduces the DNA binding affinity. Data here suggest that this hydrogen bonding network may also influence the Zn(II) binding, possibly via confining the conformation of the imidazole side chain of His97. Formation of hydrogen bond network may enthalpically favor the Zn(II) binding. A detailed thermodynamics study using isothermal titration calorimetry (ITC) on wild-type CzrA has recently been carried out in our laboratory in order to deconvolute the enthalpic and enthropic contributions to the allosteric coupling free energy that links the binding of Zn(II) and DNA to CzrA (*74*). It will be of great interest to investigate H97MeH CzrA in this context which may provide information on the energetic role of this hydrogen bonding network in Zn(II) binding. However, such study requires high concentrations of protein and the yield of the semisynthesis strategy outlined in this chapter is likely too low. Alternatively, a totally synthetic approach or one that involves an in vivo codon redefinition may be used (*114, 124*), although challenges associated with these two strategies need to be considered.

The substantial decrease in Zn(II) affinity can also be a result of a change in the structure from the additional methyl groups in the H97MeH CzrA dimer. To begin to test this idea, uniformly ^{15}N-labeled CzrA1-95-intein fusion protein was purified and the resultant ligated H97MeH CzrA investigated by ^{1}H-^{15}N NMR spectroscopy (Figure 27). The ^{1}H-^{15}N HSQC spectra for residues 1-95 of the parent H96C CzrA and H97MeH CzrA are very similar, revealing that the methyl group does not significantly perturb the protein fold in the absence or presence of Zn(II) (Figure 27A and B). Strikingly, the

chemical shift perturbations that occur upon Zn(II) binding to H96C vs. H97MeH CzrA (Figure 27C and D) are also very similar to one another, which suggests that the average conformations of these two proteins are indeed similar in both functional states. This would seem to argue against an unanticipated steric effect of the additional methyl group and is consistent with the conclusion that the binding of Zn(II) to H97MeH CzrA results in a conformational change that is similar to that of the parent H96C CzrA. In fact, the identity of the intersubunit perturbation of residues 65 and 68 in H96C and H97MeH CzrAs virtually ensures this (*65*). Thus, the methyl group does *not* intrinsically block the formation of the allosterically inhibited state in the absence of DNA.

How then does loss of this hydrogen bonding interaction nearly abrogate inhibition of DNA binding by Zn(II)? One strong possibility is that the bound DNA effectively prevents this conformational change which is required to drive CzrA off the operator. Indeed, a major role of Zn(II) binding by CzrA is to "freeze out" a conformational state(s) that has low affinity for the DNA (*65*). The $N^{\varepsilon 2}$ hydrogen bonding network may therefore be specifically required to stabilize this dynamically "rigidified" state, which at the same time, might enhance K_{Zn}. Detailed solution NMR and structural studies will be required to obtain direct support for this idea. Although the methyl group perturbations appear small, a thiazole or oxazole substitution of the imidazole side chain may further minimize any unanticipated structural perturbations that might result. It is important to point out, however, that the methyl group and thioether substitutions of the $N^{\varepsilon 2}$ atom of His61 in *Mtb* CsoR were functionally quite similar. These experiments are underway in our laboratory.

CHAPTER IV

BIOCHEMICAL PROPERTIES OF *B. subtilis* CsoR*

INTRODUCTION

In previous chapters, the characterization of *Mtb* CsoR as the founding member of a new metalloregulatory family was presented, as were insights into the mechanism of Cu(I)-dependent allosteric negative regulation of DNA binding by employing both conventional and unnatural amino acid substitution methods. Further insights into this new family of metalloregulatory proteins can be obtained from investigation of the known or proposed CsoRs from other microorganisms. In this context, known Cu(I)-sensing CsoR from *B. subtilis* (*Bsu* CsoR) is discussed in this chapter, which will be followed by a focus on a putative Cu(I)-sensing CsoR from *S. aureus* (*Sau* CsoR).

With the publication of the structure and function of *Mtb* CsoR, the characterization of *Bsu* CsoR as a Cu sensor that regulates the transcription of *copZA* operon was reported soon after. *copZ* encodes the Cu chaperone while *copA* encodes the Cu-efflux P-type ATPase (*105*). *Bsu* CsoR shares high sequence similarity with *Mtb* CsoR and has been shown to bind to a pseudo-palindromic DNA in the operator-promoter region of *copZA* operon (*Bsu* CopO) and repress the transcription (Figure 9). Addition of Cu inhibits the binding and derepresses the transcription, allowing the

---

* Reproduced in part with permission from "Molecular insights into the metal selectivity of the copper(I)-sensing repressor CsoR from *Bacillus subtilis"* Ma Z., Cowart D. M., Scott R. A. and Giedroc D. P., 2009, *Biochemistry,* 48(15), 3325-3334, Copyright [2009] American Chemical Society.

expression of CopZ/CopA proteins to traffic and efflux the excess Cu out of the cytoplasm.

Here, using a series of biochemical and biophysical experiments, we show that *Bsu* CsoR binds 1 mol equiv Cu(I) per monomer with very high affinity ($\geq 10^{19}$ M^{-1}). X-ray absorption spectroscopy (XAS) shows Cu(I) adopts, as expected, an S_2N coordination geometry similar to *Mtb* CsoR (*39*). Unlike *Mtb* CsoR, both apo and Cu(I)-bound *Bsu* CsoRs are non-dissociable tetramers in the low micromolar monomer concentration range. Size exclusion chromatography reveals apo-*Bsu* CsoR binds to a 30 bp *copZA* operator DNA (*Bsu* CopO) with a saturating stoichiometry of 8 monomers, or two tetramers, to one two-fold symmetric, pseudo-palindromic 30 bp DNA sequence. The DNA binding affinities were further determined by fluorescence anisotropy for both apo and Cu(I)-bound *Bsu* CsoRs under defined solution conditions. The Cu(I)-dependent regulation of DNA binding is abrogated in an E90A *Bsu* CsoR mutant. Interestingly, *Bsu* CsoR is also capable of binding other divalent metal ions including Co(II), Zn(II) and Ni(II), and in fact binds Ni(II) and Zn(II) with 10^8-10^9 M^{-1} affinities at equilibrium. While with weaker affinity than Cu(I), Zn(II) may well be partly bound to CsoR in vivo. However, each of these metals adopts a non-native (non-trigonal) coordination geometry and each fails to strongly negatively regulate operator DNA binding in vitro.

MATERIALS AND METHODS

Plasmid construction, protein expression and purification. The *Bsu* CsoR-pET16b expression plasmid was a generous gift of Dr. John D. Helmann (Cornell University)

(*105*). Amino acid substitutions were introduced into this plasmid by site-directed quick-change mutagenesis and the integrity of the resulting plasmids were confirmed by DNA sequencing. Wild-type and E90A *Bsu* CsoRs were expressed and purified using similar procedures as described previously for *Mtb* CsoR in Chapter II (*39, 105*). Expression plasmids containing wild type or mutant *Bsu* CsoR were transformed into *E. coli* BL21(DE3) and grown in LB media until OD_{600} reached 0.6-0.8. 0.4 mM IPTG was then added and cells were grown for additional 2 h before harvesting by low speed centrifugation. Cell pellets were suspended in 200 mL Buffer A (25 mM MES, 2 mM DTT, 1 mM EDTA, pH 5.8) and lysed by sonication. The lysate was centrifuged and 0.15% (v/v) polyethyleneimine (PEI) was added to the supernatant to precipitate the nucleic acids. *Bsu* CsoR remained in the supernatant and was subjected to $(NH_4)_2SO_4$ precipitation and the pellet was resuspended in Buffer A and dialyzed against Buffer A containing 0.05 M NaCl. The sample is then purified by SP Fast Flow, Superdex 200 size exclusion chromatography as described previously (*39*). The resultant proteins were pooled, concentrated and dialyzed against Buffer N (10 mM MES, 0.2 M NaCl, pH 6.5) in an anaerobic Vacuum Atmospheres glovebox. The purity of the final products was estimated by visualization of Coomassie-stained 18% Tris-glycine SDS-PAGE gels to be ≥90%. Protein concentration was determined by UV absorption using ε_{280nm}=1615 M^{-1} cm^{-1} and free thiols were determined by the DTNB assay to be more than 95% of expected value (*39, 105*). Less than 0.1% copper was detected by atomic absorption spectroscopy in all purified protein samples.

Cu(I) binding and BCS competition monitored by UV-vis absorption spectroscopy. These experiments were carried out anaerobically in Buffer N as described in Chapter II.

Cu(I)-binding monitored by tyrosine fluorescence. These experiments were carried out anaerobically in Buffer N as described in Chapter II.

Cu(I) X-ray absorption spectroscopy. The XAS samples were prepared anaerobically in 10 mM MES, 0.2 M NaCl, 30% (v/v) glycerol, pH 6.5 and data were collected and analyzed as described in Chapter II.

Sedimentation velocity and equilibrium experiments. All analytical ultracentrifugation experiments were carried out using a Beckman model Optima XL-I analytical ultracentrifuge equipped with an An-60 Ti rotor in the Physical Biochemistry Instrumentation Facility at Indiana University. All samples were prepared in buffer N and loaded into centerpieces inside the anaerobic glovebox. 110 μL samples for equilibrium experiments were prepared at 8 μM, 14 μM and 20 μM monomer concentrations (≈0.3, 0.5 and 0.8 OD_{230} initially) and loaded into 6-channel Epon charcoal-filled centerpieces. Intensity scans at 230 nm were taken at speeds of 19,300, 30,600 and 38,700 rpm at 20 ^{o}C. All equilibrium data were fit globally to a single species model using Ultrascan as described (*70*). For sedimentation velocity experiments, 450 μL samples were loaded into a two-channel aluminum centerpiece with 1.2 cm path length. The rotor speed was 60,000 rpm at 20^{o}C and intensity data at 230 nm were collected as a function of time. Sample concentrations were 8 μM and 20 μM *Bsu* CsoR monomer (≈0.3 and 0.8 OD_{230} initially). Data were analyzed using

Ultrascan software interfaced with a genetic algorithm and Monte Carlo analysis package essentially as described (*125-128*).

Size exclusion chromatography. A 30 bp DNA derived from the *copZA* operator-promoter region (*Bsu* CopO: 5'-TTGTAATACCCTACGGGGGTATGGTAGGAT-3' and the complementary sequence) (Operon, AL) was used for all DNA binding experiments. 10 μM DNA was mixed with different concentrations of *Bsu* CsoR monomer up to 100 μM in buffer N with 2 mM DTT in room temperature. 100 μL of each mixture was loaded onto a Tricon Superdex 200 column (GE Healthcare, NJ) on an Äkta-10 purifier. Elution profiles were obtained by monitoring the absorption at 240 nm, 260 nm and 280 nm simultaneously.

Fluorescence anisotropy. A 30 bp 5'-fluorescein labeled DNA (Operon, AL) with the same sequence as above was used. The double stranded DNA was made by mixing the labeled strand with 1.1 mol equiv of the unlabeled complementary strand. The mixture was heated at 95 ^{o}C for 10 min and then slowly cooled to room temperature. Formation of double stranded DNA was further confirmed by native TBE polyacrylamide gel electrophoresis. A typical anisotropy experiment was done with 4 nM DNA in 10 mM MES, 0.4 M NaCl, 2 mM DTT, pH 6.5 at 25^{o}C unless noted otherwise. Anisotropy was monitored by exciting the fluorescein at 487 nm. With apo- or Cu(I)-bound *Bsu* CsoRs added, the average anisotropy of 5 measurements was reported for each addition. For Ni(II)- and Zn(II)-bound *Bsu* CsoRs, 1 mol equiv of metal ions were mixed with *Bsu* CsoR as titrant; an additional 5 μM Ni(II) or Zn(II) was present in the cuvette to ensure that only the metal-bound CsoR was present during these titrations. The resulting data

were fitted to a stepwise model involving the binding of two non-dissociable tetramers to one DNA using Dynafit assuming a linear change in anisotropy with fractional saturation of the DNA (Appendix C) (*106, 110*). Since Cu(I)-bound *Bsu* CsoR does not reach saturation, the maximum anisotropy value was fixed at the same value as that obtained for apo-*Bsu* CsoR. The coupling free energy, ΔG_c, is operationally defined by ΔG_c=-RTln($K_1^{Cu}K_2^{Cu}/K_1^{apo}K_2^{apo}$), where K_1^{apo}, K_2^{apo}, K_1^{Cu} and K_2^{Cu} are stepwise DNA binding constants for apo and Cu(I)-bound *Bsu* CsoRs, respectively. This formalism for ΔG_c was used since the saturating and presumably fully repressing complex invokes two bound tetramers bound per palindromic operator DNA segment, as well as the high inverse correlation between the magnitudes of K_1 and K_2.

Other metal binding experiments. Zn(II) binding was monitored by a chelator competition assay with magfura-2 (K_{Zn}=5.0 x 10^7 M^{-1} at pH 7.0) using UV-vis absorption spectroscopy as previously described (*70, 110*). The data were fit using a competitive binding model with Dynafit (*106*) to determine the Zn(II) binding affinity (Appendix D). Co(II) and Ni(II) binding experiments were carried out as described previously (*70, 110*) in Buffer N. Ni(II) binding affinity was determined by a competition assay with EGTA (*129*). All concentrations of metal titrants were determined using atomic absorption spectroscopy.

RESULTS

Bsu CsoR binds 1 mol equiv Cu(I) per monomer with an affinity higher than that of BCS. It has been previously shown that *Bsu* CsoR regulates the expression of *copZA* operon

by binding to the promoter region and that the addition of $CuSO_4$ and DTT as reductant resulted in disruption of the DNA binding. It was therefore proposed that the DNA binding affinity of *Bsu* CsoR is regulated by Cu(I) binding. Here, we show that *Bsu* CsoR binds Cu(I) directly in vitro by both UV-vis and tyrosine fluorescence spectroscopy.

Addition of Cu(I) into an anaerobic solution of *Bsu* CsoR causes increased absorption in the ultraviolet region ($\varepsilon_{240nm}\approx16{,}000\ M^{-1}cm^{-1}$); this reports on the formation of thiolate-copper coordination bonds and the spectrum is quite similar to that of Cu(I)-saturated *Mtb* CsoR (*39, 110*). This increase is saturable at ≈1.0 mol equiv Cu(I) per monomer (Figure 28A). Significant quenching of tyrosine fluorescence is observed upon Cu(I) binding as shown in Figure 28B. Maximum quenching is achieved upon addition of ≈1.2 mol equiv Cu(I). Therefore, both UV-vis and tyrosine fluorescence suggest *Bsu* CsoR binds ≈1 Cu(I) ion per mol monomer.

The Cu(I) binding affinity was estimated by a competition experiment using BCS, a Cu(I) specific competitor which can form a $Cu(I)(BCS)_2$ complex that absorbs at 483 nm with a β_2=19.8 (*107*). Figure 29 shows the change of the absorbance at 483 nm when Cu(I) is added to a mixture of 20 μM *Bsu* CsoR monomers and 50 μM BCS. No change of absorbance is observed until about 20 μM Cu(I) is added, suggesting the Cu(I) added initially is bound to *Bsu* CsoR but not BCS. After *Bsu* CsoR is saturated with 1 mol equiv Cu(I), additional Cu(I) forms a complex with BCS reported by the linear increase of absorbance at 483 nm, which is saturated at about 45 μM total Cu(I), reporting on the formation of ≈25 μM $Cu(I)(BCS)_2$ complex. The fact that no

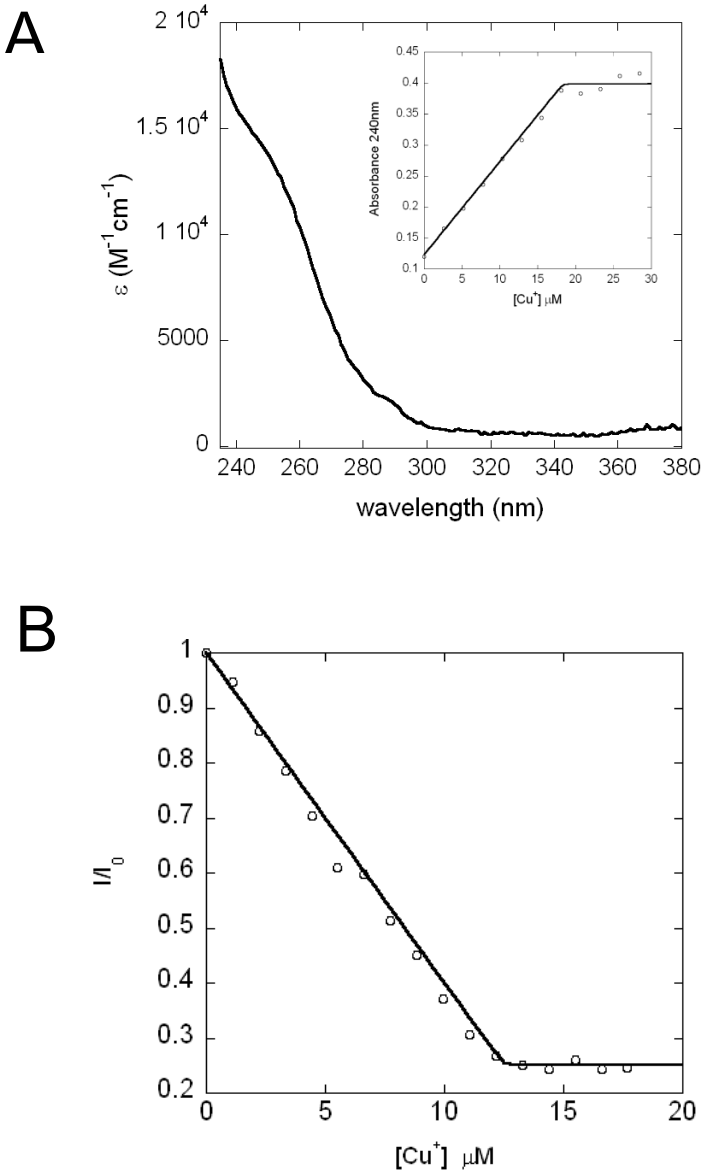

Figure 28. *Bsu* CsoR binds 1 monomer mol equiv of Cu(I). (A) Apoprotein-subtracted molar absorptivity spectrum of Cu(I):*Bsu* CsoR mixture at 1:1 molar ratio with the binding isotherm shown in the inset. (B) Anaerobic titration of 10 μM apo-*Bsu* CsoR with Cu(I) as monitored by change in tyrosine fluorescence. Conditions: 10 mM MES, 0.2 M NaCl, pH 6.5, 25^{o}C.

$Cu(I)(BCS)_2$ complex is formed until saturation of *Bsu* CsoR suggests that *Bsu* CsoR binds Cu(I) with much higher affinity than BCS. Due to the sharpness of the transition, this binding isotherm provides only a lower limit of the apparent binding affinity of $K_{Cu} \geq 10^{19}$ M^{-1} when fit to a single site binding model [1:1 Cu(I) per protomer] under these solution conditions (Table 6). Although CsoR is a tetramer (see below), microscopic binding constants for individual sites in the tetramer, and thus any cooperativity of metal binding to these sites, cannot be resolved by this assay under these conditions given the stoichiometric nature of the complex formation (Figure 12).

Cu(I) forms a trigonal S_2N coordination site in Bsu CsoR. Copper K-edge X-ray absorption spectroscopy was used to determine the structure of Cu(I) complex formed at 0.8:1 Cu(I):*Bsu* CsoR monomer molar ratio (chosen to assure that all Cu(I) was bound to protein). The pre-edge peak at 8940 eV in the edge spectrum shown in Figure 30A is consistent with a 1s→4p excitation typical for 3-coordinate Cu(I) (*122*). The Cu K-edge extended X-ray absorption fine structure (EXAFS) spectrum as well as the Fourier transforms are shown in Figure 30B; structural parameters derived from EXAFS curve fitting are shown in Table 7. The data are best fit to a 3-coordinate model, with two Cu-S interactions at 2.20 Å and a single Cu-N/O interaction (fixed at 2.05 Å). This Cu-S distance is consistent with 3-coordinate Cu(I) and is similar to the Cu-S distance previously reported for *Mtb* CsoR. Significant outer-shell scattering observed between 3 and 4 Å is consistent with the third coordinating ligand being a nitrogen atom from a His residues, possibly from His70 which corresponds to known Cu(I) ligand His61 in *Mtb* CsoR (*39*). These data are consistent with the idea that Cu(I) is coordinated by Cys45',

Table 6. Metal and DNA binding affinities and allosteric coupling free energies for metalloderivatives of wild-type and E90A *Bsu* CsoRs.

Bsu CsoR	metal	metal binding affinity[a]	DNA binding affinity[b]		ΔG_c
		(M^{-1})	K_1 (M^{-1})	K_2 (M^{-1})	(kcal/mol)
Wild-type	apo	-	3.1 (±0.8) x 10^7	8.3 (±2.2) x 10^7	-
	Cu(I)	$\geq 10^{19}$	2.9 (±0.4) x 10^6	$\leq$1.0 x 10^5	$\geq$ +5.4
	Co(II)	$\leq 10^5$	-	-	-
	Ni(II)	3.6 (±0.3) x 10^9	5.7 (±1.0) x 10^6	3.1 (±0.5) x 10^7	+1.6 (±0.3)
	Zn(II)	1.6 (±0.1) x $10^{8,c}$	1.0 (±0.3) x 10^7	1.5 (±0.4) x 10^7	+1.7 (±0.3)
E90A	apo	-	9.5 (±3.0) x 10^6	1.3 (±0.4) x 10^7	-
	Cu(I)	$\geq 10^{19}$	4.8 (±2.0) x 10^6	1.1 (±0.4) x 10^8	–0.9 (±0.4)

[a]The results of fitting to a simple 1:1 (metal:monomer) binding model. [b]Solution conditions: 10 mM MES, 0.4 M NaCl, 2 mM DTT, pH 6.5, 25 ^oC. We note that unique values of K_1 and K_2 are not readily resolved in this assay (see Methods) [c]A fit to two-site step-wise dimer binding models gives K_{Zn1}= 1.7 (±0.4) x 10^9 M^{-1}; K_{Zn2}= 4.5 (±0.3) x 10^7 M^{-1}.

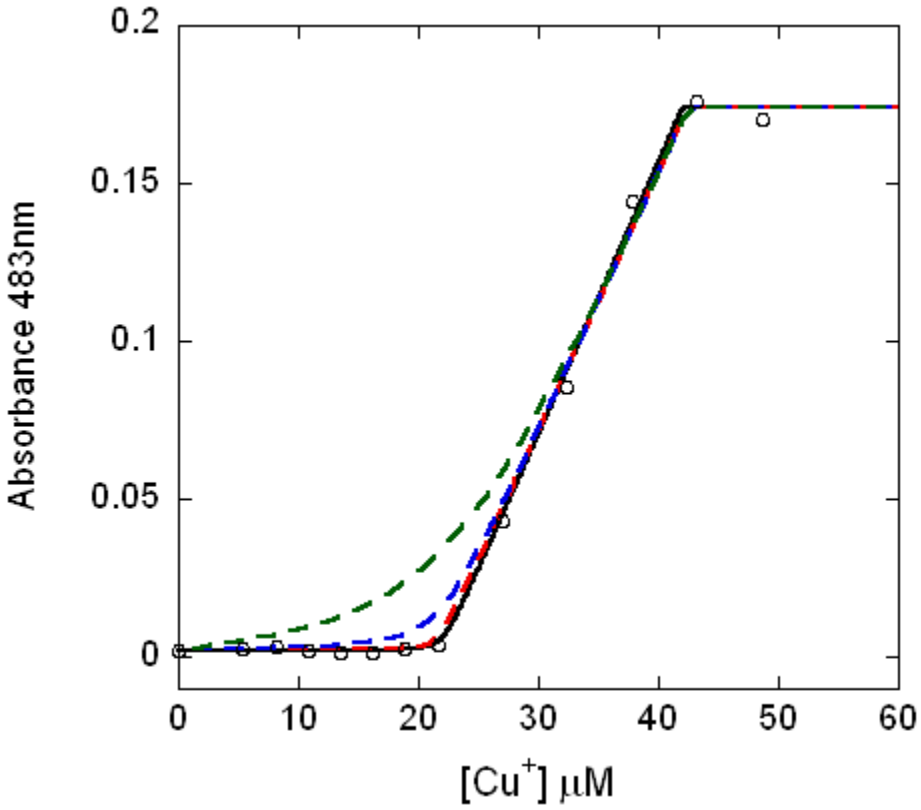

Figure 29. BCS competition experiment with wild-type *Bsu* CsoR. Different amounts of Cu(I) were mixed with 20 μM *Bsu* CsoR monomer and 50 μM BCS in buffer N with the absorption at 483 nm plotted against the total Cu(I) concentration. The solid curve represents the best-fit to a simple competition model (see text for details). The dash lines represent simulations with log K_{Cu}=17 (green), 18 (blue) and 19 (red) under the same conditions. Conditions: 10 mM MES, 0.2 M NaCl, pH 6.5.

His70 and Cys74 in *Bsu* CsoR dimer, which are analogous to the Cu(I) ligands in *Mtb* CsoR dimer. Virtually identical spectra and curve-fitting results were obtained for E90A *Bsu* CsoR, suggesting no significant change in the first-shell coordination of Cu(I) in this mutant (Figure 30C, Table 7).

Both apo and Cu(I)-bound Bsu CsoRs are tetramers. A preliminary characterization using Superdex 200 size exclusion chromatography on both apo and Cu(I)-bound *Bsu* CsoR revealed a single species roughly corresponding to a homotetramer in both cases. To better characterize the assembly state of *Bsu* CsoR in solution, analytical sedimentation equilibrium and velocity ultracentrifugation experiments were carried out with apo and Cu(I)-bound *Bsu* CsoRs in the low micromolar monomer concentration range.

The equilibrium scans were globally fit with a single ideal species model, with representative data and fits shown for the apo- and Cu(I)-bound *Bsu* CsoRs in Figure 31A and Figure 31B, respectively. For apo and Cu(I)-bound *Bsu* CsoR, the single species molecular weights of 41.0±0.5 kDa and 39.8±0.6 kDa, respectively, were obtained. This suggests that the assembly state of both forms of CsoR is tetrameric under these solution conditions (expected molecular weight of 45.9 kDa) and a lower limit of the dimer-tetramerization equilibrium constant is 10^7 $(M\ dimer)^{-1}$. This is in full agreement with results for the Ni(II)/Co(II) sensor *E. coli* RcnR (*103*), but distinct from what was previously reported for *Mtb* CsoR, where a significant dimer-tetramer equilibrium was observed (*39*). One possible explanation is that the dimer-tetramer

Table 7. XAS fitting parameters for *Bsu* CsoR[a]

Sample (k range) $\Delta k^3\chi$	Fit	Shell	R_{as} (Å)	σ_{as}^2 (Å^2)	ΔE_0 (eV)	f'[b]
WT *Bsu* CsoR	1	Cu-S_2	2.20	0.0023	-3.853	0.070
(k = 2-12Å^{-1})		Cu-N_1	<u>2.05</u>[c]	<u>0.0016</u>	[-3.853][d]	
$\Delta k^3\chi$ = 12.729		Cu-C_1	[3.04]	[0.0032]	[-3.853]	
		Cu-C_1	[3.08]	[0.0033]	[-3.853]	
		Cu-N_1	[4.21]	[0.0020]	[-3.853]	
		Cu-C_1	[4.24]	[0.0020]	[-3.853]	
E90A *Bsu* CsoR	1	Cu-S_2	2.20	0.0024	-4.322	0.076
(k = 2-12Å^{-1})		Cu-N_1	<u>2.05</u>	<u>0.0016</u>	[-4.322]	
$\Delta k^3\chi$ = 14.157		Cu-C_1	[3.04]	[0.0032]	[-4.322]	
		Cu-C_1	[3.08]	[0.0033]	[-4.322]	
		Cu-N_1	[4.21]	[0.0020]	[-4.322]	
		Cu-C_1	[4.24]	[0.0020]	[-4.322]	

[a] Shell is the chemical unit defined for the multiple scattering calculation. Subscripts denote the number of scatterers per metal. R_{as} is the metal-scatterer distance. σ_{as}^2 is a mean square deviation in R_{as}. ΔE_0 is the shift in E_0 for the theoretical scattering functions.

[b] f' is a normalized error (chi-squared):

$$f' = \frac{\left\{\sum_i \left[k^3\left(\chi_i^{obs} - \chi_i^{calc}\right)\right]^2 / N\right\}^{1/2}}{\left[\left(k^3\chi^{obs}\right)_{max} - \left(k^3\chi^{obs}\right)_{min}\right]}$$

c Underlined numbers were fixed at the indicated value (not optimized).

[d] Numbers in square brackets were constrained to be either a multiple of the above value (σ_{as}^2) or to maintain a constant difference from the above value (R_{as}, ΔE_0).

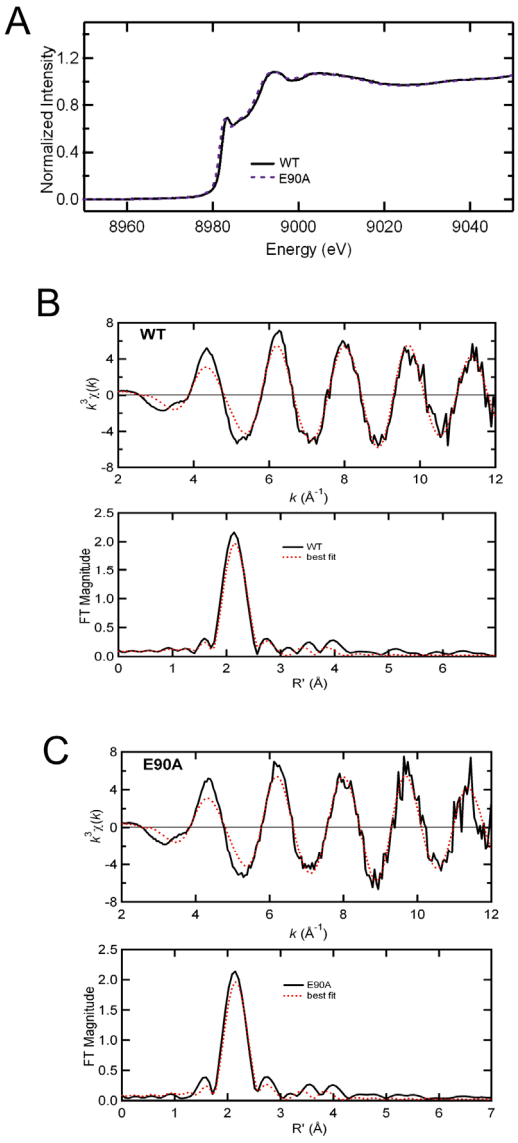

Figure 30. X-ray absorption spectroscopy (XAS) of Cu(I)-bound *Bsu* CsoR. (A) Cu K-edge X-ray absorption edge spectra of Cu(I)-bound WT (solid) and E90A *Bsu* CsoRs (dashed). Copper K-edge EXAFS spectra and the Fourier transforms (k^3 weighted, k=2-12 Å^{-1}) for Cu(I)-bound WT (B) and the E90A *Bsu* CsoRs (C). In B and C, solid curves represent the experimental data and dashed curves represent best fits with parameters compiled in Table 7.

equilibrium of *Mtb* CsoR is influenced by the 30 amino acid C-terminal tail found only in CsoR homologs from pathogenic mycobacteria.

To further confirm the assembly state and obtain further insights into the hydrodynamic properties of the apo- and Cu(I)-bound tetramers, sedimentation velocity experiments were carried out under the same solution conditions. Consistent with the equilibrium experiments, a single boundary was observed for all samples; quantitative analysis of these distribution plots is consistent with a single species of sedimentation coefficient 3.03 S for apo-*Bsu* CsoR and 3.34 S for Cu(I)-bound *Bsu* CsoR (Figure 31C and Figure 31D, respectively). The fitted parameters and predicted hydrodynamic characteristics are compiled in Table 8. These data taken collectively suggest that the dominant assembly state of each form of CsoR is a highly asymmetric tetramer with Cu(I) binding inducing a small but measurable change in the hydrodynamic properties of the molecule.

Apo-Bsu CsoR binds operator DNA with 2:1 tetramer:DNA stoichiometry. It was previously shown that *Bsu* CsoR is capable of binding to an operator in the promoter region of *copZA* operon, although the stoichiometry and affinity were not investigated in detail (*105*). Size exclusion chromatography was first used to determine the DNA binding stoichiometry (Figure 32A). Addition of 40 μM apo-*Bsu* CsoR monomer to 10 μM DNA gives rise to a new peak with an elution volume of 13.7 mL, assigned to a *Bsu* CsoR-DNA complex, with a significant fraction of free DNA. Addition of 80 μM apo-*Bsu* CsoR monomer to 10 μM DNA reveals that only the 13.7 mL peak is observed with no evidence of free DNA, suggesting that all the protein and DNA added form the

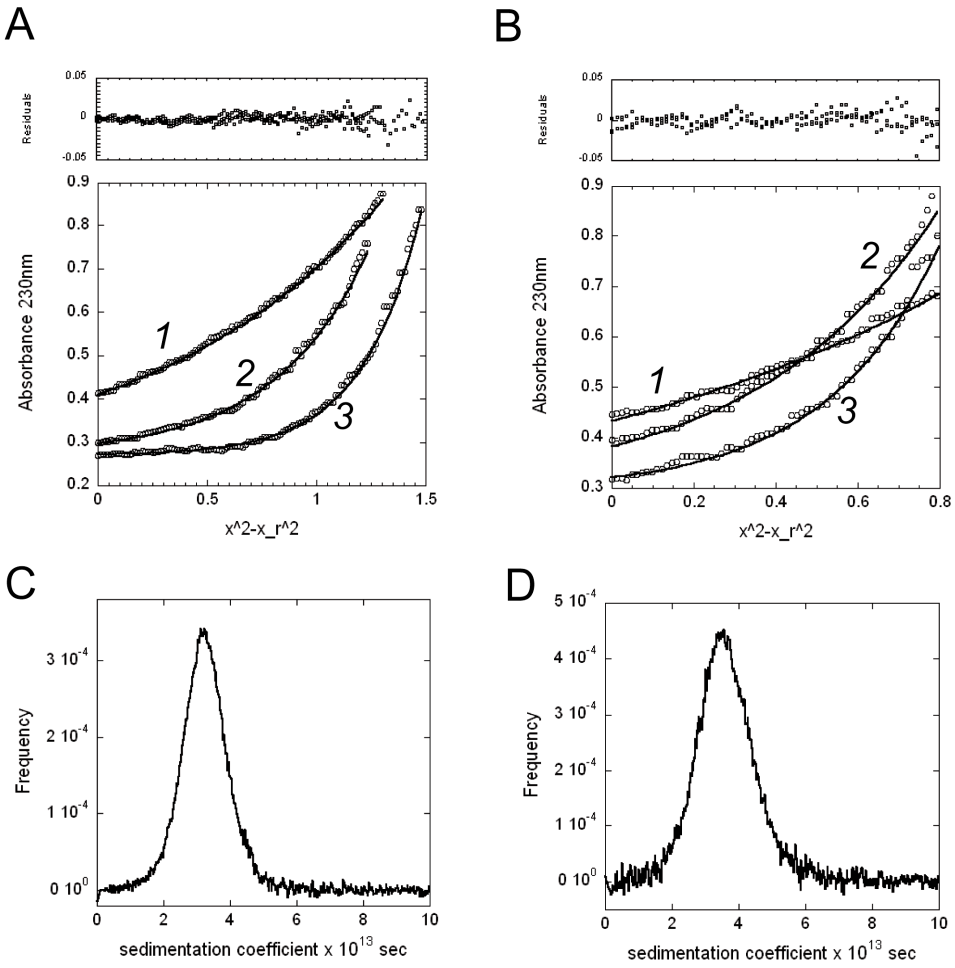

Figure 31. Analytical ultracentrifugation of apo and Cu(I)-bound *Bsu* CsoRs. (A) and (B) Representative equilibrium data with a global fit to a single ideal species model and residuals for both apo and Cu(I)-bound *Bsu* CsoR at 0.3 AU_{230}, respectively. The three data sets correspond to different rotor speeds: 1) 19,300 rpm; 2) 30,600 rpm; 3) 38,700 rpm. The solid curves show a global fit to a single ideal species model (residues in *upper panel*). (C) and (D) Distribution of sedimentation coefficient of apo and Cu(I)-bound *Bsu* CsoRs, respectively. All parameters derived from sedimentation velocity fits are compiled in Table 8.

Table 8. Summary of fitted parameters derived from the sedimentation velocity experiments with *Bsu* CsoR

CsoR	s x 10^{13} (sec)	D x 10^{7} (cm^2/sec)	RMSD	f/f_0[a]
apo (0.3 OD_{230})	3.05	6.84	0.0067	1.50
apo (0.8 OD_{230})	3.01	7.08	0.011	1.52
Cu(I)-bound (0.3 OD_{230})	3.34	6.07	0.0082	1.37
Cu(I)-bound (0.8 OD_{230})	3.34	6.10	0.0095	1.37

[a] Frictional coefficients calculated from s and D upon fixing the molecular weight of the tetramer to 45.9 kDa.

complex. Further addition of protein does not affect the protein-DNA complex peak at 13.7 mL, with only free protein peak eluting at 15.9 mL (data not shown). This suggests that the *Bsu* CsoR-DNA interaction saturates at 8:1 monomer:DNA ratio corresponding to two tetramers per DNA. Similar experiments carried out with Cu(I)-bound *Bsu* CsoR reveals the elution of only free DNA and free protein and no protein-DNA complex peak (data not shown), which is consistent with the fact that Cu(I) binding to *Bsu* CsoR significantly decreases the DNA binding affinity.

Fluorescence anisotropy experiments first carried out in buffer N (0.2 M NaCl) with 2 mM DTT with 10 nM 30 bp DNA further confirm the stoichiometry. Under these conditions, apo-*Bsu* CsoR binds the fluorescein-labeled 30 bp DNA with very high affinity ($\geq 10^9\ M^{-1}$) as revealed by the stoichiometric binding curve (Figure 32B). The binding isotherm increases linearly and saturates at about 8 *Bsu* CsoR monomers to 1 DNA, consistent with the stoichiometry determined by size exclusion chromatography. Since free *Bsu* CsoR is a stable tetramer, these data are consistent with a binding stoichiometry of two tetramers to one two-fold symmetric DNA.

DNA binding affinity of apo and Cu(I)-bound Bsu CsoRs. The apparent DNA binding affinity of apo-*Bsu* CsoR was estimated to be $2x10^7\ M^{-1}$ by electrophoretic mobility shift assay (EMSA) in 20 mM Tris, 50 mM NaCl, 1 mM DTT at pH 8.0 (*105*). To determine the binding affinity quantitatively, we performed the fluorescence anisotropy experiments in 10 mM MES, 0.4 M NaCl, 2 mM DTT, pH 6.5, 25 ^oC. Figure 33A shows a typical normalized *Bsu* CsoR-DNA binding curve monitored by fluorescence anisotropy. Since only a lower limit of tetramerization constant of $10^7\ M^{-1}$ was

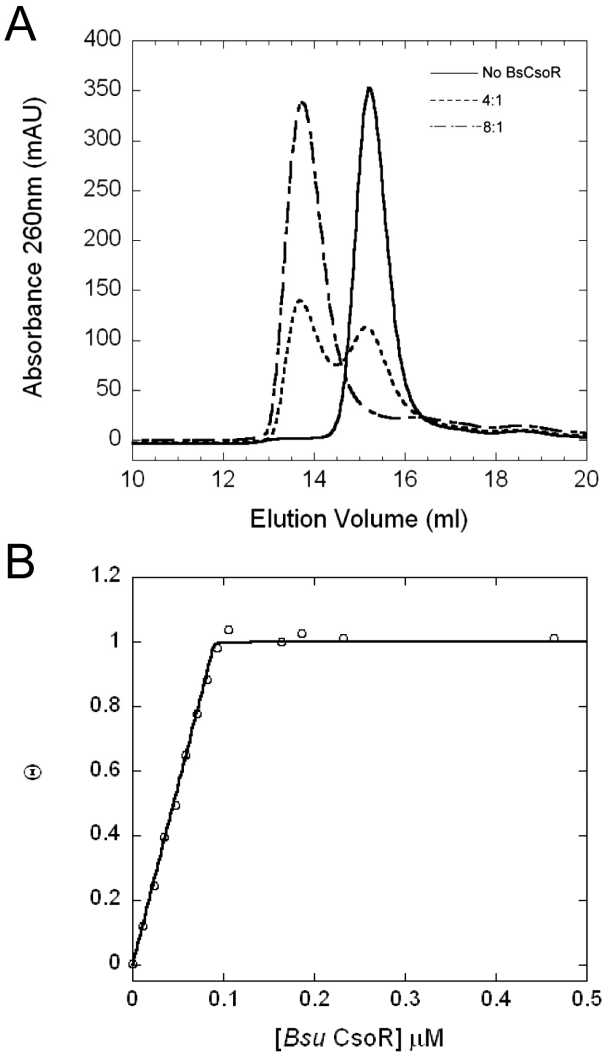

Figure 32. *Bsu* CsoR-*copZA* operator DNA binding stoichiometry. (A) Elution profile obtained with different *Bsu* CsoR:DNA ratios from a Superdex 200 column as monitored by absorption at 260nm. Conditions: 10 mM MES, 0.2 M NaCl, 2 mM DTT, pH 6.5. (B) Normalized DNA binding isotherm based on fluorescence anisotropy with 10 nM DNA in 10 mM MES, pH 6.5, 0.2 M NaCl, 2 mM DTT, 25^{o}C.

determined by analytical ultracentrifugation, these DNA binding data were fit using a stepwise binding model of two non-dissociable tetramers to one DNA (Appendix C). Apo-*Bsu* CsoR binds to the DNA with K_1^{apo}=3.1(±0.8) x 10^7 M^{-1} and K_2^{apo} = 8.3 (±2.2) x 10^7 M^{-1}, while Cu(I)-bound *Bsu* CsoR binds the same DNA with K_1^{Cu}=2.9(±0.4) x 10^6 M^{-1} and K_2^{Cu}≤1.0 x 10^5 M^{-1}. This gives an operationally defined coupling free energy (ΔG_c) ≥ 5.4 kcal/mol (Table 6). The second binding event was not observed for Cu(I)-bound protein under the experimental conditions, therefore only an upper limit for K_2^{Cu} is reported here.

DNA binding by E90A CsoR is not regulated by Cu(I) binding. How Cu(I) binding changes the conformation and/or assembly state of CsoR in a way that results in an allosterically inhibited conformation remains unclear; however, data in Chapter III suggest that Tyr35, His61 and Glu81 in *Mtb* CsoR are involved in the regulation (*39*). Therefore, to test whether *Bsu* CsoR shares an allosteric mechanism that is similar to that suggested for *Mtb* CsoR, the equivalent residue of Glu81, Glu90 in *Bsu* CsoR, was substituted with an Ala. As shown in Figure 33B, Cu(I)-bound E90A CsoR binds the 30 bp DNA with a high affinity that is similar in magnitude to that of apo-E90A CsoR, suggesting that Cu(I) binding does not negatively regulate the DNA binding affinity of this mutant. Since the Cu(I)-binding affinity (Table 6) and the coordination environment of E90A CsoR (Figure 30) are indistinguishable from those of wild-type CsoR, these data suggest that E90 plays an important role in mediating Cu(I)-dependent negative regulation of DNA binding.

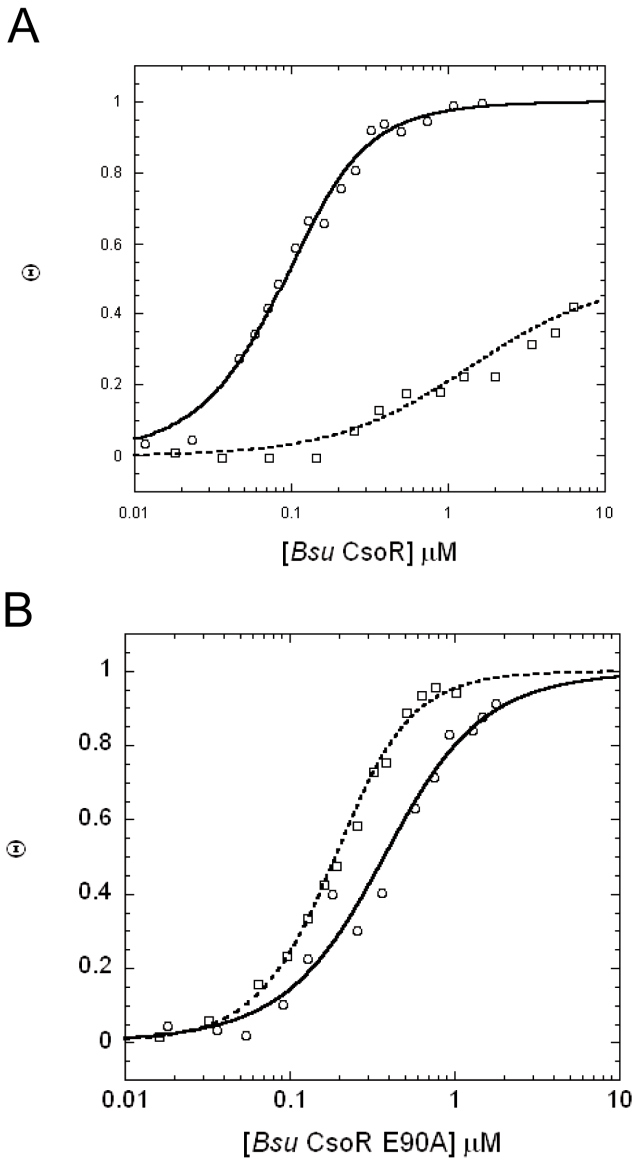

Figure 33. Normalized fluorescence anisotropy-based DNA binding isotherms of WT (A) and E90A (B) *Bsu* CsoRs acquired in the absence (○) and presence (□) of Cu(I). Curves represent the best fit using a stepwise two tetramer DNA binding model with the fitting parameters given in Table 6. Conditions: 10 mM MES, pH 6.5, 0.4 M NaCl, 2 mM DTT, 25°C.

The Binding of Zn(II), Co(II) and Ni(II) to Bsu CsoR. Although studies in *Mtb* and in *M. smegmatis* reveal that Cu(I) is the primary inducer of *csoR*-dependent gene expression, it was of interest to determine the specificity of Cu(I) binding and the degree to which other metals could allosterically regulate *copZA* operator-promoter binding. A Zn(II) titration using magfura-2 as a competition chelator shows that *Bsu* CsoR binds Zn(II) with K_{Zn}=1.6 (±0.1) x 10^8 M^{-1} (Table 6). To provide insights into the coordination geometry of Zn(II), Co(II) was used as a structural surrogate for Zn(II) (*70, 110*). Not surprisingly, Co(II) binds to *Bsu* CsoR with an affinity far lower than that of Zn(II), with $K_{Co} \leq 10^5$ M^{-1} under the same conditions. As shown in Figure 34A, Co(II) bound *Bsu* CsoR shows strong ligand-to-metal charge transfer (LMCT) at 290 nm with an ε=1500 $M^{-1}cm^{-1}$ and at 335 nm with an ε=800 $M^{-1}cm^{-1}$. The d-d transition envelope centered at ≈600 nm gives an ε≈300 $M^{-1}cm^{-1}$. These data taken together are consistent with a tetrahedral or distorted tetrahedral Co(II) complex with one or two of the Cys residues as donor atoms to the Co(II). Since Co(II) is bound tetrahedrally, Zn(II) may well bind with the same coordination geometry, although this was not directly determined here.

When apo-*Bsu* CsoR binds Ni(II), the UV-vis absorption spectrum shows a feature at ≈480 nm with a molar intensity of ε=100 $M^{-1}cm^{-1}$(Figure 34B and inset). This feature is consistent with a square planar or distorted square planar coordination geometry as observed previously for *E. coli* NikR (*129*) and nickel-substituted mutant retroviral-type zinc-finger peptides (*130*). The intense ligand-to-metal charge transfer transitions in the near ultraviolet region suggest that Cys residues are involved in coordinating Ni(II). The binding isotherm as shown in the inset of Figure 34B shows a

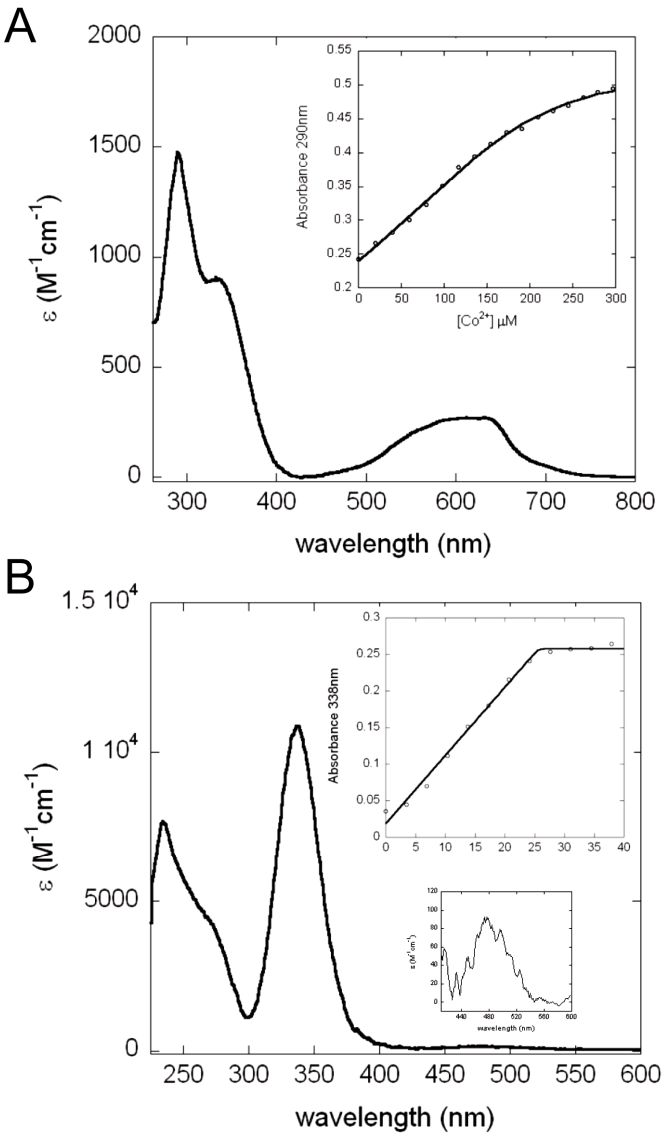

Figure 34. Co(II) and Ni(II) binding to *Bsu* CsoR. Apoprotein-subtracted molar absorptivity spectra of Co(II):*Bsu* CsoR mixture at 2:1 molar ratio (A) or Ni(II):*Bsu* CsoR mixture at 1:1 molar ratio (B). The binding isotherms shown in the insets are fitted with a simple 1:1 binding model with parameters collected in Table 6.

linear increase up to about 1.2 mol equiv Ni(II) followed by a sharp transition to a plateau, revealing that *Bsu* CsoR binds ≈1 mol equiv Ni(II) with a binding affinity $\geq 10^7$ M^{-1} (*i.e.,* stoichiometrically). The binding affinity estimated by an EGTA competition experiment was determined to be K_{Ni}=3.6(±0.3) x 10^9 M^{-1} (Table 6).

These metal binding experiments clearly show that *Bsu* CsoR is also capable of binding other divalent metal ions with widely different affinities and coordination geometries. To test whether these metal ions are significant allosteric negative effectors of DNA binding, fluorescence anisotropy experiments analogous to that shown in Figure 33 for Cu(I) were carried out with excess metal ion to ensure that the metal-bound form of the protein is the predominant species in solution. The fitted parameters are compiled in Table 6. Both Zn(II) and Ni(II) complexed *Bsu* CsoR bind to the 30 bp *copZA* operator DNA with affinity close to that of apo-*Bsu* CsoR, each resulting in only a small positive coupling free energy (Figure 35, Table 6). This is consistent with previous observations that divalent metal ions are poor regulators of DNA binding of *Mtb* CsoR both in vitro and in vivo, despite their high equilibrium affinities for these metals (*39*).

DISCUSSION

Bsu CsoR regulates the transcription of *copZA* operon, which encodes two important components of the Cu homeostasis system, the Cu-chaperone CopZ and the Cu-effluxer CopA. It is widely accepted that in both eukaryotes and prokaryotes, the intracellular trafficking of copper ions is dependent on metallochaperones which reinforces the idea that there is little or no “free” or bioavailable copper ions in the cell

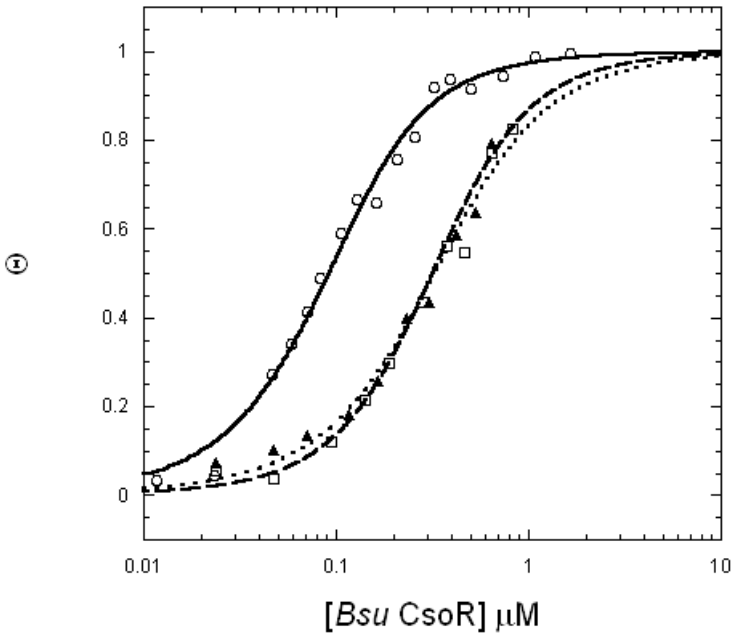

Figure 35. Normalized fluorescence anisotropy-based DNA binding isotherms of apo- (○), Zn(II)- (▲) and Ni(II)-bound (□) WT *Bsu* CsoRs. The solid, dash and dot curves represent data fit by a stepwise binding model (Figure 12, Appendix C) and the parameters are compiled in Table 6. Conditions: 10 mM MES, 0.4 M NaCl, 2 mM DTT, pH 6.5, 25^{o}C.

(*29, 131, 132*). It is still unclear how *Bsu* CsoR, as a Cu-sensor, obtains the copper ion in the cell, although one strong possibility is from CopZ. Such a CopZ-dependent transfer of Cu to *Bsu* CsoR is analogous to the accepted mechanism in *Enterococcus hirae*, where the Zn(II)-bound form of the Cu-sensor CopY acquires Cu from the Cu-chaperone CopZ with displacement of Zn(II) (*133*). Under uninduced conditions, a background level of CopZ in the cell functions as a copper chelator or buffer, perhaps delivering copper to target proteins. The ratio between apo and Cu-bound CopZ may be thermodynamically and kinetically maintained in a certain "window" by various cellular protein-protein interactions and Cu-transfer reactions. Upon Cu stress, Cu-bound CopZ may be formed quickly, therefore making it possible to transfer Cu to *Bsu* CsoR, leading to derepression of the *copZA* operon; this, in turn, results in increased expression of apo-CopZ and CopA required to efflux excess Cu out of cytosol, bringing this ratio back into a normal or unstressed range. Cu(I)-bound *Bsu* CsoR may then be degraded or potentially transfer Cu to other target proteins, *e.g.* CopA itself, via a ligand exchange reaction (*12*). It is also unknown if apo-CsoR or apo-CsoR bound to the operator is loaded with Zn(II), as has been proposed for *E. hirae* CopY.

Bsu and *Mtb* CsoRs share very high amino acid sequence identity. In particular, all three proposed Cu ligands are conserved as are two proposed "second coordination shell" residues, corresponding to Tyr35 (Tyr44 in *Bsu*) and Glu81 (Glu90 in *Bsu*) in *Mtb* CsoR. The major difference between the two CsoRs is that *Mtb* CsoR contains a unique ≈30 amino acid C-terminal tail which is missing in the previously solved crystal structure of Cu(I)-CsoR from *Mtb* (Chapter II) (*39*). Aside from this, these two CsoRs

possess very similar biochemical and biophysical properties. Both coordinate 1 monomer mol equiv of Cu(I) with very high affinity to form a trigonal planar S_2N coordination geometry with very similar Cu-S distances. It is also the case that *Bsu* CsoR is a stable tetramer in the low micromolar (monomer) concentration range, while a dimer-tetramer equilibrium was observed in previous analytical ultracentrifugation studies carried out on full-length *Mtb* CsoR (*39*). Adjacent C_2-symmetric dimers in the crystal structure of Cu(I)-bound *Mtb* CsoR pack against one another to form a tetramer with D_2 rotational symmetry. In this configuration of the tetramer, the C-terminal tail of *Mtb* CsoR would be positioned at the dimer-dimer or tetramer interface; it therefore seems possible that the flexible C-terminal tail may influence the *Mtb* CsoR tetramer. This has yet to be investigated systematically (see Chapter VI).

We find no significant differences in assembly states of the apo and Cu(I)-bound forms of *Bsu* CsoR, which are both tetrameric under the conditions investigated. Therefore, only a lower limit of the tetramerization constant (K_{tet}) of about 10^7 (M dimer)$^{-1}$ could be estimated from these data. However, differences in K_{tet} in the nanomolar concentration range cannot be ruled out by these data; if this is the case, they may be partly responsible for the different DNA binding affinities reported here for apo- and Cu(I)-CsoRs. On the other hand, the sedimentation velocity experiments show a small *increase* in sedimentation coefficient in Cu(I)-bound *Bsu* CsoR, suggesting a conformation with a smaller frictional coefficient, thus more spherical relative to the apoprotein (Table 8). However, this change may not play a primary role in allosteric

regulation of DNA binding because a similar change in sedimentation coefficient appears to characterize E90A CsoR as well (data not shown).

Understanding what happens when a particular metal sensor binds the "wrong" metal is just as important as understanding how the cognate metal ion drives regulation of gene expression (*5*). We show here that the metal binding site of *Bsu* CsoR can adopt a range of distinct coordination numbers and geometries upon binding different metal ions. Co(II), and by inference Zn(II), adopts a tetrahedral or distorted tetrahedral geometry while Ni(II) appears to form a square planar or distorted square planar geometry. Each complex incorporates one or both Cys residues in *Bsu* CsoR; in fact, it is formally possible that each employs all three Cu(I) ligands while adding a fourth ligand, perhaps from the N-terminal region like in RcnR (*103*), or from solvent. In any case, the Co(II) and Ni(II) coordination geometries are clearly distinct from that of RcnR, where each metal adopts an octahedral or pseudo-octahedral complex (*103*). Strikingly, while the binding of Cu(I) stabilizes an allosterically inhibited conformation of *Bsu* CsoR, neither Zn(II) nor Ni(II) is capable of strongly regulating the DNA binding, despite their high equilibrium affinities (albeit ≥10 orders of magnitude smaller than K_{Cu}) (Table 6). In fact, K_{Ni} for CsoR may well be comparable to K_{Ni} for the *bona fide* Ni/Co sensor *E. coli* RcnR; in contrast, K_{Co} is at least 10^4-smaller for *Bsu* CsoR (K_{Zn} has not been reported for RcnR) (*103*). These features are consistent with the emerging theme that formation of the "native" coordination geometry is most closely linked to biological metalloregulation, rather than absolute metal binding affinity (*6, 70, 113*). This, in turn, suggests that specific features of trigonal planar Cu(I) coordination

complex in CsoR may organize a "second coordination shell" of interactions used to drive defined conformational changes that are linked to Cu(I)-mediated derepression of gene expression (see Chapter III) (*39, 110*).

As discussed in the previous chapters, one strong candidate for propagating this structural change in Cu(I)-CsoRs is the $N^{\varepsilon 2}$ face of His70 (His61 in *Mtb* CsoR). The crystal structure of *Mtb* CsoR reveals that this face of the His61 imidazole ring is in close proximity to the side chains of both Glu81and Tyr35' in *Mtb* CsoR (*39*) which correspond to Glu90 and Tyr44' in *Bsu* CsoR. Glu90 is a highly conserved residue in the α3 helix of all Cu(I)-specific CsoRs, and we show here that an Ala substitution abolishes negative regulation of DNA binding without significantly interfering with the Cu(I) affinity or coordination geometry. We note that the significant quenching of the steady-state tyrosine fluorescence upon Cu(I) binding is consistent with a tyrosinate-like species, that might form as a result of hydrogen bonding of the hydroxyl proton with an as yet unidentified acceptor, an excellent candidate for which is Glu90 (*134*). Interestingly, both of these conserved residues have also been shown to be crucial for allosteric regulation in *Mtb* CsoR (see Chapter III).

CHAPTER V

BIOCHEMICAL PROPERTIES OF A PUTATIVE Cu(I)-SENSING CsoR FROM *Staphylococcus aureus*

INTRODUCTION

In the previous chapter, the transcriptional regulator *Bsu* CsoR was biochemically and biophysically characterized. The genes encoding both *Mtb* and *Bsu* CsoRs have common genomic neighbors including genes encoding a putative P-type ATPase predicted to efflux Cu(I) from the cytoplasm, and in the case of *Bsu* CsoR, a well-characterized Cu(I) metallochaperone (*135*). However, this is not always the case. Many genes encoding what we anticipate are Cu(I)-specific CsoRs do not have gene neighbors directly implicated in Cu homeostasis, thus making it difficult to predict the gene(s) that might be regulated. *S. aureus* CsoR (*Sau* CsoR) is one such example and is discussed here.

A gene encoding a putative Cu effluxing P-type ATPase CopA in the Newman strain of *Staphylococcus aureus* (NWMN_2457) was the first functionally characterized gene to be related to Cu resistance of *S. aureus* (*136*). The transcriptional level of *copA* in the laboratory strain, *S. aureus* SH1000, is strongly induced when elevated $CuSO_4$ concentrations are added to the medium. This immediately suggests that *S. aureus* must encode a regulator with a role in Cu(I) homeostasis. However, no Cu-specific metalloregulatory protein has been identified in this microorganism (*136*). Close inspection of the promoter region of *copA* reveals a GC-rich inverted repeat very similar

to the inverted repeats found in the *Mtb* CsoO and *Bsu copZA* operator-promoter regions (Figure 36) (*39, 111*). Therefore, we proposed that the *copA* gene in *S. aureus* is regulated by a CsoR, despite the fact that there are no CsoR-like proteins close to the *copA* gene (Figure 36).

A blast search using *Mtb* CsoR sequence as query reveals two CsoR homologs in the Newman strain of *S. aureus.* These are NWMN_1991 (Figure 36) and another unannotated open reading frame (ORF) between NWMN_0026 and NWMN_0027 (encoded by the complementary strand of 37974-38234). Further analysis of the protein sequences reveals that the latter contains only the x-Cys-x-Cys signature, and is classified as a putative oxidative stress sensor (*Sau* CsoR^{ox}, see Chapter VI) (Figure 9) (*103*). On the other hand, NWMN_1991 contains the x-Cys-His-Cys signature and shares many other structural features of a *bona fide* Cu sensor. This gene is tentatively designated *Sau CsoR* proposed to encode a Cu(I)-sensor that regulates the transcription of *copA* and potentially *copZ* genes and perhaps others (Figure 36).

To test this, a Δ*csoR* strain of *S. aureus* Newman was constructed in the laboratory of Dr. Eric Skaar at Vanderbilt University. Preliminary studies show that this strain is less sensitive to elevated Cu concentrations in the growth media, a phenotype that is similar to that of a *B. subtilis* Δ*csoR* strain (Appendix E) (*105*). This would occur as a result of the constitutive expression of *copA* gene, consistent with the role of CsoR as a repressor of *copA* and *copZ* transcription. As was previously done for *Mtb* and *Bsu* CsoRs, the putative *Sau* CsoR was over expressed and purified from *E. coli* and characterized biochemically. *Sau* CsoR binds one mol equiv Cu(I) per monomer with

very high affinity and x-ray absorption spectroscopy suggests a 3-coordinate Cu(I) complex, likely formed by the conserved residues Cys41, His66 and Cys70. More importantly, *Sau* CsoR binds a 39 bp DNA *cop* operator (CopO) fragment derived from the promoter region of *copA* gene, and Cu(I) binding greatly decreases the binding affinity. The findings are consistent with a derepression model established for other CsoRs.

MATERIALS AND METHODS

Plasmid construction and protein purification. The *Sau csoR* gene was initially amplified from the region 2212576-2212914 as annotated for NWMN_1991 in *S. aureus* Newman genomic DNA (provided by Dr. Eric Skaar at Vanderbilt University). It was then cloned into pET3d vector between the NcoI and BamHI restriction sites. The resultant protein after expression showed poor solubility and no DNA binding activity on a 39 bp DNA derived from the promoter of *S. aureus copA* gene (Figure 36). Further inspection of the DNA sequence of *csoR* gene revealed another initiation codon at 2212869, resulting in an ORF 15 codons shorter than the annotated CsoR with an obvious ribosome binding site just upstream of this initiation codon. A multiple sequence alignment of Cu(I)-sensing CsoRs reveals that no other CsoR contains an extended N-terminal region (Figure 9). Therefore, the region corresponding to 2212576-2212869 was hypothesized to represent the actual ORF encoding CsoR and was further amplified from the genome and cloned into pET3d vector between the NcoI and BamHI restriction sites. The second residue was changed to an alanine for cloning purposes.

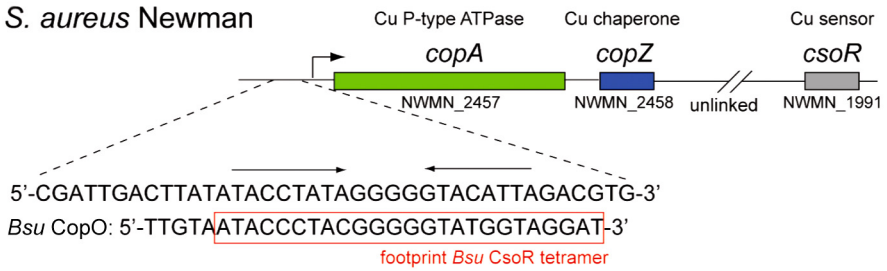

Figure 36. Genomic location of genes encoding CopA, CopZ and a putative CsoR in *S. aureus* Newman. The DNA sequence in the *copA* promoter region is also shown in comparison with *Bsu* CopO which has been shown to be bound by *Bsu* CsoR in Chapter IV (*105*).

Amino acid substitutions were introduced to this plasmid by site-directed quick-change mutagenesis. The sequences of all the resultant plasmids were verified by DNA sequencing.

Plasmids carrying wild-type or mutant *Sau* CsoRs were transformed into *E. coli* pLysS. A single colony from an LB plate containing 100 mg/L ampicillin was inoculated into 200 mL LB medium containing 100 mg/L ampicillin and grown overnight in a 37 ^{o}C shaker. 20 mL of the overnight culture was then used to inoculate 1 L of the same LB medium and grown at 37 ^{o}C until OD600 reached 0.6-0.8. 0.4 mM IPTG was then added and cells were grown for additional 2 h before harvesting by low speed centrifugation. Cells were resuspended in 200 mL Buffer E (25 mM HEPES, pH 7.0, 2 mM EDTA, 2 mM DTT) and lysed by sonication. After centrifugation, 0.15% (v/v) of PEI was added to the supernatant to precipitate the nucleic acids. Both wild-type and C41A *Sau* CsoR appeared to be in the PEI pellet which was then resuspended in Buffer E containing 0.5 M NaCl. In contrast, H66A *Sau* CsoR appeared to reside in the PEI supernatant fraction. The supernatant containing *Sau* CsoR was then subjected to ammonium sulfate precipitation and the resulting pellet was resuspended in Buffer E and dialyzed against Buffer E containing 0.05 M NaCl. The sample was then purified by Q Fast Flow column with Buffer E using a salt gradient of 0.05 – 0.5 M NaCl. Fractions containing *Sau* CsoR were combined and concentrated to a final volume of ~3 mL. 1 mL of the resultant protein was then loaded onto a Superdex 200 30/100GL size exclusion column (GE Healthcare, NJ) pre-equilibrated with Buffer E containing 0.3 M NaCl. The fractions containing *Sau* CsoR were combined and dialyzed against Buffer E containing 0.05 M

NaCl and loaded onto a MonoQ column for further purification. Fractions from MonoQ column containing *Sau* CsoR were then pooled and concentrated to a volume of ~6 mL and dialyzed into Buffer S (10 mM HEPES, 0.2 M NaCl, pH 7.0) in the glovebox. The purity of the final products was estimated by visualization of Coomassie-stained 18% Tris-glycine SDS-PAGE gels to be ≥90%. Protein concentration was determined by using a ε_{280}=1615 $M^{-1}cm^{-1}$. The free thiol content was determined by the DTNB assay to be more than 90% of expected value (2.0 expected) (*39, 105*). Less than 0.1% copper was detected by atomic absorption spectroscopy in all purified protein samples.

Cu(I) binding experiments. see Methods in Chapter II

X-ray absorption spectroscopy. see Methods in Chapter II

Size exclusion chromatography. 100 μL of 50 μM *Sau* CsoR monomer was loaded on to a Superdex 200 (GE Healthcare, NJ) column pre-equilibrated with 10 mM HEPES, 0.4 M NaCl, 2 mM DTT, pH 7.0 on an Äkta-10 purifier. The elution profile was monitored by UV absorbance at 220 nm, 260 nm and 280 nm simultaneously.

Electrophoretic mobility shift assay (EMSA). Different amounts of *Sau* CsoR (1-10 μM monomer) were mixed with 0.5 μM 39 bp DNA (CopO) (5'-CGATTGACTTATATACC TATAGGGGGTACATTAGACGTG-3') derived from the promoter region of the *S. aureus copA* gene in Buffer S containing 2 mM DTT. For Cu(I)-bound samples, *Sau* CsoRs were loaded with 1.0 mol equiv Cu(I) before adding to the DNA. After incubating for 30 min at room temperature, the mixtures were loaded onto a 6% TBE polyacrylamide gel (Invitrogen, CA) and run at 120 V for 45 min before staining with

ethidium bromide. The gel was then scanned by a Typhoon Imager (GE Healthcare, NJ) in the Physical Biochemistry Instrumentation Facility at Indiana University.

RESULTS

Sau CsoR binds 1 mol equiv Cu(I) per monomer with high affinity. To show that *Sau* CsoR binds Cu(I) in vitro, CuCl was directly titrated anaerobically into *Sau* CsoR purified from *E. coli*. Binding of Cu(I) to CsoR results in a ligand to metal charge transfer (LMCT) at about 240 nm with an $\varepsilon \approx 15000\ M^{-1}cm^{-1}$ (Figure 37). Similar features characterize Cu(I) binding to *Mtb* and *Bsu* CsoRs, suggesting two Cys-Cu(I) coordination bonds (*39, 111*). The increase of absorbance saturates upon ~1 mol equiv Cu(I) per *Sau* CsoR monomer (Figure 37 inset). Therefore, *Sau* CsoR binds 1 mol equiv Cu(I) per monomer, and two Cys residues are likely involved in the coordination.

The Cu(I) binding affinity was further quantified using a BCS competition assay in which different BCS concentrations were mixed with CuCl and *Sau* CsoR anaerobically (see Methods). When Cu(I) is added into a mixture of *Sau* CsoR and BCS, CsoR strongly competes with BCS in binding Cu(I), suggesting an affinity similar to, or higher than, BCS. Log K_{Cu} was calculated to be 18.1±0.5 by quantification of the $Cu(I)(BCS)_2$ complex in the solution based on the absorption at 483 nm. Substitution of Cys41 or His66 (equivalent of C36 and His61 in *Mtb* CsoR) with alanine results in a significant decrease in K_{Cu}, with log K_{Cu} of 14.5±0.1 and 15.3±0.1 for C41A and H66A CsoRs, respectively. These data are consistent with the scenario that these two residues are involved in Cu(I) binding.

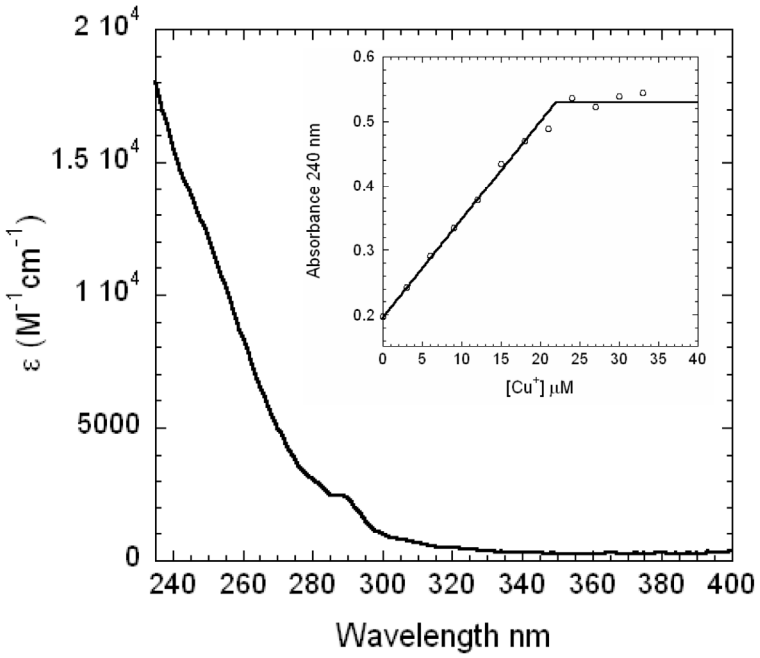

Figure 37. *Sau* CsoR binds 1 monomer mol equiv of Cu(I) with high affinity. Apoprotein-subtracted molar absorptivity spectrum of Cu(I):*Sau* CsoR mixture at 1:1 molar ratio. Inset: the binding isotherm of anaerobic titration of CuCl into 22 μM *Sau* CsoR monomer. Conditions: 10 mM HEPES, 0.2 M NaCl, pH 7.0.

Sau CsoR forms a 3-coordinate complex with Cu(I). The Cu(I) coordination geometry was further determined by x-ray absorption spectroscopy. As shown in Figure 38A, when bound to 0.8 mol equiv Cu(I), the pre-edge peak at 8940 eV is consistent with a 1s→4p excitation typical for 3-coordinate Cu(I) (Figure 38A) (*39, 111, 122*). This is very similar to what has been shown for *Mtb* CsoR 1-106 (Chapter III). The Fourier Transform as well as the Cu K-edge extended X-ray absorption fine structure (EXAFS) spectrum for *Sau* CsoR with the best fit are shown in Figure 38B and C, respectively. The fitted parameters are compiled in Table 9. The fit suggests two Cu-S interactions at 2.20 Å and one Cu-N/O interaction at 2.01 Å. The Cu-S distances are very similar to the previous reported distances for *Mtb* and *Bsu* CsoRs. The significant outer shell scattering at 3-4 Å is consistent with the third ligand being a histidine residue. *Sau* CsoR His66 corresponds to His61 in *Mtb* CsoR and His70 in *Bsu* CsoR (Figure 9), and the Cu(I) binding affinity is significantly decreased in the H66A mutant. Therefore, it is highly likely that His66 serves as the third ligand, together with Cys41 and Cys70, to form the S_2N coordination site for Cu(I).

Sau CsoR self-associates in solution. During the purification of *Sau* CsoR, it was observed that CsoR elutes from a size exclusion column much earlier than what had been previously observed for *Mtb* and *Bsu* CsoRs. This suggests that the assembly state of *Sau* CsoR may be considerably larger than a tetramer. To test this, 50 μM *Sau* CsoR monomer was loaded onto a Superdex 200 column. The elution profile revealed a highly asymmetric peak with a maximum absorbance at ~11.7 mL corresponding to a molecular weight in excess of 300 kDa (Figure 39). Such asymmetry suggests that there are

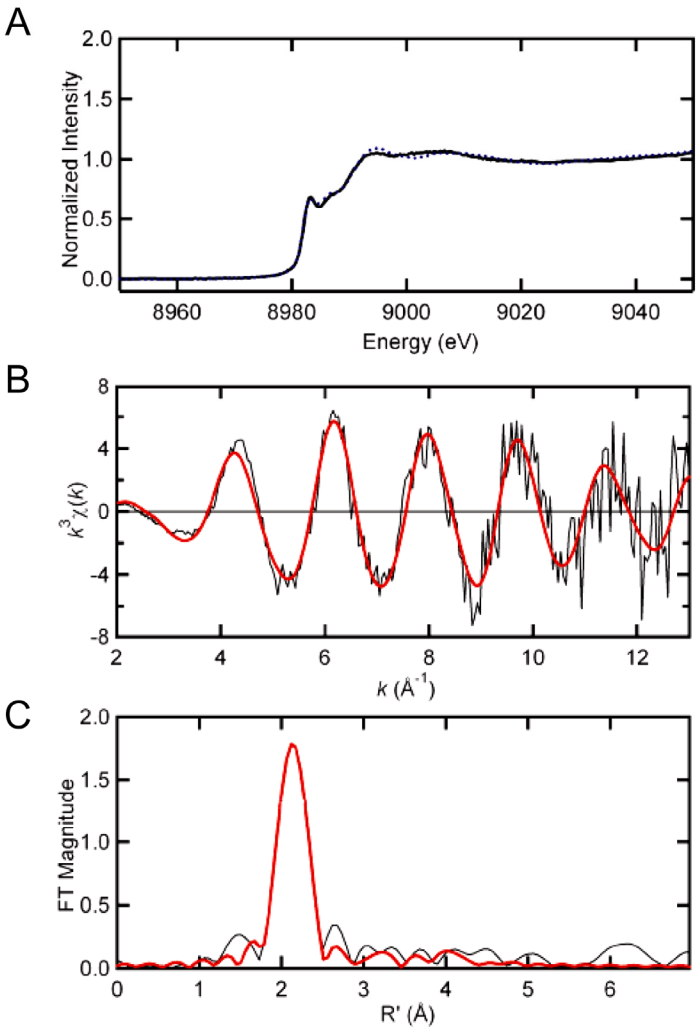

Figure 38. X-ray absorption spectroscopy (XAS) of Cu(I)-bound *Sau* CsoR. (A) Cu K-edge X-ray absorption edge spectra of Cu(I)-bound WT *Sau* CsoR (solid black) and *Mtb* CsoR 1-106 (dashed blue) exactly the same as shown in Chapter III. The Fourier transforms (k^3 weighted, k=2-12 Å^{-1}) and copper K-edge EXAFS spectrum for Cu(I)-bound WT *Sau* CsoR are shown in panels (B) and (C), respectively. The solid *red* curves in B and C represent the best fits with parameters compiled in Table 9.

Table 9. XAS fitting parameters for *Sau* CsoR[a].

Sample (*k* range) $\Delta k^3\chi$	Fit	Shell	R_{as} (Å)	σ_{as}^2 (Å^2)	ΔE_0 (eV)	f[b]
Sau CsoR	1	Cu-S_2	2.20	0.0028	-5.420	0.102
		Cu-N_1	2.01	0.0016	[-5.420][c]	
		Cu-C_1	[2.99]	[0.0032]	[-5.420]	
		Cu-C_1	[3.04]	[0.0033]	[-5.420]	
		Cu-N_1	[4.17]	[0.0020]	[-5.420]	
		Cu-C_1	[4.22]	[0.0020]	[-5.420]	

[a] Shell is the chemical unit defined for the multiple scattering calculation. Subscripts denote the number of scatterers per metal. R_{as} is the metal-scatterer distance. σ_{as}^2 is a mean square deviation in R_{as}. ΔE_0 is the shift in E_0 for the theoretical scattering functions.

[b] f' is a normalized error (chi-squared):

$$f' = \frac{\left\{\sum_i \left[k^3\left(\chi_i^{obs} - \chi_i^{calc}\right)\right]^2 / N\right\}^{1/2}}{\left[\left(k^3\chi^{obs}\right)_{max} - \left(k^3\chi^{obs}\right)_{min}\right]}$$

[c] Numbers in square brackets were constrained to be either a multiple of the above value (σ_{as}^2) or to maintain a constant difference from the above value (R_{as}, ΔE_0).

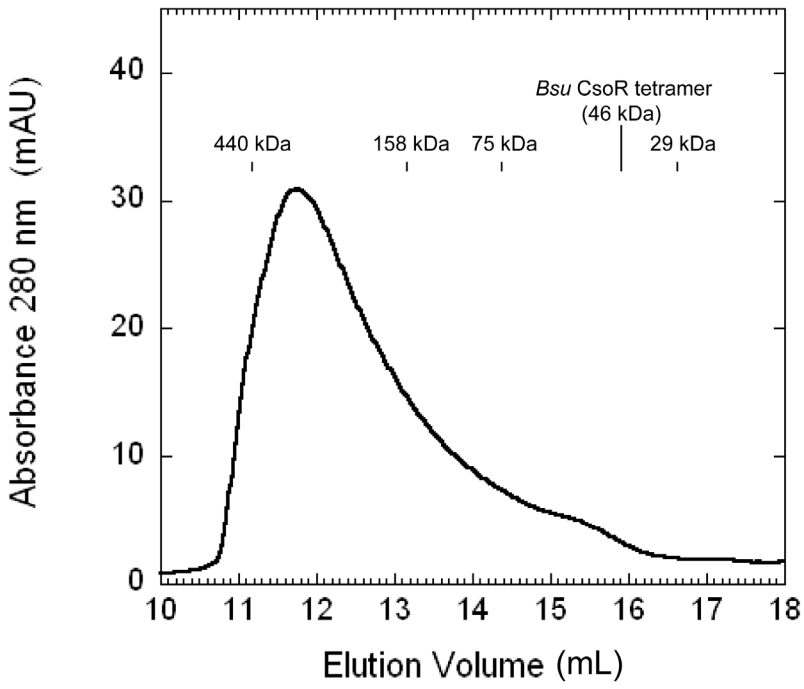

Figure 39. Elution profile of 50 μM *Sau* CsoR monomer from a Superdex G200 column. Conditions: 10 mM HEPES, 0.4 M NaCl, 2 mM DTT, pH 7.0.

multiple oligomerization states in the solution, clearly distinct from the *Bsu* CsoR tetramer, which elutes at ~15.9 mL from the same column (Figure 39); the "shoulder" in the elution profile at the same position may correspond to tetrameric *Sau* CsoR (10 mM HEPES, pH 7.0, 0.4 M NaCl, 2 mM DTT). The solution condition dependence and Cu(I) dependence of the assembly states, as well as the functional relevance, are not yet known.

DNA binding of Sau CsoR. To test whether *Sau* CsoR is involved in Cu homeostasis, a *ΔcsoR* strain was first made and its growth under different Cu concentrations in the medium was tested in collaboration with Dr. Eric Skaar's laboratory. As shown in Appendix E, wild-type *S. aureus* Newman strain shows slower growth with increasing concentrations of Cu in the medium, suggesting the elevated Cu is toxic to the cell. Interestingly, the *ΔcsoR* strain shows no such growth phenotype at Cu concentration as high as 125 μM and only 500 μM Cu in the medium appears to be toxic. These data suggest that the *ΔcsoR* strain is less sensitive to Cu-stress, which is analogous to what has been found in *ΔcsoR* strain of *B. subtilis* (*105*). Since we hypothesize that CsoR is a repressor for the *copA* gene encoding a Cu-effluxing P-type ATPase, in the *ΔcsoR* strain, *copA* gene is expected to be constitutively transcribed regardless of Cu concentration. Such transcription level of *copA* may allow the strain to be more resistant to Cu stress comparing to wild-type strain, in which *copA* gene is at least partly repressed under low Cu concentrations.

Based on these observations, it was postulated that *Sau* CsoR regulates the transcription of *copA* gene by binding to the promoter region, in a fashion similar to that

of *Mtb* and *Bsu* CsoRs. To test this, a 39 bp DNA derived from the *copA* gene promoter region (*Sau* CopO) containing an inverted repeat analogous to those of *Mtb* CsoO and *Bsu* CopO (Figure 36) is used in an eletrophoretic mobility shift assay (EMSA). As shown in Figure 40A, *Sau* CsoR is capable of forming a complex with this 39 bp DNA in the apo-form, while addition of Cu(I) to the mixtures inhibits the formation of such a complex. This is consistent with what has been shown previously for *Mtb* CsoR (Chapter II) and *Bsu* CsoR (Chapter IV), in which *Sau* CsoR in the apo-form binds to the promoter region of *copA* gene and therefore represses the transcription, while Cu(I) binding to *Sau* CsoR induces transcriptional derepression.

Furthermore, a mutation of each of the two Cu(I) ligands, Cys41 and His66, alters the DNA binding properties. As shown in Figure 40B, no H66A CsoR-DNA complex is detected under these conditions (10 mM HEPES, 0.2 M NaCl, 2 mM DTT, pH 7.0), suggesting that this mutant is unable to bind to the DNA or simply binds with very low affinity; note that this was previously established for *Mtb* H61A CsoR (Chapter II and III) (Table 1). This reveals that the key allosteric residue His66 may have a third function, which is to play a direct role in DNA binding, in addition to Cu(I) binding and allosteric coupling (Chapter III). On the other hand, *Sau* C41A CsoR is capable of binding the DNA in the presence or absence of bound Cu(I) (Figure 40B). This finding is also analogous to the findings for *Mtb* C36A CsoR (Table 1). However, the loss of Cu(I)-dependent regulation likely results from significant change in the coordination geometry and Cu(I) binding affinity, but not in the allosteric regulation pathway itself.

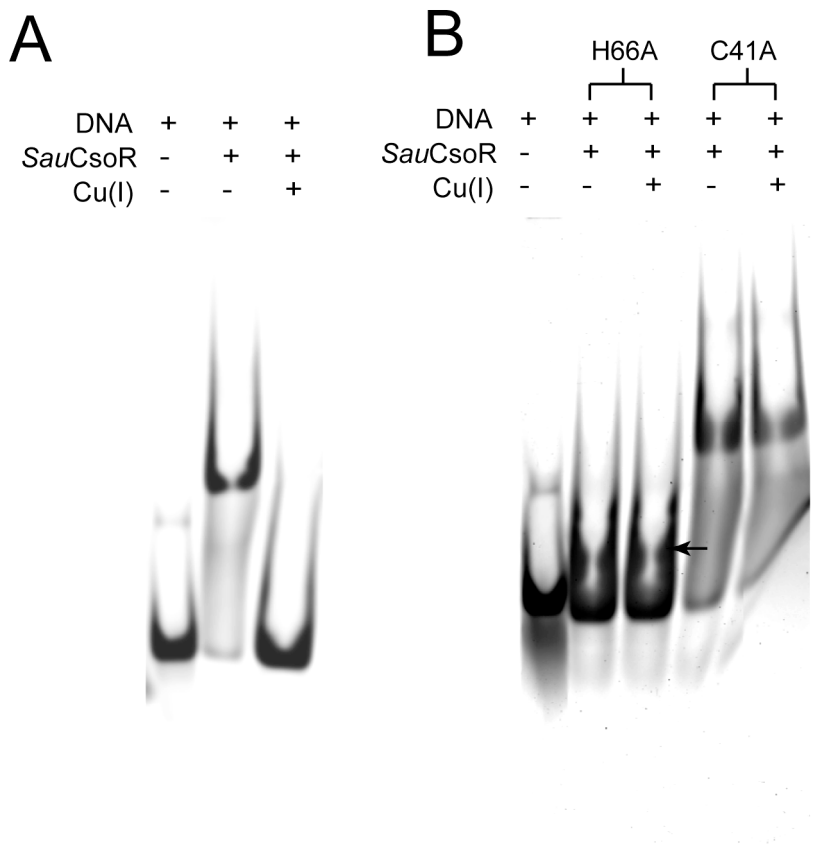

Figure 40. DNA binding of wild-type *Sau* CsoR (A) and H66A and C41A mutants (B) in absence or presence of saturating Cu(I) as monitored by EMSA. Possible non-specific H66A CsoR-DNA complex may form under the high DNA concentration (0.5 μM) used here as indicated by the arrow in panel (B). Condition: 10 mM HEPES, 0.2 M NaCl, 2 mM DTT, pH 7.0.

DISCUSSION

These data provide the first evidence that the gene designated NWMN_1991 may encode a CsoR in *S. aureus* that functions as a Cu(I)-sensor protein in regulating the transcription of *copA* required to mitigate Cu(I) stress by effluxing Cu from the cytoplasm. Both the biological and biochemical data are consistent with a derepression model similar to that described for *Mtb* and *Bsu* CsoRs, in which the apo *Sau* CsoR binds to the promoter region of *copA* gene and represses the transcription, while Cu(I) binding induces derepression.

The *Sau ΔcsoR* strain constructed by our collaborator has been found to be more resistant to Cu stress (Appendix E). The DNA binding study reported here suggests that *Sau* C41A CsoR binds to the DNA regardless of the presence of Cu(I). Therefore, a *S. aureus* strain carrying C41A CsoR is expected to repress the transcription of *copA* even under Cu stress and will be more sensitive to Cu stress when compared to the wild-type strain. Thus, C41A CsoR will function as a dominant negative mutant. On the other hand, *Sau* H66A CsoR is incapable of binding the DNA. The transcription of *copA* in a strain carrying H66A is expected to be constitutively on and may present a phenotype that is similar to that of the *ΔcsoR* strain (Appendix E**APPENDIX E**). The studies of the Cu resistance of these two strains will provide more convincing evidence to support the proposed function of *Sau* CsoR. RT-PCR experiments being carried out to determine the transcription of *copA* in these different strains comparing to wild-type strain grown under different Cu concentrations in the medium will also be necessary to verify the proposed role of CsoR in transcriptional regulation. In addition, the Cu content in these

different *S. aureus* strains is being measured by ICP-MS (*9*) with the prediction that strains with constitutive *copA* transcription will be expected to have a low cytosolic Cu content, relative to C41A CsoR-allele containing strains.

It is also noted that the gene encoding the proposed Cu-chaperone CopZ is next to *copA* (Figure 36). Although the transcription of *copZ* gene is also Cu-dependent, these two genes do not seem to be co-transcribed (*136*). Therefore, it is not yet known whether the transcription of *copZ* is also regulated by CsoR or some other as yet unknown regulator. An assay to determine whether CsoR can bind the promoter region of *copZ* as well as the transcription level of *copZ* in the *ΔcsoR* strain comparing to the wild-type strain will be required to understand this.

Efforts have also been made to quantify the DNA binding affinity of apo and Cu(I)-bound *Sau* CsoR using a fluorescence anisotropy-based assay as described in previous chapters. In fact, the DNA binding affinity of apo-*Sau* CsoR was determined to be $A_2^{apo} \approx 10^{14}$ M^{-2} with a change in the anisotropy of the fluorescein fluorescence of the 39 bp DNA consistent with a stoichiometry of two tetramers per DNA (data not shown). These characteristics are similar to that determined for apo-*Mtb* CsoR determined under similar solution conditions (Chapter II). However, when Cu(I)-bound *Sau* CsoR was titrated into the same DNA, a binding isotherm that fails to "saturate" was obtained. This is likely the result of non-specific interactions between high molecular weight CsoR aggregates and the DNA which may be enhanced by Cu(I). Systematically changing of solution conditions, *i.e.*, salt concentration and pH, failed to prevent such interactions (data not shown). Interestingly, no complex is observed in the EMSA assay carried out

here (Figure 40A), thus consistent with the idea that these interactions between Cu(I)-bound CsoR and DNA are weak and kinetically labile and thus dissociate during electrophoresis. Although the DNA binding affinity is unable to be obtained by EMSA under the conditions of high input DNA concentrations used here (~0.5 μM DNA), further experiments using ^{32}P or digoxigenin end-labeled DNA will provide a better estimate of the CopO binding affinities of apo- and Cu(I) *Sau* CsoRs (*39, 105*).

CHAPTER VI

SUMMARY AND PERSPECTIVES

SUMMARY

In this work, three Cu-sensing homologs from the newly described CsoR/RcnR metalloregulatory family have been biochemically characterized using biochemical and biophysical methods. These include the founding member, *Mtb* CsoR, a subsequently described *Bsu* CsoR and a candidate CsoR from *S. aureus*. Biochemical data reveal that *each* shares properties consistent with a role as a Cu(I) sensor in the cytosol where it regulates the transcription of genes involved in Cu homeostasis. All three CsoRs form 3-coordinate trigonal planar S_2N complexes with Cu(I) characterized by extraordinarily high affinity ($\log K_{Cu} \geq 18$). Cu(I)-binding in turn decreases the operator DNA binding affinity and leads to derepression of the genes repressed by the apo-form of these CsoRs. Efforts to explore the underlying mechanism of this allosteric negative regulation by Cu(I) using a combination of unnatural amino acid substitution and conventional mutagenesis reveal three essential residues in *Mtb* CsoR. These include the Cu(I) ligand His61 itself and two "second coordination shell" residues, Tyr35 and Glu81, which appear to be involved in propagating the allosteric response. As a result of these studies, we have proposed that upon coordination of Cu(I) via the $N^{\delta 1}$ atom of His61 (*Mtb* CsoR numbering system) , the $N^{\varepsilon 2}$ atom may form a hydrogen bonding network with Tyr35 and Glu81, which further stabilizes a conformation of the protein with low DNA binding affinity. We further establish that substitution of His61 with Ala not only alters the first

coordination sphere of the Cu(I) ion (*39*), but largely abrogates operator DNA binding. While this work provides novel molecular level insights into this new family of metalloregulatory proteins, several key unresolved issues remain (see below).

PERSPECTIVES

How does CsoR bind to its DNA operator? The Cu(I)-bound structure of *Mtb* CsoR reveals a novel protein fold with no classical DNA binding motif (Figure 8). High resolution structural studies coupled with a better understanding of the minimal structural characterization of the DNA operator will provide further insights into the protein-DNA complex and how Cu-binding inhibits the complex. A recent report on the DNA sequences bound by *E. coli* RcnR revealed that a "G-tract" flanked by short inverted repeats may characterize the minimal structural element recognized by RcnR tetramer, although the extent to which this is true for CsoRs remain to be tested (*137*). *Bsu* CsoR is likely the best structural target among the three CsoRs characterized here since it lacks the long C-terminal tail of *Mtb* CsoR, like nearly all other CsoRs (Figure 9). More importantly, *Bsu* CsoR is easily purified to very high yield from *E. coli* and as shown in Chapter IV is a stable tetramer in both apo- and Cu(I) bound states, physical properties consistent with an excellent structural target. Solution conditions (10 mM MES, 50 mM NaCl, 2 mM TCEP, pH 6.0, 40 ^{o}C) have been established that give rise to ≥80% of the number of expected backbone amide correlations in a fully deuterated sample in a ^{1}H-^{15}N HSQC NMR spectrum. These spectra may well permit detailed NMR studies of the CsoR tetramer and the tetramer-DNA complex. At a minimum, these

preliminary spectra certainly argue for a rotationally symmetric complex with D_2 symmetry (data not shown).

Alternatively, crystallography could be used to solve the high resolution structure of *Bsu* CsoR-DNA complex, as well as that of apo and Cu(I)-bound *Bsu* CsoR. The DNA binding stoichiometry and affinity determined here along with previous footprinting results (*105*) provide crucial information that can be used to screen crystallization conditions for the protein-DNA complex. A comparison of all three allosteric states will provide detailed insights as to how this putative hydrogen bonding network drives allosteric inhibition of DNA binding. Such studies are also critical for our understanding of how His61 stabilizes the complex with DNA.

Other biochemical methods can also be used to probe the DNA binding surface on CsoR. For example, a pulse-chase mass spectrometry-based ratiometric lysine modification scheme has been developed in our laboratory to identify which Lys residues in CsoR are protected from reaction with a chemical reagent when bound to DNA. Alternatively, H/D exchange mass spectrometry could also be used to obtain dynamics information from backbone amide protons in the event that NMR studies ultimately fail (*138*).This approach can also be used to probe more subtle conformational changes upon Cu(I) binding, as has been described in *B. subtilis* MntR, a Mn(II)-regulatory protein (*139*). The biochemical data here clearly suggest that *Bsu* CsoR is also capable of binding Zn(II) and Ni(II) with high affinity, but the binding of these divalent metal ions are unable to induce a conformation that is characterized by low-affinity

DNA binding. These non-inducing metal ions can serve as good controls in developing this method, as has been shown for MntR (*139*).

Role of the C-terminal tail of Mtb CsoR. As discussed, *Mtb* CsoR has a unique C-terminal tail consisting of ≈30 amino acids residues, ≈18 of which are highly conserved in pathogenic mycobacteria (through V104; Figure 9). An unexpected finding was that this region plays an important role in DNA binding (Chapter II) since truncation of the tail before residue 106 significantly decreases the DNA binding affinity. The conserved residues in the tail are mostly neutral and hydrophobic in nature, and are therefore unlikely to interact directly with the DNA. One possibility is that the tail influences the oligomerization or the conformational state of CsoR in solution or when bound to DNA.

The crystallographic structure of Cu(I)-bound CsoR reveals that the tetramer may form as a dimer of dimers, with the α3 helices positioned at the dimer-dimer interface. Therefore, although the C-terminal tail is not resolved in the structure, it is very likely to be found at this interface where it could potentially stabilize the tetramer or alternatively change the distance between positively charged patches on one face of the tetramer (*39*). This may also suggest the exciting possibility that another protein, *e.g.*, a Cu chaperone, might bind to this tail and thereby mediate disassembly of the protein-DNA complex in some way. In any case, a systematic study on the assembly state of the full-length *Mtb* CsoR as well as the deletion mutants will likely shed considerable light on understanding the fundamental role of the C-terminal tail in *Mtb* CsoR.

From where does CsoR obtain Cu(I) inside of the cell? Due to the toxicity of free Cu(I) ions, there is likely to be little bioavailable Cu(I) in the cell (*38*). Therefore, it is not yet

known how CsoR obtains its Cu(I) ion. *B. subtilis* provides an excellent opportunity with which to investigate this problem since the Cu chaperone CopZ, a good candidate for Cu delivery to CsoR, has been extensively structurally and biochemically characterized (*112, 135, 140, 141*). Intermolecular Cu(I) transfer from the Cu chaperone to the target proteins usually occurs via an intermolecular ligand exchange reaction (Figure 41) (*12*). Our detailed structural and thermodynamic knowledge of both *Bsu* CsoR and CopZ (*111, 112, 141*) will allow us to readily test whether CopZ is capable of transferring Cu(I) to CsoR, in a mechanism that is analogous to that proposed for CopZ and the Cu regulatory repressor CopY in *E. hirae* (*142*). It would be interesting to examine both the kinetic and thermodynamic aspects of the transfer reaction. Kinetically, Cu(I) transfer through a ligand exchange reaction is expected to be much faster than a mechanism where Cu(I) first dissociates from CopZ and then binds to CsoR, because Cu(I)-CopZ affinity is very high and k_{off} for Cu(I) should be very slow (*112*). The significant quenching of the tyrosine fluorescence upon Cu(I) binding to CsoR (Chapter IV) provides an excellent probe with which to monitor such a transfer event. It would also be interesting to carry out such a kinetics study in presence of DNA to determine the rate at which CsoR dissociates from the DNA in presence of Cu(I)-bound CopZ by fluorescence anisotropy.

Cu(I) transfer can also be monitored under equilibrium conditions as shown for CopY and CopA using size-exclusion chromatography (*142, 143*). Since CsoR forms a tetramer (~45 kDa) and CopZ (~8 kDa) is monomeric, these two proteins can easily be separated from one another in a mixture. More importantly, the Cu content of the

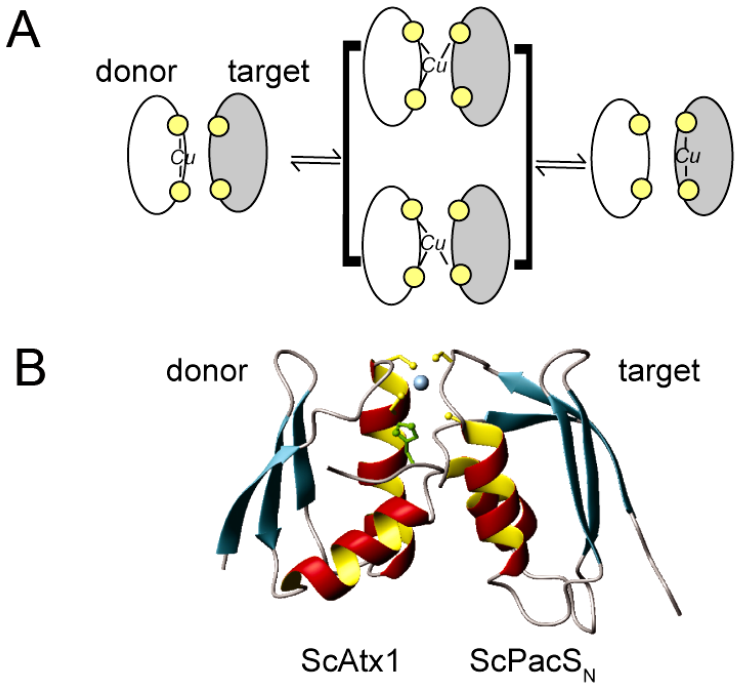

Figure 41. Intermolecular Cu(I) transfer by a ligand exchange reaction. (A) Schematic model of Cu(I) exchange between a Cu(I) donor metallochaperone and a Cu(I) target protein, *e.g.,* the MBD of a P-type ATPase. The structural intermediate shown in brackets is a transiently formed Cu(I)-cross linked intermolecular complex (*29*), a three-dimensional NMR-based model of which is shown in (B) for the complex between the Cu(I) chaperone ScAtx1 and the N-terminal MBD of PacS from *Synechocystis* PCC 6803 (*144*).

individual fractions can be easily measured by atomic absorption spectroscopy or ICP-MS to follow Cu(I) transfer (*142*). Finally, although the ligand exchange reaction likely involves the formation of a transient metal-mediated protein-protein intermediate that may be difficult to detect using standard biochemical methods, such an short-lived transfer intermediate has been captured and studied by NMR spectroscopy in other systems (*12*). The fact that *B. subtilis* CopZ has been extensively studied by NMR spectroscopy greatly facilitates such experiments (*135, 141*).

Function of the CsoR-like putative oxidative stress sensors. As discussed in Chapter I, the amino acids in the W-X-Y-Z "signature" positions of CsoR/RcnR family sensors (see Figure 10) suggest the hypothesis that a group of CsoR orthologs with x-Cys-x-Cys motif may sense oxidative stress or function in sulfur metabolism in some way. A survey of the genomic neighborhoods of these genes reveals common neighbors such as rhodanese homology domain proteins and/or a putative glyoxalase I, the latter of which facilitates resistance to oxidative stress and carbonyl electrophiles (*1, 103*). However, there is as yet no direct biological or biochemical evidence in support of this hypothesis.

Investigation of a homology model of these putative oxidative stress sensing CsoRs reveals that the two conserved Cys residues are likely in close proximity (analogous to Cys36 and Cys65' in *Mtb* CsoR) with which to reversibly form a disulfide bond under oxidizing conditions. This may then induce a conformational change in the dimer (or tetramer) as well, which will in turn regulate the DNA binding affinity. Oxidative stress sensing via formation of a reversible disulfide bond has been shown in several oxidative stress sensors, including the *P. aeruginosa* MexR from MarR family

(*104*) and *E. coli* OxyR from LysR family (Figure 2) (*145*). However, it should be pointed out that the pK_a and reduction potential of the Cys pair must be tuned in such a way that reversible disulfide bond formation can occur in the cytosolic milieu over a range of reduction potentials accessible in oxidatively stressed vs. non-stressed cells.

To begin to investigate the function of these CsoR-like proteins, candidate CsoR^{ox} containing x-Cys-x-Cys signatures from *S. pneumoniae* (SPD_0073) and *S. aureus* Newman (Figure 42) have been expressed in *E. coli* and purified to homogeneity in our laboratory. We also have access to deletion strains made in collaboration with Drs. Malcolm Winkler (Indiana University) and Eric Skaar (Vanderbilt University), respectively. Although functional characterization of these strains is in progress, preliminary data suggest that both proteins are purified as partially oxidized dimers (unlike *bona fide* Cu sensors) which suggests that the reduction potential of this Cys pair may well be more negative than in the Cu sensors (Ma, Z. et al., unpublished observations). In addition, *Sau* CsoR^{ox} purified from *E. coli* is capable of binding to the DNA derived from this promoter region of NWMN_0027 under reducing conditions *in vitro*. We therefore hypothesize that *Sau* CsoR^{ox} regulates the transcription of NWMN_0027, although further biological and biochemical experiments are required to fully understand the functional importance and mechanism of derepression of this subfamily of regulators.

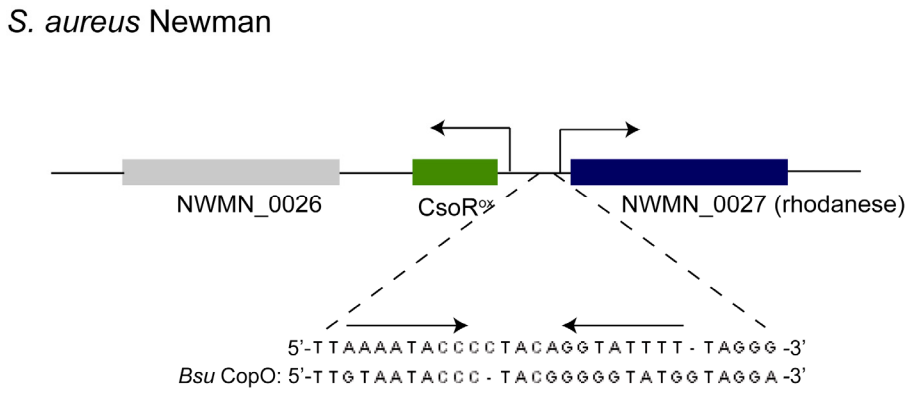

Figure 42. Genetic localization of the gene encoding *Sau* CsoR^{ox}. The DNA sequence in the promoter region of NWMN_0027 is shown in comparison with *Bsu* CopO (see Chapter IV). NWMN_0027 encodes a putative rhodanese homology domain often associated with cyanide detoxification, sulfur trafficking via formation of Cys persulfides and iron-sulfur protein biogenesis (*146*).

REFERENCES

1. Ma, Z., Jacobsen, F. E., and Giedroc, D. P. (2009) Coordination chemistry of bacterial metal sensing and transport, *Chem. Rev. in press*.

2. Waldron, K. J., Rutherford, J. C., Ford, D., and Robinson, N. J. (2009) Metalloproteins and metal sensing, *Nature 460*, 823-830.

3. Lippard, S. J., and Berg, J. M. (1994) *Principles of Bioinorganic Chemistry*, University Science Books, Mill Valley, CA.

4. Tottey, S., Waldron, K. J., Firbank, S. J., Reale, B., Bessant, C., Sato, K., Cheek, T. R., Gray, J., Banfield, M. J., Dennison, C., and Robinson, N. J. (2008) Protein-folding location can regulate manganese-binding versus copper- or zinc-binding, *Nature 455*, 1138-1142.

5. Waldron, K. J., and Robinson, N. J. (2009) How do bacterial cells ensure that metalloproteins get the correct metal?, *Nat. Rev. Microbiol. 7*, 25-35.

6. Giedroc, D. P., and Arunkumar, A. I. (2007) Metal sensor proteins: nature's metalloregulated allosteric switches, *Dalton Trans.*, 3107-3120.

7. Outten, C. E., and O'Halloran, T. V. (2001) Femtomolar sensitivity of metalloregulatory proteins controlling zinc homeostasis, *Science 292*, 2488-2492.

8. Maier, R., Benoit, S., and Seshadri, S. (2007) Nickel-binding and accessory proteins facilitating Ni-enzyme maturation in Helicobacter pylori, *BioMetals 20*, 655-664.

9. Finney, L. A., and O'Halloran, T. V. (2003) Transition metal speciation in the cell: Insights from the chemistry of metal ion receptors, *Science 300*, 931-936.

10. Bandyopadhyay, S., Chandramouli, K., and Johnson, M. K. (2008) Iron-sulfur cluster biosynthesis, *Biochem. Soc. Trans. 036*, 1112-1119.

11. Graham, A. I., Hunt, S., Stokes, S. L., Bramall, N., Bunch, J., Cox, A. G., McLeod, C. W., and Poole, R. K. (2009) Severe zinc depletion of Escherichia coli: Roles for high affinity zinc binding by ZinT, zinc transport and zinc-independent proteins, *J. Biol. Chem. 284*, 18377-18389.

12. Banci, L., Bertini, I., Cantini, F., Felli, I. C., Gonnelli, L., Hadjiliadis, N., Pierattelli, R., Rosato, A., and Voulgaris, P. (2006) The Atx1-Ccc2 complex is a metal-mediated protein-protein interaction, *Nat. Chem. Biol. 2*, 367-368.

13. Wu, C. C., Rice, W. J., and Stokes, D. L. (2008) Structure of a copper pump suggests a regulatory role for its metal-binding domain, *Structure 16*, 976-985.

14. Lu, M., and Fu, D. (2007) Structure of the zinc transporter YiiP, *Science 317*, 1746-1748.

15. Davis, A. V., and O'Halloran, T. V. (2008) A place for thioether chemistry in cellular copper ion recognition and trafficking, *Nat. Chem. Biol. 4*, 148-151.

16. Zhang, L., Koay, M., Maher, M. J., Xiao, Z., and Wedd, A. G. (2006) Intermolecular transfer of copper ions from the CopC protein of Pseudomonas syringae. Crystal structures of fully loaded Cu(I)Cu(II) forms, *J. Am. Chem. Soc. 128*, 5834-5850.

17. Gold, B., Deng, H., Bryk, R., Vargas, D., Eliezer, D., Roberts, J., Jiang, X., and Nathan, C. (2008) Identification of a copper-binding metallothionein in pathogenic mycobacteria, *Nat. Chem. Biol. 4*, 609-616.

18. Blindauer, C. A., Harrison, M. D., Robinson, A. K., Parkinson, J. A., Bowness, P. W., Sadler, P. J., and Robinson, N. J. (2002) Multiple bacteria encode metallothioneins and SmtA-like zinc fingers, *Mol. Microbiol. 45*, 1421-1432.

19. Andrews, S. C., Robinson, A. K., and Rodriguez-Quinones, F. (2003) Bacterial iron homeostasis, *FEMS Microbiol. Rev. 27*, 215-237.

20. Solioz, M., and Stoyanov, J. V. (2003) Copper homeostasis in Enterococcus hirae, *FEMS Microbiol. Rev. 27*, 183-195.

21. Cavet, J. S., Borrelly, G. P., and Robinson, N. J. (2003) Zn, Cu and Co in cyanobacteria: selective control of metal availability, *FEMS Microbiol. Rev. 27*, 165-181.

22. Ward, S. K., Hoye, E. A., and Talaat, A. M. (2008) The global responses of Mycobacterium tuberculosis to physiological levels of copper, *J. Bacteriol. 190*, 2939-2946.

23. Magnani, D., Barre, O., Gerber, S. D., and Solioz, M. (2008) Characterization of the CopR regulon of Lactococcus lactis IL1403, *J. Bacteriol. 190*, 536-545.

24. Macomber, L., and Imlay, J. A. (2009) The iron-sulfur clusters of dehydratases are primary intracellular targets of copper toxicity, *Proc. Natl. Acad. Sci. 106*, 8344-8349.

25. Dong, J., Atwood, C. S., Anderson, V. E., Siedlak, S. L., Smith, M. A., Perry, G., and Carey, P. R. (2003) Metal binding and oxidation of amyloid-beta within isolated senile plaque cores: Raman microscopic evidence, *Biochemistry 42*, 2768-2773.

26. Rasia, R. M., Bertoncini, C. W., Marsh, D., Hoyer, W., Cherny, D., Zweckstetter, M., Griesinger, C., Jovin, T. M., and Fernandez, C. O. (2005) Structural characterization of copper(II) binding to alpha-synuclein: Insights into the bioinorganic chemistry of Parkinson's disease, *Proc. Natl. Acad. Sci. 102*, 4294-4299.

27. Bocharova, O. V., Breydo, L., Salnikov, V. V., and Baskakov, I. V. (2005) Copper(II) inhibits in vitro conversion of prion protein into amyloid fibrils, *Biochemistry 44*, 6776-6787.

28. Eakin, C. M., Berman, A. J., and Miranker, A. D. (2006) A native to amyloidogenic transition regulated by a backbone trigger, *Nat. Struct. Mol. Biol. 13*, 202-208.

29. Rae, T. D., Schmidt, P. J., Pufahl, R. A., Culotta, V. C., and O'Halloran, T. V. (1999) Undetectable intracellular free copper: the requirement of a copper chaperone for superoxide dismutase, *Science 284*, 805-808.

30. Noyce, J. O., Michels, H., and Keevil, C. W. (2006) Potential use of copper surfaces to reduce survival of epidemic meticillin-resistant Staphylococcus aureus in the healthcare environment, *J. Hosp. Infect. 63*, 289-297.

31. Francis, M. S., and Thomas, C. J. (1997) Mutants in the CtpA copper transporting P-type ATPase reduce virulence of Listeria monocytogenes, *Microb. Pathog. 22*, 67-78.

32. Mitrakul, K., Loo, C. Y., Hughes, C. V., and Ganeshkumar, N. (2004) Role of a Streptococcus gordonii copper-transport operon, copYAZ, in biofilm detachment, *Oral. Microbiol. Immunol. 19*, 395-402.

33. Rensing, C., and Grass, G. (2003) Escherichia coli mechanisms of copper homeostasis in a changing environment, *FEMS Microbiol. Rev. 27*, 197-213.

34. Blindauer, C. A., Harrison, M. D., Parkinson, J. A., Robinson, A. K., Cavet, J. S., Robinson, N. J., and Sadler, P. J. (2001) A metallothionein containing a zinc finger within a four-metal cluster protects a bacterium from zinc toxicity, *Proc. Natl. Acad. Sci. 98*, 9593-9598.

35. Barkay, T., Miller, S. M., and Summers, A. O. (2003) Bacterial mercury resistance from atoms to ecosystems, *FEMS Microbiol. Rev. 27*, 355-384.

36. Qin, J., Rosen, B. P., Zhang, Y., Wang, G., Franke, S., and Rensing, C. (2006) Arsenic detoxification and evolution of trimethylarsine gas by a microbial arsenite S-adenosylmethionine methyltransferase, *Proc. Natl. Acad. Sci. 103*, 2075-2080.

37. Ye, J., Kandegedara, A., Martin, P., and Rosen, B. P. (2005) Crystal structure of the Staphylococcus aureus pI258 CadC Cd(II)/Pb(II)/Zn(II)-responsive repressor, *J. Bacteriol. 187*, 4214-4221.

38. Changela, A., Chen, K., Xue, Y., Holschen, J., Outten, C. E., O'Halloran, T. V., and Mondragon, A. (2003) Molecular basis of metal-ion selectivity and zeptomolar sensitivity by CueR, *Science 301*, 1383-1387.

39. Liu, T., Ramesh, A., Ma, Z., Ward, S. K., Zhang, L., George, G. N., Talaat, A. M., Sacchettini, J. C., and Giedroc, D. P. (2007) CsoR is a novel Mycobacterium tuberculosis copper-sensing transcriptional regulator, *Nat. Chem. Biol. 3*, 60-68.

40. Safo, M. K., Zhao, Q., Ko, T. P., Musayev, F. N., Robinson, H., Scarsdale, N., Wang, A. H., and Archer, G. L. (2005) Crystal structures of the BlaI repressor from Staphylococcus aureus and its complex with DNA: insights into transcriptional regulation of the bla and mec operons, *J. Bacteriol. 187*, 1833-1844.

41. Orth, P., Schnappinger, D., Hillen, W., Saenger, W., and Hinrichs, W. (2000) Structural basis of gene regulation by the tetracycline inducible Tet repressor-operator system, *Nat. Struct. Biol. 7*, 215-219.

42. Traore, D. A., El Ghazouani, A., Ilango, S., Dupuy, J., Jacquamet, L., Ferrer, J. L., Caux-Thang, C., Duarte, V., and Latour, J. M. (2006) Crystal structure of the apo-PerR-Zn protein from Bacillus subtilis, *Mol. Microbiol. 61*, 1211-1219.

43. Kliegman, J. I., Griner, S. L., Helmann, J. D., Brennan, R. G., and Glasfeld, A. (2006) Structural basis for the metal-selective activation of the manganese transport regulator of Bacillus subtilis, *Biochemistry 45*, 3493-3505.

44. Schreiter, E. R., Wang, S. C., Zamble, D. B., and Drennan, C. L. (2006) NikR-operator complex structure and the mechanism of repressor activation by metal ions, *Proc. Natl. Acad. Sci. 103*, 13676-13681.

45. Hong, M., Fuangthong, M., Helmann, J. D., and Brennan, R. G. (2005) Structure of an OhrR-ohrA operator complex reveals the DNA binding mechanism of the MarR family, *Mol. Cell 20*, 131-141.

46. Schüttelkopf, A. W., Boxer, D. H., and Hunter, W. N. (2003) Crystal Structure of Activated ModE Reveals Conformational Changes Involving Both Oxyanion and DNA-binding Domains, *J. Mol. Biol. 326*, 761-767.

47. Wang, Y., Hemmingsen, L., and Giedroc, D. P. (2005) Structural and functional characterization of Mycobacterium tuberculosis CmtR, a PbII/CdII-sensing SmtB/ArsR metalloregulatory repressor, *Biochemistry 44*, 8976-8988.

48. Stoyanov, J. V., Hobman, J. L., and Brown, N. L. (2001) CueR (YbbI) of Escherichia coli is a MerR family regulator controlling expression of the copper exporter CopA, *Mol. Microbiol. 39*, 502-511.

49. Strausak, D., and Solioz, M. (1997) CopY is a copper-inducible repressor of the Enterococcus hirae copper ATPases, *J. Biol. Chem. 272*, 8932-8936.

50. De Pina, K., Desjardin, V., Mandrand-Berthelot, M. A., Giordano, G., and Wu, L. F. (1999) Isolation and characterization of the nikR gene encoding a nickel-responsive regulator in Escherichia coli, *J. Bacteriol. 181*, 670-674.

51. Patzer, S. I., and Hantke, K. (1998) The ZnuABC high-affinity zinc uptake system and its regulator Zur in Escherichia coli, *Mol. Microbiol. 28*, 1199-1210.

52. Busenlehner, L. S., Pennella, M. A., and Giedroc, D. P. (2003) The SmtB/ArsR family of metalloregulatory transcriptional repressors: Structural insights into prokaryotic metal resistance, *FEMS Microbiol. Rev. 27*, 131-143.

53. Campbell, D. R., Chapman, K. E., Waldron, K. J., Tottey, S., Kendall, S., Cavallaro, G., Andreini, C., Hinds, J., Stoker, N. G., Robinson, N. J., and Cavet, J. S. (2007) Mycobacterial cells have dual nickel-cobalt sensors: sequence relationships and metal sites of metal-responsive repressors are not congruent, *J. Biol. Chem. 282*, 32298-32310.

54. Wu, J., and Rosen, B. P. (1993) Metalloregulated expression of the ars operon, *J. Biol. Chem. 268*, 52-58.

55. Morby, A. P., Turner, J. S., Huckle, J. W., and Robinson, N. J. (1993) SmtB is a metal-dependent repressor of the cyanobacterial metallothionein gene smtA: identification of a Zn inhibited DNA-protein complex, *Nuceic Acids Res. 21*, 921-925.

56. Cavet, J. S., Graham, A. I., Meng, W., and Robinson, N. J. (2003) A cadmium-lead-sensing ArsR-SmtB repressor with novel sensory sites. Complementary metal discrimination by NmtR AND CmtR in a common cytosol, *J. Biol. Chem. 278*, 44560-44566.

57. Harvie, D. R., Andreini, C., Cavallaro, G., Meng, W., Connolly, B. A., Yoshida, K., Fujita, Y., Harwood, C. R., Radford, D. S., Tottey, S., Cavet, J. S., and Robinson, N. J. (2006) Predicting metals sensed by ArsR-SmtB repressors: allosteric interference by a non-effector metal, *Mol. Microbiol. 59*, 1341-1356.

58. Liu, T., Golden, J. W., and Giedroc, D. P. (2005) A zinc(II)/lead(II)/cadmium(II) -inducible operon from the Cyanobacterium anabaena is regulated by AztR, an alpha3N ArsR/SmtB metalloregulator, *Biochemistry 44*, 8673-8683.

59. Thelwell, C., Robinson, N. J., and Turner-Cavet, J. S. (1998) An SmtB-like repressor from Synechocystis PCC 6803 regulates a zinc exporter, *Proc. Natl. Acad. Sci. 95*, 10728-10733.

60. Liu, T., Chen, X., Ma, Z., Shokes, J., Hemmingsen, L., Scott, R. A., and Giedroc, D. P. (2008) A Cu(I)-sensing ArsR family metal sensor protein with a relaxed metal selectivity profile, *Biochemistry 47*, 10564-10575.

61. Busenlehner, L. S., Weng, T. C., Penner-Hahn, J. E., and Giedroc, D. P. (2002) Elucidation of primary (alpha(3)N) and vestigial (alpha(5)) heavy metal-binding sites in Staphylococcus aureus pI258 CadC: evolutionary implications for metal ion selectivity of ArsR/SmtB metal sensor proteins, *J. Mol. Biol. 319*, 685-701.

62. Busenlehner, L. S., and Giedroc, D. P. (2006) Kinetics of metal binding by the toxic metal-sensing transcriptional repressor Staphylococcus aureus pI258 CadC, *J. Inorg. Biochem. 100*, 1024-1034.

63. Apuy, J. L., Busenlehner, L. S., Russell, D. H., and Giedroc, D. P. (2004) Ratiometric pulsed alkylation mass spectrometry as a probe of thiolate reactivity in different metalloderivatives of Staphylococcus aureus pI258 CadC, *Biochemistry 43*, 3824-3834.

64. Ordoñez, E., Thiyagarajan, S., Cook, J. D., Stemmler, T. L., Gil, J. A., Mateos, L. M., and Rosen, B. P. (2008) Evolution of metal(loid) binding sites in transcriptional regulators, *J. Biol. Chem. 283*, 25706-25714.

65. Arunkumar, A. I., Campanello, G. C., and Giedroc, D. P. (2009) Solution structure of CzrA in the DNA-bound state: Insights into metal-induced allosteric

regulation in ArsR/SmtB family metal sensor proteins, *Proc. Natl. Acad. Sci. In Press*.

66. Eicken, C., Pennella, M. A., Chen, X., Koshlap, K. M., VanZile, M. L., Sacchettini, J. C., and Giedroc, D. P. (2003) A metal-ligand-mediated intersubunit allosteric switch in related SmtB/ArsR zinc sensor proteins, *J. Mol. Biol. 333*, 683-695.

67. Liu, T., Nakashima, S., Hirose, K., Shibasaka, M., Katsuhara, M., Ezaki, B., Giedroc, D. P., and Kasamo, K. (2004) A novel cyanobacterial SmtB/ArsR family repressor regulates the expression of a CPx-ATPase and a metallothionein in response to both Cu(I)/Ag(I) and Zn(II)/Cd(II), *J. Biol. Chem. 279*, 17810-17818.

68. Hirose, K., Ezaki, B., Liu, T., and Nakashima, S. (2006) Diamide stress induces a metallothionein BmtA through a repressor BxmR and is modulated by Zn-inducible BmtA in the cyanobacterium Oscillatoria brevis, *Toxicol. Lett. 163*, 250-256.

69. VanZile, M. L., Chen, X., and Giedroc, D. P. (2002) Structural characterization of distinct alpha3N and alpha5 metal sites in the cyanobacterial zinc sensor SmtB, *Biochemistry 41*, 9765-9775.

70. Pennella, M. A., Shokes, J. E., Cosper, N. J., Scott, R. A., and Giedroc, D. P. (2003) Structural elements of metal selectivity in metal sensor proteins, *Proc. Natl. Acad. Sci. 100*, 3713-3718.

71. Cavet, J. S., Meng, W., Pennella, M. A., Appelhoff, R. J., Giedroc, D. P., and Robinson, N. J. (2002) A nickel-cobalt-sensing ArsR-SmtB family repressor. Contributions of cytosol and effector binding sites to metal selectivity, *J. Biol. Chem. 277*, 38441-38448.

72. Qin, J., Fu, H. L., Ye, J., Bencze, K. Z., Stemmler, T. L., Rawlings, D. E., and Rosen, B. P. (2007) Convergent evolution of a new arsenic binding site in the ArsR/SmtB family of metalloregulators, *J. Biol. Chem. 282*, 34346-34355.

73. Banci, L., Bertini, I., Cantini, F., Ciofi-Baffoni, S., Cavet, J. S., Dennison, C., Graham, A. I., Harvie, D. R., and Robinson, N. J. (2007) NMR structural

analysis of cadmium sensing by winged helix repressor CmtR, *J. Biol. Chem. 282*, 30181-30188.

74. Grossoehme, N. E., and Giedroc, D. P. (2009) Thermodynamic investigation of the energies driving allosteric coupling in CzrA *J. Am. Chem. Soc. Submitted*.

75. Saha, R. P., and Chakrabarti, P. (2006) Molecular modeling and characterization of Vibrio cholerae transcription regulator HlyU, *BMC Struct. Biol. 6*, 24.

76. Mandal, S., Chatterjee, S., Dam, B., Roy, P., and Das Gupta, S. K. (2007) The dimeric repressor SoxR binds cooperatively to the promoter(s) regulating expression of the sulfur oxidation (sox) operon of Pseudaminobacter salicylatoxidans KCT001, *Microbiology 153*, 80-91.

77. Gueune, H., Durand, M.-J., Thouand, G., and DuBow, M. S. (2008) The ygaVP Genes of Escherichia coli Form a Tributyltin-Inducible Operon, *Appl. Environ. Microbiol. 74*, 1954-1958.

78. Lund, P. A., Ford, S. J., and Brown, N. L. (1986) Transcriptional regulation of the mercury-resistance genes of transposon Tn501, *J. Gen. Microbiol. 132 (Pt 2)*, 465-480.

79. O'Halloran, T., and Walsh, C. (1987) Metalloregulatory DNA-binding protein encoded by the merR gene: isolation and characterization, *Science 235*, 211-214.

80. Lund, P. A., and Brown, N. L. (1989) Regulation of transcription in Escherichia coli from the mer and merR promoters in the transposon Tn501, *J. Mol. Biol. 205*, 343-353.

81. O'Halloran, T. V., Frantz, B., Shin, M. K., Ralston, D. M., and Wright, J. G. (1989) The MerR heavy metal receptor mediates positive activation in a topologically novel transcription complex, *Cell 56*, 119-129.

82. Permina, E., Kazakov, A., Kalinina, O., and Gelfand, M. (2006) Comparative genomics of regulation of heavy metal resistance in Eubacteria, *BMC Microbiol. 6*, 49.

83. Outten, C. E., Outten, F. W., and O'Halloran, T. V. (1999) DNA distortion mechanism for transcriptional activation by ZntR, a Zn(II)-responsive MerR homologue in Escherichia coli, *J. Biol. Chem. 274*, 37517-37524.

84. Frantz, B., and O'Halloran, T. V. (1990) DNA distortion accompanies transcriptional activation by the metal-responsive gene-regulatory protein MerR, *Biochemistry 29*, 4747-4751.

85. Checa, S. K., Espariz, M., Audero, M. E., Botta, P. E., Spinelli, S. V., and Soncini, F. C. (2007) Bacterial sensing of and resistance to gold salts, *Mol. Microbiol. 63*, 1307-1318.

86. Lee, S. W., Glickmann, E., and Cooksey, D. A. (2001) Chromosomal locus for cadmium resistance in Pseudomonas putida consisting of a cadmium-transporting ATPase and a MerR family response regulator, *Appl. Environ. Microbiol. 67*, 1437-1444.

87. Borremans, B., Hobman, J. L., Provoost, A., Brown, N. L., and van Der Lelie, D. (2001) Cloning and functional analysis of the pbr lead resistance determinant of Ralstonia metallidurans CH34, *J. Bacteriol. 183*, 5651-5658.

88. Heldwein, E. E., and Brennan, R. G. (2001) Crystal structure of the transcription activator BmrR bound to DNA and a drug, *Nature 409*, 378-382.

89. Godsey, M. H., Baranova, N. N., Neyfakh, A. A., and Brennan, R. G. (2001) Crystal structure of MtaN, a global multidrug transporter gene activator, *J. Biol. Chem. 276*, 47178-47184.

90. Utschig, L. M., Bryson, J. W., and O'Halloran, T. V. (1995) Mercury-199 NMR of the metal receptor site in MerR and its protein-DNA complex, *Science 268*, 380-385.

91. Shewchuk, L. M., Verdine, G. L., Nash, H., and Walsh, C. T. (1989) Mutagenesis of the cysteines in the metalloregulatory protein MerR indicates that a metal-bridged dimer activates transcription, *Biochemistry 28*, 6140-6145.

92. Jian, X., Wasinger, E. C., Lockard, J. V., Chen, L. X., and He, C. (2009) Highly Sensitive and Selective Gold(I) Recognition by a Metalloregulator in Ralstonia metallidurans, *J. Am. Chem. Soc. 131*, 10869-10871.

93. Watanabe, S., Kita, A., Kobayashi, K., and Miki, K. (2008) Crystal structure of the [2Fe-2S] oxidative-stress sensor SoxR bound to DNA, *Proc. Natl. Acad. Sci. 105*, 4121-4126.

94. Brown, N. L., Stoyanov, J. V., Kidd, S. P., and Hobman, J. L. (2003) The MerR family of transcriptional regulators, *FEMS Microbiol. Rev. 27*, 145-164.

95. Ralston, D. M., and O'Halloran, T. V. (1990) Ultrasensitivity and heavy-metal selectivity of the allosterically modulated MerR transcription complex, *Proc. Natl. Acad. Sci. 87*, 3846-3850.

96. Newberry, K. J., Huffman, J. L., Miller, M. C., Vazquez-Laslop, N., Neyfakh, A. A., and Brennan, R. G. (2008) Structures of BmrR-Drug Complexes Reveal a Rigid Multidrug Binding Pocket and Transcription Activation through Tyrosine Expulsion, *J. Biol. Chem. 283*, 26795-26804.

97. Portmann, R., Poulsen, K. R., Wimmer, R., and Solioz, M. (2006) CopY-like copper inducible repressors are putative 'winged helix' proteins, *Biometals 19*, 61-70.

98. Cobine, P. A., George, G. N., Jones, C. E., Wickramasinghe, W. A., Solioz, M., and Dameron, C. T. (2002) Copper transfer from the Cu(I) chaperone, CopZ, to the repressor, Zn(II)CopY: metal coordination environments and protein interactions, *Biochemistry 41*, 5822-5829.

99. Cantini, F., Banci, L., and Solioz, M. (2009) The copper-responsive repressor CopR of Lactococcus lactis is a 'winged helix' protein, *Biochem. J. 417*, 493-499.

100. Singleton, C., and Le Brun, N. E. (2007) Atx1-like chaperones and their cognate P-type ATPases: copper-binding and transfer, *Biometals 20*, 275-289.

101. Iwig, J. S., Rowe, J. L., and Chivers, P. T. (2006) Nickel homeostasis in Escherichia coli - the rcnR-rcnA efflux pathway and its linkage to NikR function, *Mol. Microbiol. 62*, 252-262.

102. Rodriguez, G. M., and Smith, I. (2006) Identification of an ABC transporter required for iron acquisition and virulence in Mycobacterium tuberculosis, *J. Bacteriol. 188*, 424-430.

103. Iwig, J. S., Leitch, S., Herbst, R. W., Maroney, M. J., and Chivers, P. T. (2008) Ni(II) and Co(II) sensing by Escherichia coli RcnR, *J. Am. Chem. Soc. 130*, 7592-7606.

104. Chen, H., Hu, J., Chen, P. R., Lan, L., Li, Z., Hicks, L. M., Dinner, A. R., and He, C. (2008) The Pseudomonas aeruginosa multidrug efflux regulator MexR uses an oxidation-sensing mechanism, *Proc. Nat. Acad. Sci. 105*, 13586-13591.

105. Smaldone, G. T., and Helmann, J. D. (2007) CsoR regulates the copper efflux operon copZA in Bacillus subtilis, *Microbiology 153*, 4123-4128.

106. Kuzmic, P. (1996) Program DYNAFIT for the analysis of enzyme kinetic data: application to HIV proteinase, *Anal. Biochem. 237*, 260-273.

107. Xiao, Z., Loughlin, F., George, G. N., Howlett, G. J., and Wedd, A. G. (2004) C-terminal domain of the membrane copper transporter Ctr1 from Saccharomyces cerevisiae binds four Cu(I) ions as a cuprous-thiolate polynuclear cluster: sub-femtomolar Cu(I) affinity of three proteins involved in copper trafficking, *J. Am. Chem. Soc. 126*, 3081-3090.

108. Xue, Y., Davis, A. V., Balakrishnan, G., Stasser, J. P., Staehlin, B. M., Focia, P., Spiro, T. G., Penner-Hahn, J. E., and O'Halloran, T. V. (2008) Cu(I) recognition via cation-[pi] and methionine interactions in CusF, *Nat. Chem. Biol. 4*, 107-109.

109. Xiao, Z., Donnelly, P. S., Zimmermann, M., and Wedd, A. G. (2008) Transfer of Copper between Bis(thiosemicarbazone) Ligands and Intracellular Copper-Binding Proteins. Insights into Mechanisms of Copper Uptake and Hypoxia Selectivity, *Inorg. Chem. 47*, 4338-4347.

110. Liu, T., Chen, X., Ma, Z., Shokes, J., Hemmingsen, L., Scott, R. A., and Giedroc, D. P. (2008) A CuI-Sensing ArsR Family Metal Sensor Protein with a Relaxed Metal Selectivity Profile, *Biochemistry 47*, 10564-10575.

111. Ma, Z., Cowart, D. M., Scott, R. A., and Giedroc, D. P. (2009) Molecular Insights into the Metal Selectivity of the Copper(I)-Sensing Repressor CsoR from Bacillus subtilis, *Biochemistry 48*, 3325-3334.

112. Zhou, L., Singleton, C., and Le Brun, N. E. (2008) High Cu(I) and low proton affinities of the CXXC motif of Bacillus subtilis CopZ, *Biochem. J. 413*, 459-465.

113. Pennella, M. A., Arunkumar, A. I., and Giedroc, D. P. (2006) Individual metal ligands play distinct functional roles in the zinc sensor Staphylococcus aureus CzrA, *J. Mol. Biol. 356*, 1124-1136.

114. Wang, L., Xie, J., and Schultz, P. G. (2006) Expanding the genetic code, *Annu. Rev. Biophys. Biomol. Struct. 35*, 225-249.

115. Muralidharan, V., and Muir, T. W. (2006) Protein ligation: an enabling technology for the biophysical analysis of proteins, *Nat. Methods 3*, 429-438.

116. Lee, S., Arunkumar, A. I., Chen, X., and Giedroc, D. P. (2006) Structural insights into homo- and heterotropic allosteric coupling in the zinc sensor S. aureus CzrA from covalently fused dimers, *J Am Chem Soc 128*, 1937-1947.

117. VanZile, M. L., Chen, X., and Giedroc, D. P. (2002) Allosteric negative regulation of smt O/P binding of the zinc sensor, SmtB, by metal ions: a coupled equilibrium analysis, *Biochemistry 41*, 9776-9786.

118. Lee, Y. H., Dorwart, M. R., Hazlett, K. R., Deka, R. K., Norgard, M. V., Radolf, J. D., and Hasemann, C. A. (2002) The crystal structure of Zn(II)-free Treponema pallidum TroA, a periplasmic metal-binding protein, reveals a closed conformation, *J. Bacteriol. 184*, 2300-2304.

119. Delaglio, F., Grzesiek, S., Vuister, G. W., Zhu, G., Pfeifer, J., and Bax, A. (1995) NMRPipe: a multidimensional spectral processing system based on UNIX pipes, *J. Biomol. NMR 6*, 277-293.

120. Goddard, T. D., and Kneller, D. G. Sparky 3, University of California, San Francisco.

121. Dawson, P. E., and Kent, S. B. H. (2000) Synthesis of native proteins by chemcial ligation, *Annu. Rev. Biochem. 69*, 923-960.

122. Kau, L. S., Spira-Solomon, D. J., Penner-Hahn, J. E., Hodgson, K. O., and Solomon, E. I. (1987) X-ray absorption-edge determination of the oxidation-state and coordination-number of copper - application to the type-3 site in rhus-vernicifera laccase and its reaction with oxygen, *J. Am. Chem. Soc. 109*, 6433-6442.

123. Arunkumar, A. I., Pennella, M. A., Kong, X., and Giedroc, D. P. (2007) Resonance assignments of the metal sensor protein CzrA in the apo-. Zn2- and DNA-bound (42 kD) states, *Biomol. NMR Assign. 1*, 99-101.

124. Kent, S. B. H. (2009) Total chemical synthesis of proteins, *Chem. Soc. Rev. 38*, 338-351.

125. Brookes, E., and Demeler, B. (2006) Genetic Algorithm Optimization for Obtaining Accurate Molecular Weight Distributions from Sedimentation Velocity Experiments, in *Analytical Ultracentrifugation VIII*, pp 33-40.

126. Brookes, E., and Demeler, B. (2008) Parallel computational techniques for the analysis of sedimentation velocity experiments in UltraScan, *Colloid. Polym. Sci. 286*, 139-148.

127. Demeler, B., and Brookes, E. (2008) Monte Carlo analysis of sedimentation experiments, *Colloid. Polym. Sci. 286*, 129-137.

128. Tan, X., Kagiampakis, I., Surovtsev, I. V., Demeler, B., and Lindahl, P. A. (2007) Nickel-Dependent Oligomerization of the Alpha Subunit of Acetyl-

Coenzyme A Synthase/Carbon Monoxide Dehydrogenase, *Biochemistry 46*, 11606-11613.

129. Wang, S. C., Dias, A. V., Bloom, S. L., and Zamble, D. B. (2004) Selectivity of metal binding and metal-induced stability of Escherichia coli NikR, *Biochemistry 43*, 10018-10028.

130. Chen, X., Chu, M., and Giedroc, D. P. (2000) Spectroscopic characterization of Co(II)-, Ni(II)-, and Cd(II)-substituted wild-type and non-native retroviral-type zinc finger peptides, *J. Biol. Inorg. Chem. 5*, 93-101.

131. Rosenzweig, A. C., and O'Halloran, T. V. (2000) Structure and chemistry of the copper chaperone proteins, *Curr. Opin. Chem. Biol. 4*, 140-147.

132. Rosenzweig, A. C. (2001) Copper delivery by metallochaperone proteins, *Acc. Chem. Res. 34*, 119-128.

133. Cobine, P. A., George, G. N., Jones, C. E., Wickramasinghe, W. A., Solioz, M., and Dameron, C. T. (2002) Copper transfer from the Cu(I) chaperone, CopZ, to the repressor, Zn(II)CopY: metal coordination environments and protein interactions, *Biochemistry 41*, 5822-5829.

134. Dietze, E. C., Wang, R. W., Lu, A. Y. H., and Atkins, W. M. (1996) Ligand Effects on the Fluorescence Properties of Tyrosine-9 in Alpha 1-1 Glutathione S-Transferase, *Biochemistry 35*, 6745-6753.

135. Banci, L., Bertini, I., Del Conte, R., Markey, J., and Ruiz-Duenas, F. J. (2001) Copper trafficking: the solution structure of Bacillus subtilis CopZ, *Biochemistry 40*, 15660-15668.

136. Sitthisak, S., Knutsson, L., Webb, J. W., and Jayaswal, R. K. (2007) Molecular characterization of the copper transport system in Staphylococcus aureus, *Microbiology 153*, 4274-4283.

137. Iwig, J. S., and Chivers, P. T. (2009) DNA Recognition and Wrapping by *E. coli* RcnR, *J. Mol. Biol. In Press*.

138. Busenlehner, L. S., and Armstrong, R. N. (2005) Insights into enzyme structure and dynamics elucidated by amide H/D exchange mass spectrometry, *Arch. Biochem. Biophys. 433*, 34-46.

139. Golynskiy, M., Li, S., Woods, V. L., Jr., and Cohen, S. M. (2007) Conformational studies of the manganese transport regulator (MntR) from Bacillus subtilis using deuterium exchange mass spectrometry, *J. Biol. Inorg. Chem. 12*, 699-709.

140. David S. Radford, Margaret A. Kihlken, Gilles P.M. Borrelly, Colin R. Harwood, Nick E. Brun, and Jennifer S. Cavet. (2003) CopZ from *Bacillus subtilis* interacts in vivo with a copper exporting CPx-type ATPase CopA, *FEMS Microbiol. Lett. 220*, 105-112.

141. Banci, L., Bertini, I., and Del Conte, R. (2003) Solution structure of Apo CopZ from *Bacillus subtilis*: further analysis of the changes associated with the presence of copper, *Biochemistry 42*, 13422-13428.

142. Cobine, P., Wickramasinghe, W. A., Harrison, M. D., Weber, T., Solioz, M., and Dameron, C. T. (1999) The Enterococcus hirae copper chaperone CopZ delivers copper(I) to the CopY repressor, *FEBS Lett. 445*, 27-30.

143. Gonzalez-Guerrero, M., and Arguello, J. M. (2008) Mechanism of Cu+-transporting ATPases: soluble Cu+ chaperones directly transfer Cu+ to transmembrane transport sites, *Proc. Natl. Acad. Sci. 105*, 5992-5997.

144. Banci, L., Bertini, I., Ciofi-Baffoni, S., Kandias, N. G., Robinson, N. J., Spyroulias, G. A., Su, X. C., Tottey, S., and Vanarotti, M. (2006) The delivery of copper for thylakoid import observed by NMR, *Proc. Natl. Acad. Sci. 103*, 8320-8325.

145. Zheng, M., Aring, slund, F., and Storz, G. (1998) Activation of the OxyR Transcription Factor by Reversible Disulfide Bond Formation, *Science 279*, 1718-1722.

146. Mueller, E. G. (2006) Trafficking in persulfides: delivering sulfur in biosynthetic pathways, *Nat. Chem. Biol. 2*, 185-194.

APPENDIX A

Dynafit script for Cu(I)-BCS competition assay for CsoR

```
[task]
        data = equilibria
        task = fit

[mechanism]

        Cu + M + M <==> Cu.M2 : K1 assoc.

        Cu + P2 <==> Cu.P2 : K3 assoc.


[concentrations]
        P2 = 22 , M = 50

[constants]
        K1 = 63000000, K3 = 1000000000000 ?

[equilibria]
        directory ./data/CsoR/
        extension txt
        variable Cu
        file BCS | response M = 0.00021 , Cu.M2 = 0.01079

[output]
        directory ./output/CsoR/BCS

[end]
```

APPENDIX B

DNA binding of wild-type and mutant *Mtb CsoO*s tested by gel-filtration[a] (10 mM HEPES, 0.2 M NaCl, 2 mM DTT, pH 7.0)

	DNA sequences	Binding
WT 50bp	5' ACTCCTTGGGTAGCCCACCCCCAGTGGGGTGGGATACCATGAACGGGTGA 3'	2 tetramers[b]
WT 28bp	GTAGCCCACCCCCAGTGGGGTGGGATAC	2 tetramers
CsoO-3	GTAGCCCACCCCCAGTGGGGT	weak[c]
CsoO-4	GTAGCCCAAAAACAGTGGGGT	no[d]
CsoO-5	GTAGCCCAACTGAAGTGGGGT	no
CsoO-6	ACCCCCAGTGGGGTGGGATAC	weak
CsoO-7	ACCCCCAGTCTGATGGGATAC	no

[a] 10 μM DNA was mixed with 80 μM *Mtb* CsoR monomer in 10 mM HEPES, 0.2 M NaCl, 2 mM DTT, pH 7.0.

[b] All protein-DNA complex and no free DNA detected (Figure 16A).

[c] Free DNA as well as a broad peak of protein-DNA complex and free protein detected.

[d] All free DNA and no binding.

APPENDIX C

Dynafit script for CsoR-DNA interaction

```
[task]
        data = equilibria
        task = fit
[mechanism]
        CsoR + D <==> CsoR.D : K1 assoc.
        CsoR + CsoR.D <==> CsoR2.D : K2 assoc.
[concentrations]
        D = 0.01
[constants]
        K1 = 10 ? , K2 = 10 ?
[equilibria]
        directory ./data
        extension txt
        variable CsoR
        file CsoR | response D = 11.69 , CsoR.D = 12.1  ,  CsoR2.D = 12.7
[output]
        directory ./output/CsoR
[end]
```

APPENDIX D

Dynafit script for Zn(II)-magfura-2 competition assay for CzrA

```
[task]
        data = equilibria
        task = fit

[mechanism]
        P + P <==> P2 : Kdim assoc.
        Zn + M* <==> Zn.M* : K1 assoc.
        Zn + P2 <==> Zn.P2 : K2 assoc.
        Zn + Zn.P2 <==> Zn2.P2 : K3 assoc.

[concentrations]
        M* = 2.4  , P = 1.67

[constants]
        Kdim=0.17 , K1 = 50  , K2 = 5000 ?, K3=100 ?

[equilibria]
        directory ./data
        extension txt
        variable Zn
        file lig325_2 | response M* = 22191, Zn.M* = 98217
        file lig379_2 | response M* = 54667, Zn.M* = 16037

[output]
        directory ./output/CzrAlig

[end]
```

APPENDIX E

Growth curves obtained for wild-type (A) and putative *ΔcsoR* locus (B) *S. aureus* Newman strain at different Cu concentrations added to the medium. These experiments were carried out in Dr. Erik Skaar's laboratory at Vanderbilt University.

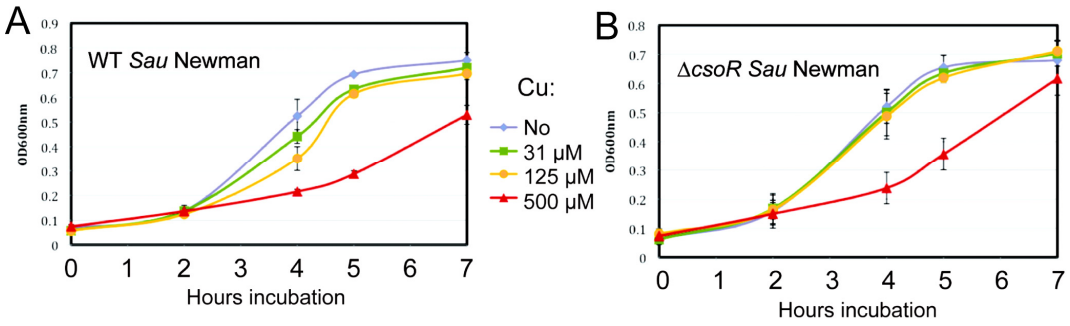

VITA

Name: Zhen Ma

Address: 800 E. Kirkwood
Chemistry Department
Indiana University
Bloomington, IN 47405

Email Address: maz@indiana.edu

Education: B.S., Biological Sciences, Fudan University, 2004
Ph.D., Biochemistry, Texas A&M University, 2009

Publications:

Liu, T., Ramesh, A., Ma, Z., Ward, S. K., Zhang, L., George, G. N., Talaat, A. M., Sacchettini, J. C., and Giedroc, D. P. (2007) CsoR is a novel *Mycobacterium tuberculosis* copper-sensing transcriptional regulator, *Nat. Chem. Biol. 3*, 60-68.

Liu, T., Chen, X., Ma, Z., Shokes, J., Hemmingsen, L., Scott, R. A., and Giedroc, D. P. (2008) A Cu(I)-sensing ArsR family metal sensor protein with a relaxed metal selectivity profile, *Biochemistry 47*, 10564-10575.

Ma, Z., Cowart, D. M., Scott, R. A., and Giedroc, D. P. (2009) Molecular Insights into the Metal Selectivity of the Copper(I)-Sensing Repressor CsoR from *Bacillus subtilis*, *Biochemistry 48*, 3325-3334.

Ma, Z., Jacobsen, F. E., and Giedroc, D. P. (2009) Coordination Chemistry of Bacterial Metal Sensing and Transport, *Chem. Rev. In press*. (doi: 10.1021/cr900077w)

Ma, Z., Cowart, D.M., Zhang, L., Ward, B.P., Arnold, R.J., DiMarchi, R.D., George, G.N., Scott, R.A. and Giedroc D.P. (2009) Unnatural Amino Acid Substitution as a Probe of the Allosteric Coupling Pathway in a Mycobacterial Cu(I)-sensor, *Submitted.*